

DESIGN AND PERFORMANCE OF LEAD SYSTEMS FOR THE ANALYSIS OF ATRIAL SIGNAL COMPONENTS IN THE ECG

THÈSE N° 3565 (2006)

PRÉSENTÉE LE 7 JUILLET 2006

À LA FACULTÉ SCIENCES ET TECHNIQUES DE L'INGÉNIEUR
Laboratoire de traitement des signaux 1
SECTION DE GÉNIE ÉLECTRIQUE ET ÉLECTRONIQUE

ÉCOLE POLYTECHNIQUE FÉDÉRALE DE LAUSANNE

POUR L'OBTENTION DU GRADE DE DOCTEUR ÈS SCIENCES

PAR

Zenichi IHARA

Bachelor of Science in Electrical Engineering, Sophia University, Tokyo, Japon
et de nationalité japonaise

acceptée sur proposition du jury:

Prof. J. R. Mosig, président du jury
Dr J.-M. Vesin, directeur de thèse
Dr K. Aminian, rapporteur
Prof. L. Kappenberger, rapporteur
Prof. A. van Oosterom, rapporteur



ÉCOLE POLYTECHNIQUE
FÉDÉRALE DE LAUSANNE

Lausanne, EPFL

2006

To the future unforeknown.

To be “normal” is the ideal aim for the unsuccessful, for all those who are still below the general level of adaptation. But for people of more than average ability, people who never found it difficult to gain successes and to accomplish their share of the world’s work – for them the moral compulsion to be nothing but normal signifies the bed of Procrustes – deadly and insupportable boredom, a hell of sterility and hopelessness.

– CARL GUSTAV JUNG. *Problems of Modern Psychotherapy* (1929)⁵⁵ –

Prologue

What drives a person to write a thesis? The passion for knowledge and science? The promise of a better life, or success? Can it be otherwise some kind of an ethically-inspired categorical imperative,⁵⁶ or, because it is the material proof of the ontological primacy of one's will over his reason?⁸⁴ It may also be, for love of the city of Geneva, because we stand to gain much more through suffering than by avoidance of it.^{7,8}

Anyhow, in my case I believe it was conviction. I had chosen to write it, and I have written it. This is the record of my activity as a doctoral student at EPFL for the past four years and a half. Thank you for being interested, whoever you are, and I hope you find *something* that makes you not regret taking this text in your hands.

So, please do, like everybody else does, begin at the beginning and go on till you come to the end: then stop.¹²

Acknowledgments

Notwithstanding the ambitious dedication and the pretentious quotation on the first page, this thesis was certainly not a lone struggle. It was a team work like nothing else. This is an address of heartfelt gratitude to the people who counted in the achievement of the work.

Professors

I would like to express my foremost gratitude and respect to **Jean-Marc Vesin**, my director of thesis and my master of signal processing. Thank you for teaching me, thank you for accepting me, thank you for backing me and thank you for being my supervisor. Although I still don't really know what *SVD* is about, as embarrassing as it is to admit, I confirm Matlab does it very well.

I owe the most part of the research work presented in this thesis to the professor **Adriaan van Oosterom** who, as my mentor, followed me, guided me and supported me throughout the entire academic work that led to this dissertation. Indeed, the driving force of this thesis that impelled my will can be summed up to the cheerful, affectionate and unforgettable encouragement he gave me four months before the deadline for submission: *"One down, three more to go!"*.*

Many thanks to Mrs. **Judith van Oosterom** for the correction of English manuscripts.

I feel deeply grateful to the founder and leader of the Lausanne Heart group, the professor **Lukas Kappenberger**. The initiative and feedback from the medical field is most essential in biomedical engineering, and an addition of a broad vision with ideas and inspiration always gave us exciting stimulations. The variety of activities of the group with conferences and workshops around Europe and the US was also a speciality of Lausanne Heart. I appreciated the numerous pedagogical opportunities provided as anybody else in the group. In that respect, I would also like to mention the countess Ida Rossi-Di-Montelera and the grants from her Theo-Rossi-Di-Montelera Foundation that kept our substantial productivity alive, as well as Medtronic Europe, the Swiss Governmental Commission of

*I was walking down the corridor of the laboratory one evening, lighthearted with the good news of my journal paper being accepted. I came across the professor and told him the news. He looked happy, put his thumb up, and continued... Most surprisingly, it worked. I shall recognize the power of will.⁸⁵

Innovative Technologies (CTI), and the Swiss National Sciences Foundation (SNSF).

During the initial stages of my studies, Lausanne Heart had many interactions with the professor **Craig S. Henriquez**. His expertise in diverse fields as well as his accurate and inspiring feedbacks were always of high value for us. I hope to see you again and discuss about all the things I was ignorant of then.

Another person I would like to mention from the United States is the professor **Alan Garfinkel**. I acknowledge on behalf of the Lausanne Heart group the most constructive advice on the use of the Courtemanche model so we would sit around the big table. I would like to thank you personally about the practical work session in Monaco on probability and statistics.

The director of Signal Processing Institute (ITS), the professor **Murat Kunt** is the very person who accepted me in the laboratory for the doctoral studies. I would like to extend my deep expression of appreciation. His finest jokes always had me in stitches. Also, my acknowledgments go to all the professors of ITS for the intriguing discussions and feedback they offered me; the professor **Daniel Mlynek**, professor **Jean-Philippe Thiran**, professor **Touradj Ebrahimi**, professor **Pierre Vandergheynst** – thank you for signing me in the Italian class – and professor **Pascal Frossard**.

The professors who welcomed me in the postgraduate program of biomedical engineering, namely the professor **Pavel Kučera** and professor **Daniel Bertrand** for the intensive physiology classes incommensurably educative, as well as the professor **Jean-Jacques Meister** for the biomechanics class and for accepting my candidature. The doctor **Kamiar Aminian** offered me the diploma project in the field of human gait analysis, and I am especially grateful and honored for his being a member of the jury of my thesis.

At last but not the least, all the professors who taught me the basis of electrical and electronics engineering at Sophia University, of whom my mentor notably, the professor **Kiyoshi Nakayama**. I would not be in this field had it not been for him and his electromagnetism classes. I am sorry I missed your valedictory lecture.

The band of brothers

My direct and closest colleagues, *a.k.a.* **les Jean-Marc boys** of Signal Processing Laboratory (LTS). They supported me during the writing of my thesis, cheered me up, and gave me a kick in the back at the moment of critical decision. We have been helping each other in the substantial work of Lausanne Heart. We were together all the time, went to expeditions everywhere. I do what I do best, you do what you do best.⁶⁵ Good luck.

Olivier “peanuts” Blanc welcomed me to Lausanne Heart. It has been a while since he left the group, but he founded the solid basis of Lausanne Heart that once began in trials and errors. His thesis work is the concrete base for the rest of us all.

Vincent “the brain” Jacquemet is the gray matter of the group. Where there is an input, there is an output. His thesis work and achievements as a postdoc have been

sustaining most of the material results of Lausanne Heart. Off the record, not many people in the field – not even ourselves sometimes – are aware of the fact that the center pillar of Lausanne Heart is no one but him. I wish him all the best for his next step and my blessing goes to the people working at his next destination. As for the group, and Switzerland, a significant change will inevitably be.

Mattia “bicycle” Bertschi studied as an expert in the biophysical modeling of the large intestine. He did not work in Lausanne Heart in a strict sense, yet is definitely a part of the JM boys and our best friend. A man of integrity and hospitality. He has a great family in the beautiful Ticino, and he is a daddy now.

Lam “the delicatessen” Dang participated in the postgraduate course in biomedical engineering where I met him. Thank you for looking me after like a brother. His lifestyle based on his surprising skill of adaptation and flexibility made him a role model of human relations for the rest of the group.

Mathieu “the last trapper” Lemay is the québécois who brought change in the group. The wind from another continent enriched the C₂H₅OH content of the discipline. His carousal attribute in the fun of living shepherded the others to their own hereditary nature. We had very much fun in Monaco and in Prague. Do not forget the revenge for Billy Joel’s *Honesty*; as for me, I will flip the crêpe on the next occasion. And thank you so much for helping me decide.

Yann “the boar of Porrentruy” Prudat is the brobdingnagian Jurassian. He is kind, and he is big. I wish you good luck with the data from Milano. Don’t drink too much.

Although not officially a member of the JM boys, **Nathalie Virag** is the core factor of Lausanne Heart managing the various projects. I thank her in particular for the organization of the “jet-set” workshops. And thank you as well for giving me precious knowledge prior to my dramatic interview at *you-know-where*.

Colleagues

I would like to mention the doctors of the Lausanne University Hospital Center (CHUV), namely **Etienne Pruvot** and **Andrei Forclaz** for providing us clinical data and answering to medical questions; the nurse assigned to the NAF project, **Véronique Prudent** for the clinical recordings of ECG; and from Radboud University Medical Centre, **Rudi Hoekema** for the cooperation in the studies involving the geometries of the human thorax.

All colleagues of LTS, the people around me from the day I entered the lab to the day I depart. The alumni, **Andrea Cavallaro**, **Diego Santa Cruz**, **Raphaël Grobois**, **Torsten Butz**, **François Mendels**, **Frédéric Décaillet**, **Eduardo Solanas Vilar**, **Meritxell Bach Cuadra**, **Elena Salvador**, **Rosa Maria Figueras i Ventura**, **Òscar Divorra Escoda**, **Patric Hagmann**, **Gary Garcia Molina**, **Xavier Bresson**, **Iva Bogdanova**, **Olivier Cuisenaire** and many more. I especially thank **Nicolas Aspert** and **Olivier Steiger** for teaching me good music. They opened the door to great works –

and fondue parties – including Mahler’s symphonies and Beethoven’s quartets in addition to the sole inclination to Bach that I had. It is true that “*My heart, which is so full to overflowing, has often been solaced and refreshed by music...*”.⁶¹ **Lisa Jonasson** is the very special colleague. She is the first person whom I spoke with in the lab, most probably because she is a blonde Swede (kidding). She represents the entire friendship and memorable moments spent with the colleagues of LTS. Moreover, she cooks delicious panna cotta with berries. **Elisa Drelie Gelasca** is the other special colleague. We started our doctoral life on the very same day, and she finished well before me... Anyway, in the end, we found ourselves in the same office. I appreciated her company heartily besides her being a sweet honey-blonde Italian. She represents the entire resplendence of the LTS girls.

To all fellows currently at LTS working hard. Thank you so much for your support and being around with jokes and smile on your face. **Dragana Viceić, Ruth Campos Casillas, Nawal Houhou, Valérie Duay**, the three **Ivana’s (Arsić, Radulović and Tošić)**, **Karin Schnass, Patricia Besson**, and all the rest... I’m kidding: **Philippe Jost, Dan Jurca, David Marimón Sanjuán, Francisco Javier Sánchez Castro, Yannick Maret, Julien Meynet, Gianluca Monaci, Ulrich Hoffmann, Yves Wiaux, et alii**. For those heading towards their doctorate, the least I can say is that I hope you get it done smoothly and sharply. I believe the statement made 25 centuries ago still stands, that is, “*Though we have heard of stupid haste in war, cleverness has never been seen associated with long delays.*”.⁹² Concentration must be the key.

Special thanks to the secretaries of ITS, **Marianne Marion, Fabienne Vionnet Monterde**, and **Aline Gruaz**. I was always impressed by the efficiency and the precision of Marianne’s work. Thank you for taking care of us all the time. Not to be forgotten is the system engineer and network administrator of the lab, **Gilles Auric**. In an environment in which the use of integrated electronic circuits known as PC is most essential as the principal tool for work, Gilles exorcized my haunted informatics environment an uncountable number of times. Thank you! I will keep in mind what you once said about conquering the world.



William-Adolphe Bouguereau (1825-1905), Biblis (1884).

Friends

There is never enough space to thank one's good friends, the time spent with whom we cherish more than anything. Because we cannot be aware of the great moments we enjoy devotedly as they stream around us, it is always in the past tense that we reminisce the enjoyment. "*I was assailed by memories of a life that wasn't mine anymore, but one in which I'd found the simplest and most lasting joys.*",⁹ accompanied with a slight bitter taste of melancholy. Good friends are sources of vivacity when weary of the *gentle indifference*⁹ often surrounding us. They inspire us, motivate us and make us live. We speak and we think together. "*The important thing isn't the soundness or otherwise of the argument, but for it to make you think.*",¹⁰ says one. My most precious friends, thank you!

The friend I care for the most who had the strongest impact on my perception of human relations is **Nicole Kate Roduit**. Because "*A compliment is something like a kiss through a veil.*",⁴⁴ I would like to embrace her gently in appreciation for the time spent together. She is an irreplaceable person I came to know in Lausanne, with whom I enjoyed the everlasting dialogues on existential themes. My feeling of upmost affection goes with you, Nickie.

The friend I would like to acknowledge above all is **Marc Hensler**. Since the first day I stepped foot à **l'école des Allières**, we have been best friends for over 20 years now. I am in Switzerland today loving Geneva and speaking French all owing to him. There is too much to be recounted here, so let me just tell you this. See you soon, my friend.

All my friends in Geneva, **Marie Schaer**, **Mikaël Rouvinez**, **Fabien Pizzirusso**, **Johan Markwalder** and **René Glaus**, thank you for the good times we spent on various occasions.

The classmates of elementary school who were my first contact with Switzerland and Geneva: **Stéphanie Koller**, **Laurence Plantard**, **Laurent Pierroz**, **Anne-Gaëlle Francioli** and all. You are the source of who I am now. I will be looking forward to the next class reunion.

And my friends in Lausanne, **Kumiko Oshima**, **Sonya Elmer**, **Mariska Ruoss**, **Danielle Ramseier** for your Berner sympathy, **Maïté Terraz** for the candles and oil, and **Nicola Scolari**, *ci vedremo presto per una pinta di Maredsous*.

My friends in Japan. I feel extremely fortunate to have good friends in every environment. **Yuta Muramatsu** and all my friends from the secondary school and high school; **Hisashi Aomori**, **Yasumasa Kawakita** and my dear fellows from the university.

Family

The greatest expression of gratitude goes to my family(ies). My parents, brother and sister, and the whole family. My father was the person who convinced me to stay at EPFL for the doctoral studies and I am grateful for his pushing me in this direction.

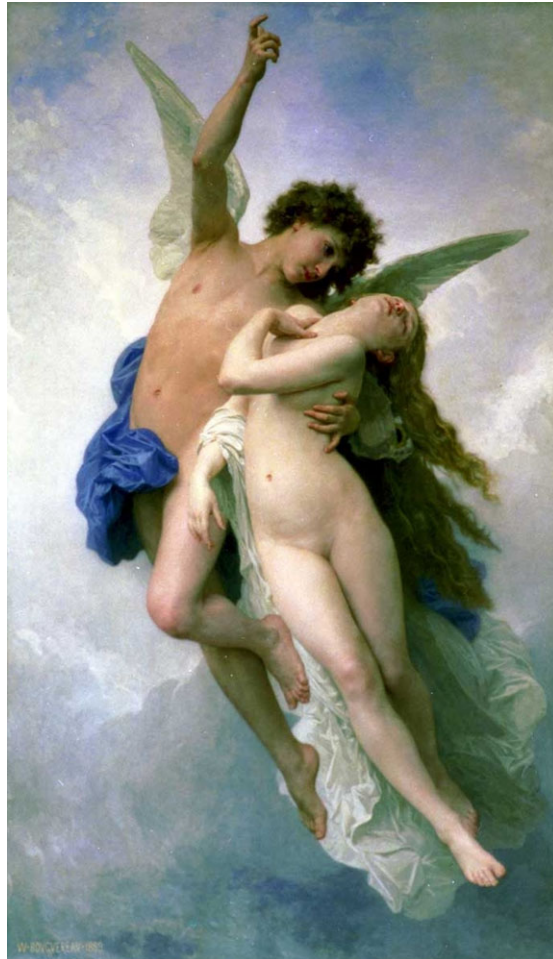
The **Hensler's**, my second family in Geneva. Marc's parents, **André**, **Elfie**, and Marc's

sister **Michèle** who always welcomed me to their home as if I had always been a member of the family. I could never thank them enough.

The **Horie's** helped me a lot when I arrived in Lausanne knowing nothing about life in Lausanne and at EPFL. Mr. and Mrs. Horie, thank you very much.

And to the future...

The redaction of my thesis advanced swiftly for one thanks to the motivation I acquired from the people who found me out: Mister **Barry W. Wilson**, Monsieur **Jean-Luc Butel**, Mister **Stephen R. La Neve** and Mister **Marshall Stanton**. I cannot but think that probabilistic processes do eventually govern peoples' lives. I shall be prepared when the die is cast. After all, tomorrow is another day!⁷⁰



William-Adolphe Bouguereau (1825-1905), Psyché et l'Amour (1889).

Table of contents

Prologue	v
Acknowledgments	vii
Table of contents	xiii
Abstract	xvii
Version abrégée	xxi
List of acronyms	xxv
List of figures	xxviii
List of tables	xxix
1 Introduction	3
1.1 Καρδία	3
1.2 Bioelectricity of the heart	5
1.3 Body surface potentials and Electrocardiogram	8
1.3.1 Vectorcardiogram	10
1.4 Cardiac arrhythmias and atrial fibrillation	10
1.5 This thesis	12
1.5.1 Atrial fibrillation in the heart of modern society	12
1.5.2 Atrial repolarization as observable during the PQ interval (<i>chapter 2</i>)	14
1.5.3 Adaptation of the standard 12-lead ECG system dedicated to the analysis of atrial fibrillation (<i>chapter 3</i>)	14
1.5.4 Performance of a lead system dedicated to atrial fibrillation: appli- cation to clinical data (<i>chapter 4</i>)	15

1.5.5	Vectorcardiographic lead systems for the characterization of atrial fibrillation (<i>chapter 5</i>)	16
2	Atrial repolarization during PQ interval	17
2.1	Introduction	17
2.2	Materials	17
2.3	Methods	19
2.3.1	Definition of terms	19
2.3.2	Processing the signals	19
2.3.3	Extracted features	21
2.3.4	Statistics	22
2.4	Results	24
2.4.1	From the RMS curve	24
2.4.2	From the 64-lead signals:	24
2.4.3	From the VCG	25
2.5	Discussion	26
2.5.1	Locations of extreme potentials	28
2.5.2	Involvement of atrial repolarization	30
2.6	Limitations	30
2.7	Conclusion	31
3	OACG lead system	33
3.1	Introduction	33
3.2	Materials and methods	34
3.2.1	Simulated atrial fibrillation	34
3.2.2	Equivalent source strength	36
3.2.3	Computation of body surface potentials	36
3.2.4	Simulated body surface potentials	37
3.2.5	Information content	38
3.2.6	Search methods	39
3.2.7	Evaluation Method	40
3.3	Results	40
3.3.1	Number of independent signals	40
3.3.2	The new lead system	40
3.3.3	Evaluation of OACG	43
3.4	Discussion	43

3.5	Limitations	45
3.6	Conclusion	45
4	Clinical application of new lead systems	47
4.1	Introduction	47
4.2	Methods	48
4.2.1	Lead systems	48
4.2.2	Clinical AF signals	50
4.2.3	VA cancellation	51
4.2.4	The complexity index	52
4.3	Results	53
4.3.1	VA cancellation	53
4.3.2	The complexity index	53
4.4	Discussion	55
4.5	Limitations	56
4.6	Conclusion	57
5	VCG lead systems for AF	59
5.1	Introduction	59
5.2	Designing VCG lead systems	60
5.3	Materials and Methods	64
5.3.1	Geometries of the human thorax	64
5.3.2	Model of the human atria	65
5.3.3	Simulated atrial fibrillation	65
5.3.4	Body Surface Potentials during AF	66
5.3.5	Design of the Lead Systems	67
5.3.6	Evaluation Method	69
5.4	Results	70
5.4.1	Evaluation of the gold standard	70
5.4.2	Dedicated transfer coefficients	71
5.4.3	The optimal 7-electrode montage	72
5.4.4	Performance	73
5.4.5	Validation	74
5.5	Discussion	74
5.6	Limitations	77
5.7	Conclusion	77

6	Conclusions	79
6.1	Achievements	79
6.1.1	Chapter 2	
	<i>Atrial repolarization as observable during the PQ interval</i>	79
6.1.2	Chapter 3	
	<i>Adaptation of the standard 12-lead ECG system dedicated to the analysis of atrial fibrillation</i>	80
6.1.3	Chapter 4	
	<i>Performance of a lead system dedicated to atrial fibrillation: application to clinical data</i>	80
6.1.4	Chapter 5	
	<i>Vectorcardiographic lead systems for the characterization of atrial fibrillation</i>	81
6.1.5	Answers to the questions	82
6.2	Perspective	82
	Bibliography	93
	Curriculum vitae	95
	Epilogue	99

Abstract

For over a century, electrocardiology has been observing human cardiac activity through recordings of electrocardiograms (ECG). The potential differences derived from the nine electrodes of the standard 12-lead ECG, placed at their designated positions, are the expression of electric dynamics of which the heart is the source. According to well-defined protocols and established criteria of diagnosis, the signals of the electrocardiogram are used as indicators of cardiac pathology.

However, of the four chambers of the human heart, each of which has a specific function, most attention in cardiology has been traditionally placed on the ventricles. This has meant that the conventional ECG system is focused on the observation of ventricular activity, and might not be optimal in studying the activity of the atria. The increasing prevalence of atrial fibrillation in the general population, with its inherent severe complications as well as the known social and economic impacts of the disease, has elicited studies investigating body surface potentials of atrial arrhythmias, invariably pivoted on the standard ECG.

The aim of this thesis is to investigate the conception and validation of a lead system targeted at the analysis of atrial fibrillation. This new lead system should be dedicated and optimized to capturing a maximal amount of information about the atrial electric activity taking place during fibrillation, but at the same time be well anchored to the standard ECG configuration, in view of its application in clinical practice. This constraint has led to the use of the same number of electrodes, nine, while leaving at least half of these, five, in their initial positions.

In the first part of this thesis, observations of body surface potential maps during normal atrial activity are discussed. The objective was to study the involvement of atrial repolarization in body surface potentials. While studying ECG signals recorded with 64-lead systems from 73 patients, special attention was devoted to the processing of low-amplitude signals. The local potential extremes were found at positions not sampled by the standard leads. Moreover, the PQ segment was found to be not *electrically silent*, the time course of the potential distribution being very similar to that during the P wave but for a reversed polarity and about 3-fold lower magnitudes. The results demonstrate a significant involvement of atrial repolarization during the PQ interval, and a small dispersion of atrial action potential durations.

In the second part, the design and evaluation of a new optimized lead system (OACG) dedicated to atrial fibrillation is presented, based on a biophysical-model study. Considering the material constraint mentioned above, the locations of four of the six precordial electrodes were optimized while leaving the remaining five electrodes of the standard ECG system in place. The analysis was based on episodes of eleven different variants of AF simulated by a biophysical model of the atria positioned inside an inhomogeneous thorax. The optimization criterion used was derived from the singular value decomposition of the data matrices. The four new electrode positions increased the ratio of the eighth to the first singular value of the data matrices of the new configuration about five-fold compared to that of the conventional electrode positions. The OACG lead system produces a more complete view on AF compared to that of the conventional the standard 12-lead system.

The third part treats the evaluation of the newly-designed OACG lead system in its application to clinical signals. Atrial fibrillation signals were recorded in patients at the nine electrode positions of 1) the standard 12-lead ECG, 2) a heuristically designed lead system, the ACG lead system, and 3) the OACG lead system. After cancellation of the ventricular signals, an information measure was derived from the singular value decomposition of the atrial signals. The resulting values obtained from the three lead systems were compared. For the limited number of recordings made available from the OACG lead system, consistently higher values of the information measure were obtained with the OACG lead system compared to the standard ECG or ACG. The ECG is clearly suboptimal in the analysis of atrial fibrillation and the OACG lead system provides a more complete view of its complex dynamics.

The electric cardiac activity can be represented as the time course of a current dipole source placed inside a homogeneous thorax, the vectorcardiogram (VCG). The fourth and final topic of this thesis concerns the design of a VCG lead system committed to atrial fibrillation. Body surface potentials during atrial fibrillation were simulated by using a biophysical model of the human atria and thorax. The XYZ components of the equivalent dipole were derived from the Gabor-Nelson equations. These served as the gold standard while searching for methods to derive the vectorcardiogram from a limited number of electrode positions and their transfer coefficients. Six electrode configurations and dedicated matrices were tested using episodes of simulated atrial fibrillation and 25 different thorax models. The OACG lead system, including one electrode on the back, reduced the RMS-based relative estimation error in comparison with that of the well-known Frank lead system. The Frank lead system was found to be suboptimal for estimating the VCG during AF. Alternative electrode configurations should include at least one electrode on the back.

The overall conclusion regarding these results can be recapitulated as a suboptimality of the standard 12-lead ECG system with respect to the analysis of atrial fibrillation. The key features of atrial activity are well present in body surface potentials, but appear at locations not covered by the standard lead system. While anchoring more than half of its electrodes at their conventional positions, the four new electrode positions optimized in regard to the information extraction exhibited higher performance in a biophysical-model study. The

application of such an adapted lead system with its customized transfer coefficients to clinical signals promises a considerable improvement in the analysis of atrial fibrillation. The lead system with one electrode on the back of the thorax, allowing a three-dimensional capture of the complex dynamics of atrial fibrillation signals, demonstrated its utility in its application for deriving the VCG representation of the source estimation.

Keywords

Atrial fibrillation, biophysical model, body surface potential, depolarization,
electrocardiogram, lead system, repolarization, vectorcardiogram.

Version abrégée

Durant son histoire, l'électrocardiologie a traité l'activité cardiaque notamment à travers l'électrocardiogramme (ECG) enregistré sur la surface du corps humain. Les différences de potentiel électrique mesurées par les neuf électrodes placées à des positions spécifiques sont des expressions de la dynamique électrique dont le cœur est la source. A l'aide de protocoles bien définis et des critères de diagnostic établis, les signaux de l'électrocardiogramme fournissent des indications précieuses sur une pathologie cardiaque éventuelle.

Cependant, parmi les quatre chambres du cœur humain, dont chacune a un rôle spécifique, le centre d'intérêt de la cardiologie a longtemps été placé sur les ventricules. Cela signifie que le système d'ECG conventionnel est focalisé sur l'observation de l'activité ventriculaire, et pourrait ne pas être adapté à l'analyse de l'activité auriculaire. L'augmentation de la prévalence de la fibrillation auriculaire dans la population générale, ses symptômes liés à des complications graves ainsi que les impacts socio-économiques de cette pathologie ont conduit à l'investigation des potentiels de surface de l'arythmie auriculaire, basée invariablement sur le système d'ECG standard.

Le but du travail présenté dans cette thèse est la conception et l'évaluation d'un nouveau système d'enregistrement focalisé sur l'analyse de la fibrillation auriculaire. Le nouveau système doit être optimisé pour l'obtention d'un maximum d'informations sur l'activité électrique des oreillettes, mais en même temps ancré sur la configuration standard de l'ECG eut égard à son application en clinique.

Dans la première partie de cette thèse, la représentation du potentiel de surface a été étudiée pendant l'activité auriculaire normale. L'objectif était d'observer l'implication de la repolarisation auriculaire dans le potentiel de surface. En utilisant les signaux d'ECG enregistrés avec des systèmes de 64 électrodes sur 73 sujets, une attention particulière a été apportée au traitement des signaux de faible amplitude. Les extrema locaux du potentiel ont été trouvés dans des régions qui ne sont pas couvertes par le système standard. De plus, le segment PQ ne s'est pas avéré «électriquement silencieux». Sa distribution de potentiel au cours du temps était très similaire à celle durant l'onde P mais d'une polarité inversée, et une magnitude trois fois inférieure. Ces résultats démontrent une implication significative de la repolarisation auriculaire pendant l'interval PQ, et une faible dispersion des durées du potentiel d'action auriculaire.

Deuxièmement, la conception et l'évaluation d'un nouveau système d'enregistrement (OACG) dédié à la fibrillation auriculaire est présenté dans une étude utilisant un modèle biophysique. Par rapport aux contraintes matérielles susmentionnées, les positions de quatre parmi les six électrodes précordiales sont optimisées en laissant les cinq restantes à leur position standard. L'analyse a été basée sur onze différents épisodes de fibrillation auriculaire simulés par un modèle biophysique des oreillettes humaines placé dans un thorax inhomogène. Le critère d'optimisation est dérivé de la décomposition en valeurs singulières des matrices de données. Les quatre nouvelles positions d'électrodes ont augmenté le rapport de la huitième à la première valeur singulière d'un facteur cinq par rapport au système conventionnel. Le système OACG produit une vue plus complète de la fibrillation auriculaire comparé au système d'ECG standard.

Le troisième volet traite de l'application de ce nouveau système au signaux cliniques. Les signaux de fibrillation auriculaire ont été enregistrés avec le système d'ECG standard ainsi qu'un système conçu heuristiquement (ACG), et le système optimisé (OACG). Après suppression des signaux ventriculaires, la même mesure d'information que précédemment a été dérivée par la décomposition en valeurs singulières des signaux auriculaires. Les valeurs obtenues par les trois systèmes ont été comparées. Avec les réserves dues au nombre limité d'enregistrements avec le système OACG, ce dernier a démontré des valeurs constamment supérieures par rapport à l'ECG standard ou l'ACG. Le système standard de l'ECG est clairement sous-optimal pour l'analyse de la fibrillation auriculaire et l'OACG apporte une meilleure vision de la dynamique complexe de cette pathologie.

L'activité cardiaque électrique peut être représentée comme une évolution au cours du temps d'un dipôle de courant placé dans un thorax homogène, le vectorcardiogram (VCG). La dernière partie de cette thèse est consacrée à la conception d'un système de VCG dédié à la fibrillation auriculaire. Les potentiels de surface pendant la fibrillation auriculaire ont été simulés avec un modèle biophysique des oreillettes humaines et de thorax. Les composants XYZ du dipôle équivalent ont été dérivés par les équations de Gabor et Nelson. Ils ont servi d'étalon à la recherche de méthodes pour la dérivation du VCG à partir d'un nombre limité de positions d'électrodes et des coefficients de transfert correspondants. Six configurations d'électrodes et de matrices de transfert ont été testées en utilisant les épisodes de fibrillation auriculaire simulés et 25 différents modèles de thorax. Le système OACG, avec la particularité d'avoir une électrode dorsale, a réduit l'erreur relative d'estimation par rapport au système bien connu de Frank. Ce dernier est sous-optimal pour estimer le VCG pendant la fibrillation auriculaire. Une configuration alternative devrait posséder au moins une électrode dans le dos.

La constatation générale vis-à-vis de ces résultats se résume à une sous-optimalité du système standard de l'ECG dans le contexte de l'analyse de la fibrillation auriculaire. Les caractéristiques clef de la fibrillation auriculaire, la dépolarisation et repolarisation, sont bien présentes, mais apparaissent en des régions qui ne sont pas couvertes par le système standard. En ancrant plus de la moitié des électrodes à leur position initiale, les quatre nouvelles positions d'électrodes optimisées vis-à-vis de l'extraction d'information ont fourni de

meilleures performances dans une étude utilisant un modèle biophysique. L'application de cette démarche promet des progrès considérables dans l'analyse de la fibrillation auriculaire. L'électrode dorsale, permettant une capture tridimensionnelle de la dynamique complexe des signaux de fibrillation auriculaire, a démontré son utilité pour la représentation VCG de l'estimation de source.

Liste des mots-clefs

Fibrillation auriculaire, modèle biophysique, potentiel de surface,
dépolarisation, électrocardiogramme, système de dérivations,
repolarisation, vectorcardiogramme.

List of acronyms

Acronyms

AA	Atrial activity
ACG	Atriacardiogram
AF (Afib)	Atrial fibrillation
AP	Action potential
APD	Action potential duration
AV node	Atrioventricular node
BEM	Boundary element method
BSP	Body surface potential
BSPM	Body surface potential mapping
ECG	Electrocardiogram
EDL	Equivalent double layer
MDL	Minimum description length
NAF project	New look on atrial fibrillation
OACG	Optimized atriacardiogram
RMS	Root mean square
SA node	Sinoatrial node
SD	Standard deviation
SVD	Singular value decomposition
VA	Ventricular activity
VCG	Vectorcardiogram
VF (Vfib)	Ventricular fibrillation
WCT	Wilson central terminal

List of figures

1.1	Heart and lungs, from an older version of Gray's anatomy (1918).	4
1.2	Schematic of blood flow inside the heart.	5
1.3	Action Potential propagation.	5
1.4	Action Potentials.	6
1.5	Surface potential observed by Augustus Waller (1889).	7
1.6	First ECG by Einthoven (1903).	8
1.7	Positions of electrodes used in a standard 12-lead ECG.	9
1.8	ECG graph.	10
1.9	VCG lead system.	11
1.10	PQRST complex.	13
2.1	RMS curves, derived from 64-lead data of one of the subjects, used for defining features and used in the various preprocessing steps.	20
2.2	Estimated densities of the location of the extreme potential values as observed in the 64-lead signals of 73 healthy subjects.	25
2.3	Directional representation of the dipole source orientations.	27
2.4	Example of the vector data during the PQ interval.	28
2.5	Body surface potential generated by a dipole inside the thorax.	29
3.1	Display of the biophysical model used in this study and two of the lead systems studied.	35
3.2	Example of the ECG of lead V1 during AF.	38
3.3	MDL functions computed from the body surface potentials of the reference thorax.	41
3.4	The proposed OACG lead system.	42
3.5	The distributions of m values derived from different lead systems, computed on the 11 simulations of AF, shown as mean \pm SD.	42

3.6	The mean values of the optimization criterion α_8 computed on all simulated AF for each of the 25 thoraxes.	43
4.1	The lead systems.	49
4.2	Cancellation of ventricular activity.	53
4.3	Dynamics of α_8	54
4.4	Singular value spectra.	55
4.5	Paired statistics of α_8	56
5.1	Dipole components during atrial fibrillation.	60
5.2	Examples of simulated AF as visible in the ECG.	62
5.3	The electrode montages of the lead systems.	68
5.4	The performance of the VCG lead systems.	71
5.5	The validation of the lead systems.	75

List of tables

2.1	Basic statistics of subjects.	18
2.2	Time features of the 73 subjects.	24
2.3	Extreme potentials of the 73 subjects.	26
2.4	Directional data.	27
3.1	Specifications of simulated AF.	36
3.2	Details of the statistics presented in figure 3.6.	44
4.1	Basic statistics of patients.	51
5.1	Frank transfer coefficients.	62
5.2	Optimized transfer coefficients for lead systems using 7 electrodes.	72
5.3	Optimized transfer coefficients for lead systems using 9 electrodes.	73
5.4	Statistical values of figure 5.4.	74
5.5	Statistical values of figure 5.5	75

Dissertation

Introduction

1

1.1 Καρδια

THE human heart, the most studied organ in biology, is a hollow mass of mainly striated muscle fibers. It is most essential to life, since its function is to pump blood through the blood vessels to the entire body by repeated, rhythmic contractions. It is situated slightly to the left of the middle of the thorax, underneath the breastbone (the sternum), at a position surrounded by the lungs (figure 1.1).³² It is the active center of the human cardiovascular system, circulating blood in the entire organism as a medium for transporting substances such as oxygen, nutrients, blood cells, enzymes, antibodies, as well as collecting the corresponding counterparts as wastes, toxins or external agents for disposal.

The heart consists of four chambers, namely the two upper atria and the two lower ventricles. The number of chambers followed the evolutionary pattern of the vertebrates, which prevents a blend of arterial and venous blood in the closed circulatory system. The high energy consumption of homeotherms, *i.e.* the avian and mammals, requested a higher efficiency of oxygen transport by clearly separating oxygenated and deoxygenated hemoglobin within the circuit. Indeed, the number of the chambers in the heart in terms of their specific functions as well as their structures and geometries are important in the expression of the pathology of this organ studied in this work. The atria serve as buffers for blood entering the heart from which it is transferred to the ventricles. The ventricles are the actual pumps that propel the blood into the circulatory system. The valves between the atria and ventricles maintain coordinated unidirectional blood flow from the atria to the ventricles. The venous blood returning from the peripheral vessels enters the right atrium, through which it passes to the right ventricle and is sent to the lungs through the pulmonary artery. The

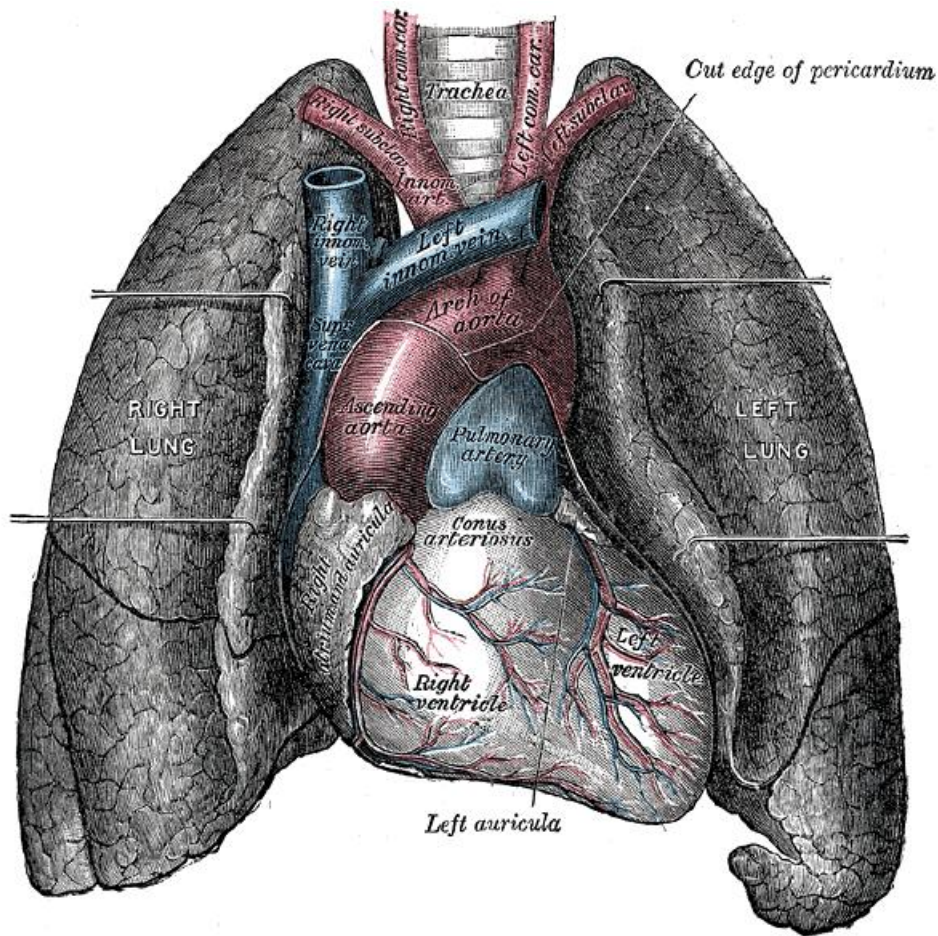


Figure 1.1 – Heart and lungs. Henry Gray, *Anatomy of the Human Body* (1918).³²

blood, rich with oxygen and free of carbon dioxide by diffusion at the pulmonary alveoli, is passed to the left atrium from which it enters the left ventricle. The latter forces the blood into the aorta from which it enters the entire circulatory system (figure 1.2). Every normal single beat of the heart involves a sequence of these well-organized events, which constitutes the cardiac cycle.

In a cardiac cycle, the aforementioned sequence consists of three major stages, namely the atrial systole, the ventricular systole and the complete cardiac diastole. The atrial systole is the phase which comprises the contraction of the atria and the corresponding influx of blood into the ventricles. Once the blood has fully left the atria, the atrioventricular valves close, preventing backflow into the atria. This closing of the valves (semilunar and atrioventricular) is the origin of the familiar beating sounds of the heart. The ventricular systole consists of the ventricular contraction and the efflux of blood into the circulatory system. Once the blood is expelled from the ventricles, the pulmonary and aortic semilunar valves close. The final complete cardiac diastole involves the relaxation of the atria and

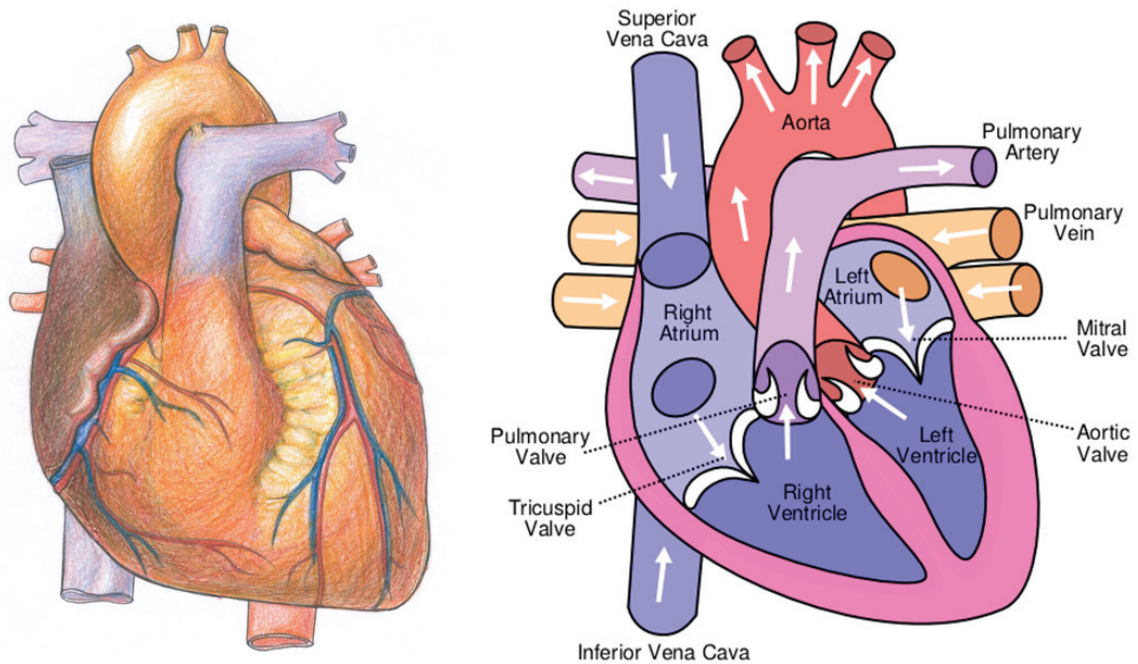


Figure 1.2 – Heart as the main pump of the cardiovascular system. Schematic diagram of blood flow in the human heart and nomenclature of principal anatomical features. Copyright, Kathy Mak and GNU Free Documentation License.

ventricles in preparation for the refilling phase of circulating blood. The whole cycle of blood circulation within the system is governed almost completely by the fluid mechanics regulated by the muscular contraction of the heart.

1.2 Bioelectricity of the heart

The cardiac muscle, a spontaneously contracting, self-exciting tissue, develops the driving force governing the fluid mechanics of the circulatory system by converting biochemical energy to kinetic energy. The contraction of the muscle is triggered by an electric stimulation, that is, the onset of an bioelectric signal called the action potential (AP).

The action potential is the general term for an all-or-none active electric impulse travel-

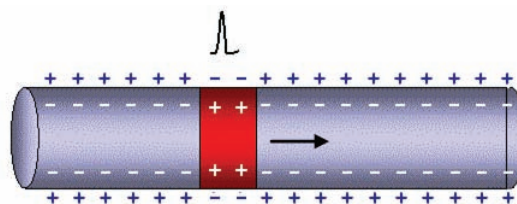


Figure 1.3 – Schematic of action potential propagation over a cell membrane.

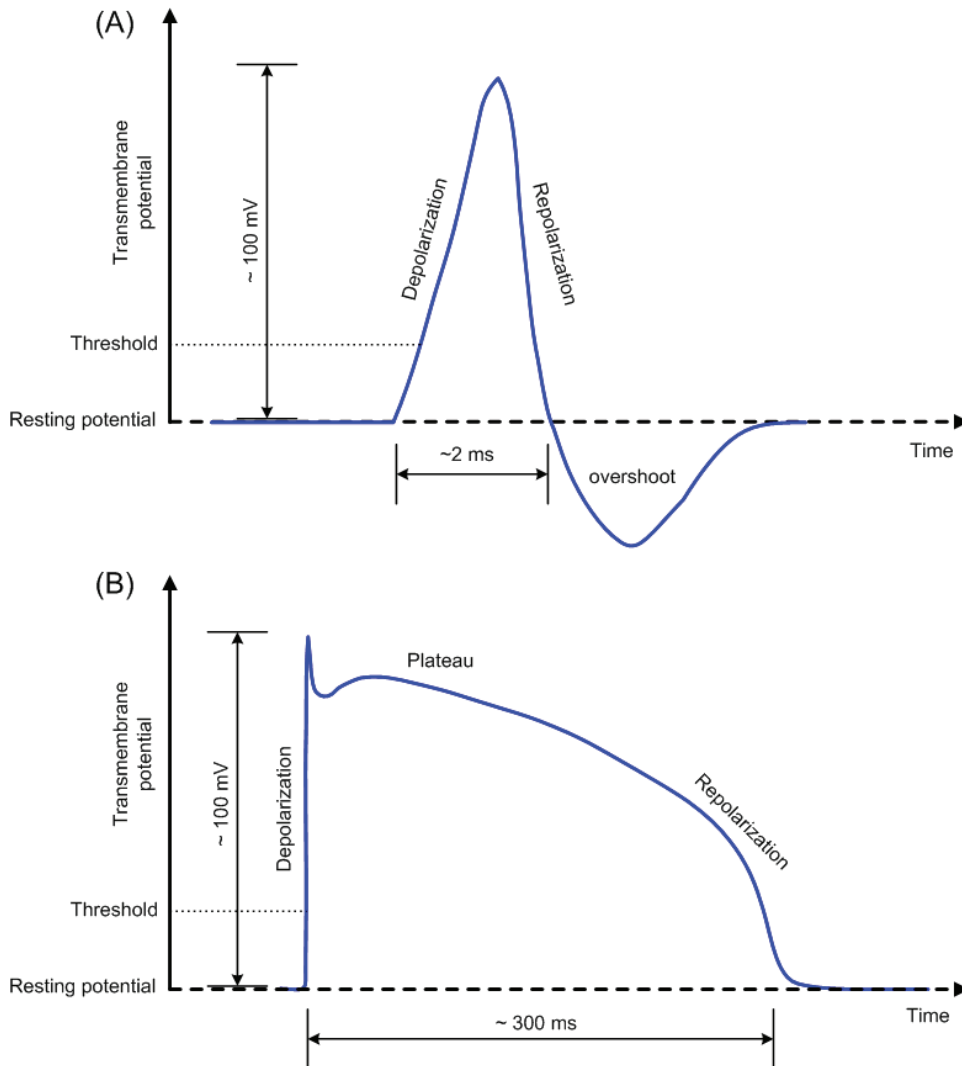


Figure 1.4 – Action potentials. **(A)** AP of neurocytes. **(B)** AP of cardiomyocytes

ing along the cell membrane (figure 1.3). In the neural system, it functions as a messenger between cells, while in muscles, it regulates the contraction of fibers. It is generated by exchanges of electrically charged ions across the cell membrane via ion channels,⁹⁰ creating a local potential bias above a triggering threshold between the two sides of the membrane. In its relaxed state, the inside of a cardiac myocyte is at a negative potential with respect to the outside, the resting potential. If the absolute value of this resting potential is reduced below a threshold level, a cascade of ion kinetics is induced, entailing chain reactions of potential dynamics propagation to the surrounding cell membrane (figure 1.4). The resting potential of a cell membrane is generated by an electrochemical equilibrium of charges (ions) on each of the sides of the membrane. The action potential reflects the local acute non-linear depolarization from this resting potential, followed by a repolarization phase of return to the resting potential. The dynamics of the inward and outward electric current

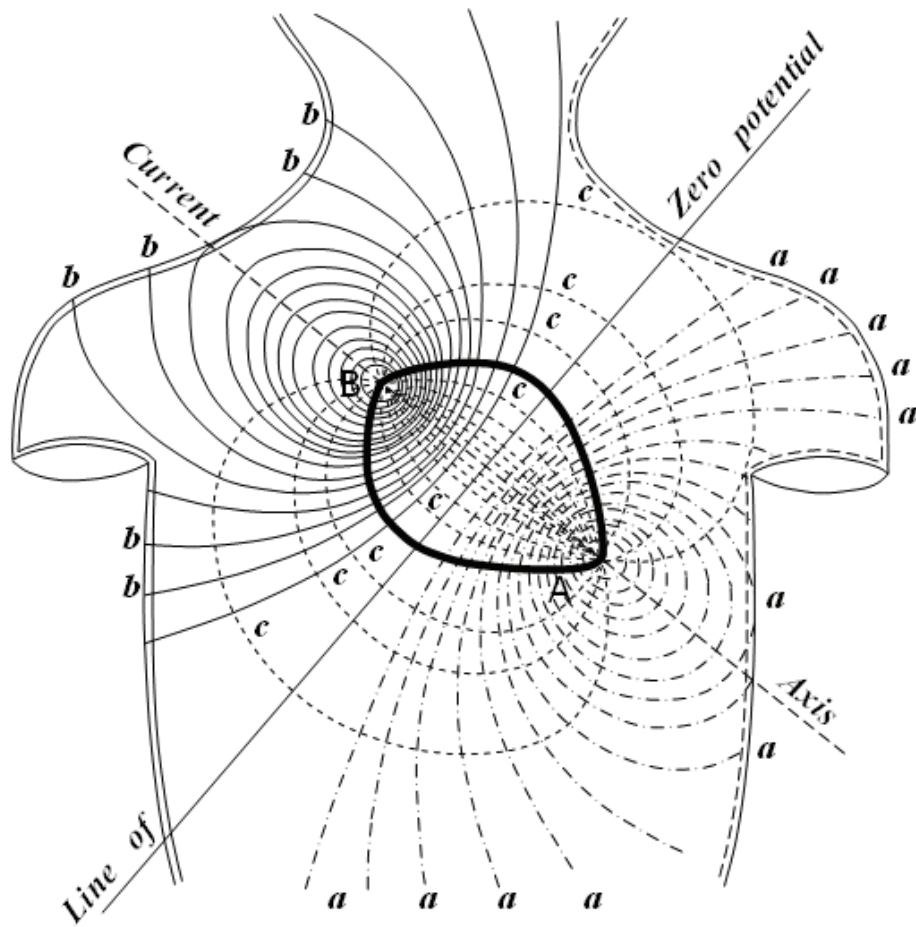


Figure 1.5 – *Potential inequalities over the body surface, by Augustus D. Waller (1889).*¹⁰⁷

is regulated by the opening and closing of the gates (ion channels) and is ruled by the electrochemical diffusion of the ions.⁷⁹ The transport of ions that regenerate the initial equilibrium is an active procedure carried out by the ion pumps. There is a brief time interval, called the refractory period, during which the membrane is not excitable between two successive action potentials.

In the case of cardiac muscle, the action potential is the signal that activates the contraction of the cardiomyocytes by propagating from cell to cell over the whole tissue. There are, nonetheless, preferential pathways along fast conducting bundles that effect the organization of the contraction of the chambers.

The rhythmic sequence of the cardiac cycle is initiated by the sinoatrial (SA) node and regulated by the atrioventricular (AV) node. The sinoatrial node, known as the cardiac pacemaker, is located in the upper front wall of the right atrium and is responsible for the initiation of action potential propagation that contracts the atria. Once the propagation reaches the atrioventricular node, situated in the lower right atrium, it is conducted through

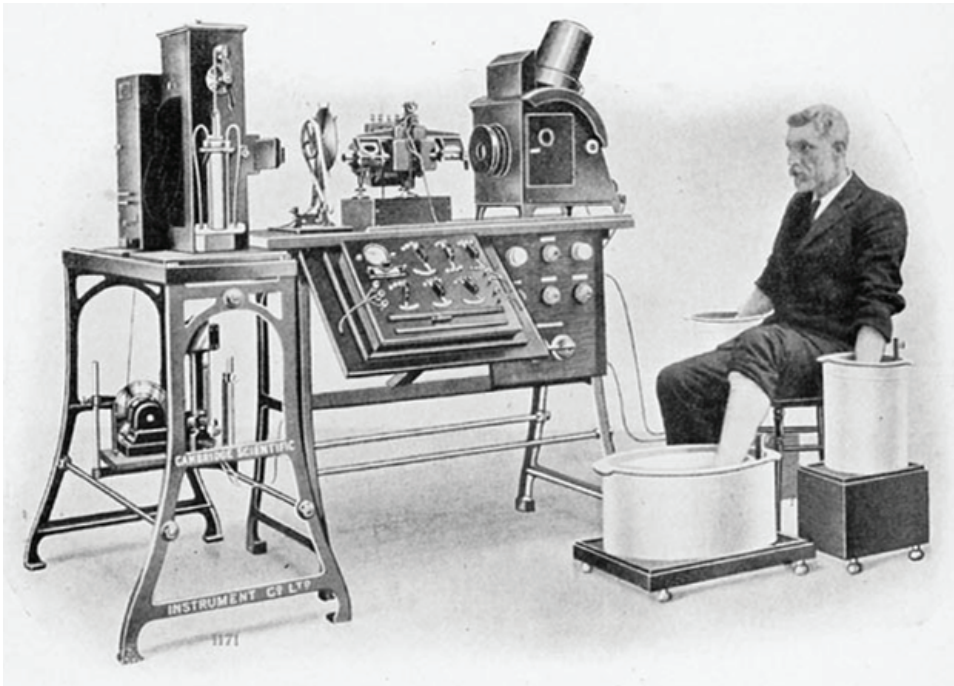


Figure 1.6 – *Picture of an early ECG recording performed by Willem Einthoven in 1903.*

the bundle of His, the left and right bundle branches, and to an extensive network of Purkinje fibers which trigger the contraction of the ventricles. The AV node regulates the timing of transmission of the excitation to the ventricles, creating a delay between the contractions of the two groups of chambers which enhances the filling of the ventricles prior to their contraction.

The physiological activity of the myocardium involves associated electromagnetic phenomena that are expressed as electric potential dynamics inside the entire body. As early as in the 19th century it became clear that the heart generated electricity. The first to systematically approach the heart from an electrical point of view was Augustus Waller, working in St Mary's Hospital in Paddington, London.¹⁰⁷ He used a mercury capillary electrometer to measure the electromotive changes on the body surface arising from the beat of the mammalian heart, and of the human heart in particular (figure 1.5).

1.3 Body surface potentials and Electrocardiogram

The electromagnetism linked to the electrophysiology of the heart is a direct expression of the cardiac mechanical function. Hence, the observation of the electric activity as body surface potentials (BSP) is an efficient and non-invasive manner of estimating the functional state of the heart. The time course of the resulting potential differences between any two points on the body surface is called Electrocardiogram (ECG). Following Waller,

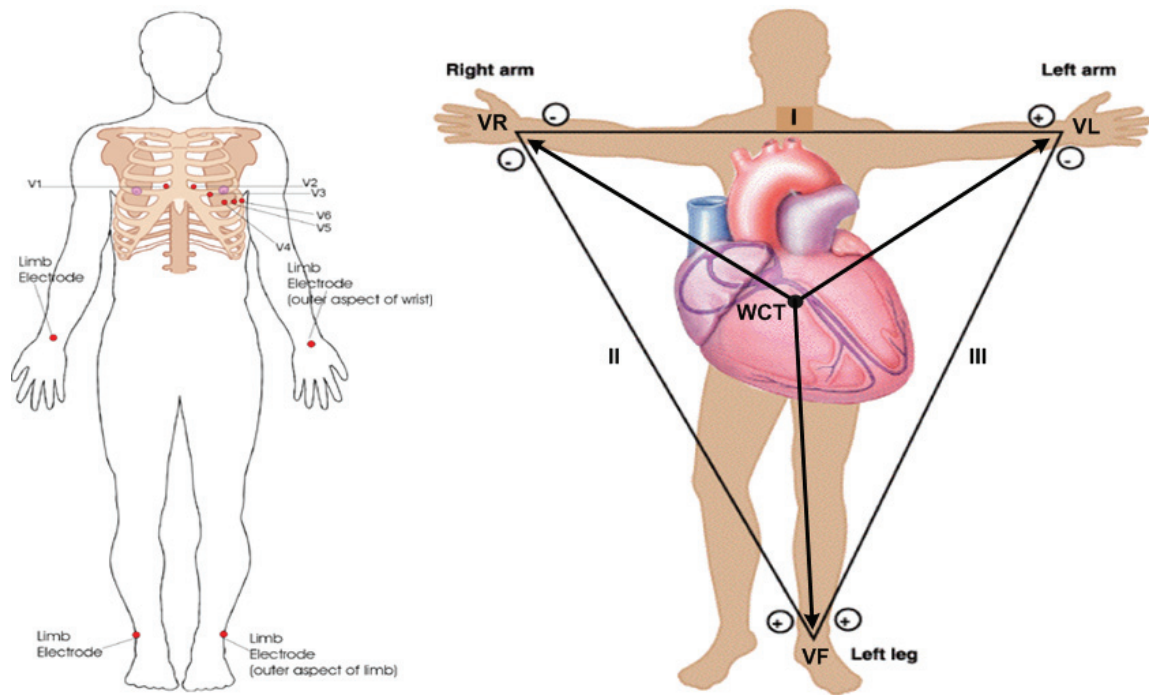


Figure 1.7 – Electrode positions of a standard 12-lead ECG and the derived leads. The three limb electrodes form an equilateral triangle in the frontal plane called the Einthoven triangle (right panel). The potential reference for all other leads is Wilson's Central Terminal (WCT) defined as the mean value of the potentials at electrodes VR, VL and VF, corresponding to the position of the center of gravity of Einthoven's triangle.

a major breakthrough in cardiac electrophysiology was reached when Willem Einthoven, working in Leiden, the Netherlands, used a string galvanometer in 1901 to record ECGs. By measuring the potential differences between the two hands and the left foot (figure 1.6), Einthoven assigned the letters P, Q, R, S and T to the various deflections, and described the electrocardiographic features of a number of cardiovascular disorders.²⁴ He received the *Nobel Prize in Physiology or Medicine* for his discovery in 1924.

Nowadays, the electrodes used in clinical practice to record the *standard 12-lead ECG* are placed on the two hands (VR and VL), the left foot (VF), and at six precordial positions (V1 to V6) as presented in figure 1.7. These *nine* electrodes located over the surface of the human body capture the electric activity of the heart from different angles reconstructing the spatial dynamics of the heart's electric activity. A display of the three limb leads in the form of a triangle on the frontal plane is referred to as Einthoven's triangle. The mean value of the instantaneous potentials, is used as the reference of the ECG signals, known as the Wilson Central Terminal (WCT) reference (figure 1.7).

The ECG is the prime tool in cardiology, and has its main function in screening and diagnosis of cardiovascular diseases in clinical practice. Because of the strong link (direct and indirect) between cardiac function and electric potential dynamics observable on the body surface, many cardiac diseases can be monitored through the expressed potential dif-

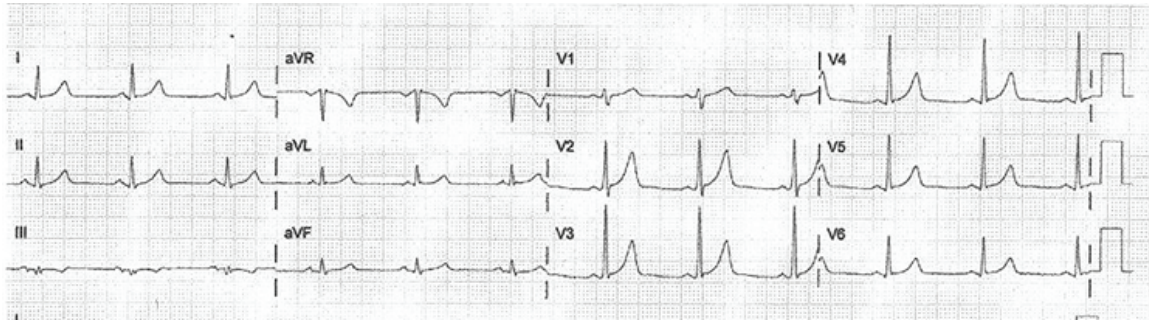


Figure 1.8 – An example of standard ECG recording during normal sinus rhythm. The twelve derivations are potential differences specifically defined between electrodes. I, II and III are potential differences between the limb electrodes as shown in figure 1.7. aVR, aVL and aVF are the “augmented” VR, VL and VF, respectively, signifying the 1.5-fold voltage between the corresponding electrode and the WCT reference. This is a historical custom in which, for instance, aVR was measured as $VR - \frac{1}{2}(VL + VF)$, which simply resulted as $aVR = \frac{3}{2}VR$. V1 to V6 are the potential differences between the corresponding precordial electrodes and the WCT reference.

ferences. According to the well-established definition of waveforms observable on each lead, the ECG has a wide use for indicating pathologies such as cardiac arrhythmias, ischaemia, or conduction abnormalities.

1.3.1 Vectorcardiogram

Cardiac activity expressed as electric potential differences over the body surface is a projection of the dynamics of the heart’s electric sources onto a surface (body). It is the result of the electric conduction of the generated currents through the inhomogeneous volume conductor that the human thorax is. The signals observed on the body surface contain spatial information concerning the electric activity of the heart. One of the methods used for describing the heart’s electric activity approximates the generator as one current dipole placed inside a homogeneous thorax. The resulting estimate is called the vectorcardiogram (VCG).

The VCG is a characterization of the total activity of the heart using three time-varying signals as the strengths of the xyz components of a current dipole in a homogeneous thorax. Each component is derived from a linear combination of potentials observed at dedicated electrode positions (*e.g.* figure 1.9), of which the best-known variant is that proposed by Frank in 1956.²⁶ The details and theory of VCG are explained in Chapter 5.

1.4 Cardiac arrhythmias and atrial fibrillation

Among abnormalities of the cardiovascular system, historically the most studied is cardiac arrhythmia*. Drug therapies were already carried out in the 18th century, while the inves-

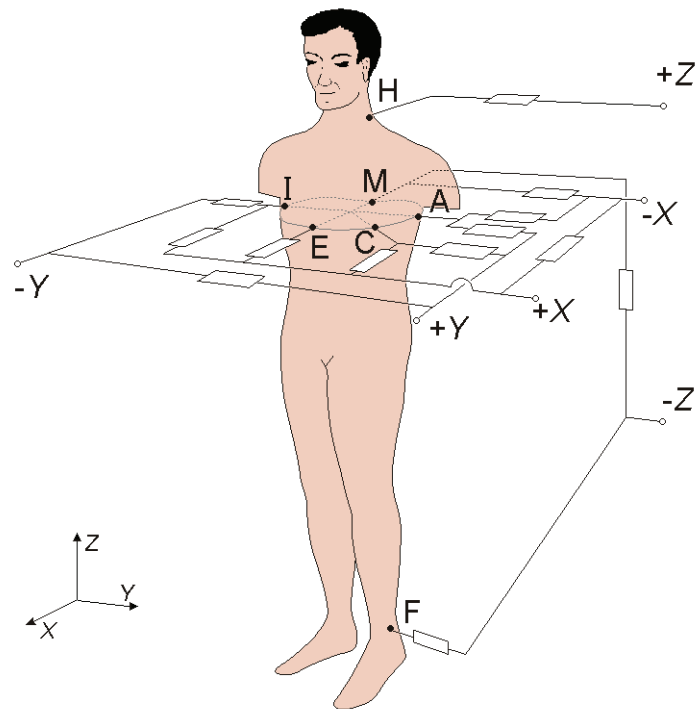


Figure 1.9 – An example of a VCG lead system. The components of the three-dimensional vector are derived as weighted sums of the potentials measured at dedicated electrode positions.⁶⁴

tigation of the electromotive aspect of cardiac arrhythmia, as summarized above, started in the 19th century.¹⁰⁶

There are mainly three types of cardiac arrhythmias: *bradycardia*, *tachycardia* and *fibrillation*. Bradycardia is a slow rhythm of less than 60 bpm, that may be life threatening. Tachycardia is considered present when the heart rate is above 100 bpm, and dangerous only when it exhibits irregular activity. The normal fast rate developed by exercise is called sinus tachycardia. The most serious variety of arrhythmia is fibrillation. This occurs when the heart muscle adopts a quivering motion instead of a normal, regular rhythm. Fibrillation can occur in the ventricles (ventricular fibrillation) or the atria (atrial fibrillation); Ventricular fibrillation (VF, Vfib) is always a medical emergency. If left untreated, ventricular fibrillation will lead to death within minutes. When a heart goes into Vfib, effective pumping of the blood stops. Vfib is considered a form of cardiac arrest, and an individual suffering from it will not survive unless cardiopulmonary resuscitation (CPR) or electric defibrillation is provided immediately. Atrial fibrillation is the quivering, chaotic motion in

*The heart was recognized as the center of life as early as in the epoch of the ancient Egyptians. It was believed to be stimulated by the Sun-God as his expression in man, as the source of wisdom and soul. Irregular or feeble pulse was a sign associated with diseases, and eventually death. The treatment of cardiac arrhythmias was therefore of foremost importance. As a parallel, the most recent trend is, following the vogue of life science, the quest for identifying signs in genetics as explanations for idiopathic cardiac dysfunctions such as sudden cardiac death.

the atria.^{72,73,83} Although it does not typically give rise to a direct medical emergency, it is often a cradle of more severe pathologies as will be presented in the next section. The center of interest of this study is atrial fibrillation.

1.5 This thesis

Historically, electrocardiology has been focusing its interest on the entire cardiac cycle, and specifically on ventricular activity. Ventricular disorders have been studied in depth because of their acute severity. Atrial arrhythmias, on the other hand, have not been the focus of intense research until recently. There are several reasons for this, but it is notably because atrial disorders are often not directly linked to death, and also because the expression of atrial activity observable on the standard 12-lead ECG leads is so small that it was long considered to be unsuitable for diagnostic procedures.

This thesis, part of the work of the Lausanne Heart group, aims at unveiling the expression of atrial activity on the body surface. It does so by studying the need for, and potential of finding ECG leads dedicated to atrial fibrillation. One of the important motivations that initiated this work is that the primary ECG, be it conceived by Einthoven or adapted later by other electrophysiologists, was founded on a heuristic and empirical basis, inspired by a quite primitive insight into the dynamics of the electric activity of the heart. Qualification of the cardiac activity by the signals recorded by the nine electrodes placed at their dedicated positions literally follows the practice of methodologies established almost a hundred years ago. Although the global usefulness of the standard ECG is proven by the history of electrocardiology, it is by no means certain that the actual lead system is optimal for the analysis of atrial fibrillation.

The message of this thesis is, indeed, that the conventional, standard 12-lead ECG system is not optimal for studying some types of cardiac arrhythmias, notably atrial fibrillation (AF), and that there are other methods of handling body surface potentials within the limitations of an easy-to-use non-invasive clinical practice and current equipment. This final section of the general introduction describes the focus of the studies, the background of the problems, the objectives, and provides an overview of the specific topics that are treated in the subsequent chapters.

Each chapter constituting the body of this thesis was the specific topic of a research task, corresponding to accepted or submitted journal papers. The references are shown at the end of my Curriculum Vitae.

1.5.1 Atrial fibrillation in the heart of modern society

Atrial fibrillation (AF, Afib) is the most common form of sustained cardiac arrhythmia in humans. In a recent study, it was established that 2% of the general population is affected, while the prevalence increases to over 10% in the elderly over 65 years.^{13,27} The prevalence

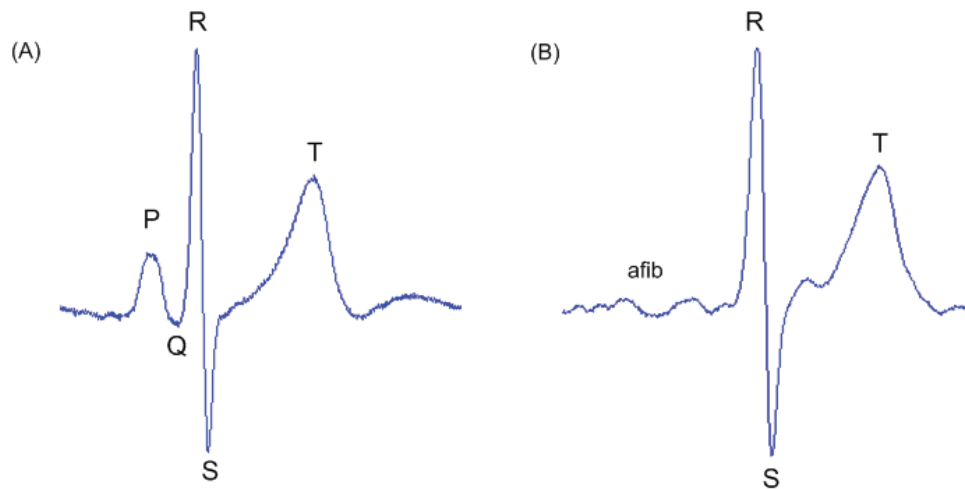


Figure 1.10 — An example of waveform of a cardiac cycle observed on the standard ECG. **(A)** During normal sinus rhythm. The labels by the waves are those defined by Einthoven. The P wave reflects the depolarization of the atria. The QRS complex represents the depolarization of the ventricles, and the T wave reflects their repolarization. **(B)** During AF. The P wave is replaced by a continuously ongoing series of AF wavelets.

continues to rise as the general life expectancy increases. Electrophysiologically, AF is an electric propagation disorder of atrial cardiomyocytes caused by functional or histological anomaly of the tissue, in which the regular periodic action potential propagation from the sinoatrial node is replaced by disorganized, meandering multiple wavelets over the whole surface of the atria. Moreover, repetitive or sustained chronic AF modifies the electrophysiological and even the structural property of the cardiac tissue in an irreversible pathological way. Development of thrombosis due to the stagnant blood in the atria can eventually induce a cerebral embolism. At the present time, noninvasive curative treatment is not possible.

The interest in AF has grown, related to the socioeconomic impact of this pathology. However, the information regarding the atrial electric activity is limited, which clearly hampers the diagnostic procedures. As can be seen in figure 1.10a, atrial activity accounts for only a small portion of the cardiac cycle observed as body surface potentials, namely the P wave. The magnitude of the electric activity in ventricles is much stronger (especially the left ventricle) compared to that of the atria. The small amount of information on normal atrial activity available is replaced during AF by a fibrillatory wave (f wave) having a very low amplitude (figure 1.10b).

The questions that arose and motivated the research were the following:

- **What can we see of atrial electric activity on the body surface?**
- **Can we learn more about atrial fibrillation from body surface potentials?**

- **How can we capture the information more effectively?**

Integrated research: biophysics and signal processing

In order to research which information is contained in the body surface potentials that express the electric dynamics of the atria, computer modeling and signal processing approaches were integrated in the work presented in this manuscript.⁵⁷

1.5.2 Atrial repolarization as observable during the PQ interval (*chapter 2*)

In this chapter, the focus is on the clinical body surface potentials during normal atrial electric activity. It has long been believed that the only content of atrial activity observable on the body surface was its depolarization phase in a normal cardiac rhythm (the P wave), and that everything else was totally hidden in the following sequence of ventricular activation. This was considered as “*common sense*” in cardiology, and even the definition of electrocardiography characterizes the signals in the period succeeding the P wave as “*electrically silent*”. This is believed even these days, although several observations in the past have indicated that potential dynamics was present in this segment on the body surface potentials.^{69,89}

The objective of this study was to assess the involvement of atrial repolarization in body surface potentials. To this end electrocardiograms of healthy subjects recorded using a 64-lead system were analyzed. The data analysis focused on the PQ intervals, while devoting special attention to the low-amplitude signals during the PQ segment: the segment from the end of the P wave till onset QRS. The data were analyzed by inspecting body surface potential maps and the *XYZ* signals of the vector cardiogram. Standard P wave features such as the amplitude or vector direction were found to have normal values.

The positions on the thorax exhibiting local potential extremes were studied. By defining specific time features respectively at the apex of the depolarization phase and in the middle of the PQ segment, the distributions of potential extremes as well as the dipole polarity and magnitude were documented.

1.5.3 Adaptation of the standard 12-lead ECG system dedicated to the analysis of atrial fibrillation (*chapter 3*)

The work presented in chapter 2 shows that during normal activity, the main features of body surface potentials of atrial activity appeared at locations far from those covered by the standard lead system. In the work presented in chapter 3, the interest was focused on the signals of atrial fibrillation. Based on previous observations, the goal was to search for a combination of a limited number of electrodes that maximizes, within the practical constraints, the capture of the dynamics of AF signals.

The objective of this study was to design a new lead system aimed at studying atrial

fibrillation, more oriented to the extraction of information, while being anchored to the existing standard 12-lead ECG system. It was prompted by our current interest in the search for a classification of different types of AF and their relationship with the underlying etiology of the disease.

The locations of 4 of the 6 precordial electrodes were optimized, while leaving the remaining 5 of the 9 electrodes of the standard 12-lead system in place. The analysis was based on episodes of 11 different variants of AF simulated by a biophysical model of the atria positioned inside an inhomogeneous thorax. The optimization criterion used was derived from the singular value decomposition of the data matrices. While maintaining VR, VL, VF, V1 and V4, the 4 new electrode positions increased the information content obtained from the body surface potentials during AF. In an independent evaluation, the same procedure was carried out by applying the new (OACG: optimized atricardiogram) leads to each of the other 25 inhomogeneous models of the thorax, and comparing the information content in each of the 11 AF episodes when using the electrodes of the new lead system as well as those of the standard leads.

1.5.4 Performance of a lead system dedicated to atrial fibrillation: application to clinical data (*chapter 4*)

A new lead system has been designed in a biophysical model-based investigation presented in chapter 3. The positions of the 9 electrodes of the standard 12-lead ECG system were optimized, within constraints of practicability, with respect to the information extraction from atrial activity during AF. The work presented in this chapter is the application of the OACG lead system to clinical signals in order to assess the actual performance of the underlying methodology. It is an ongoing study for which we so far lack a sufficient amount of clinical data recorded with the OACG lead system. According to the initiative of the NAF project, *New look at Atrial Fibrillation*, formulated by the Lausanne Heart Group, we started documenting clinical recordings of body surface potentials from patients with AF in 2003. A gross total of over 120 recordings of individual patients are to be found in the database so far. The original project was conceived using the standard ECG and its heuristic variant, the ACG lead system only.

The objective of the study presented is to evaluate the performance of a lead system dedicated to the analysis of atrial fibrillation in its application to clinical data. The difference between simulated AF and clinical recordings is the inevitable inclusion of the ventricular components in the signals. In order to obtain continuous sequences of atrial activity only, the ventricular activity is considered as undesirable perturbation and is removed.

AF signals were recorded from 30 patients at the nine electrode positions of the standard 12-lead ECG, as well as of those of two novel lead systems, ACG and OACG. After cancellation of the ventricular signals, an information measure was derived from the singular value decomposition of the atrial signals. The resulting values obtained from the three lead systems were compared.

1.5.5 Vectorcardiographic lead systems for the characterization of atrial fibrillation (*chapter 5*)

The electric (current) source of the atria as is explained in chapter 3 can be approximated in a mathematical context by an equivalent current dipole source inside a homogeneous volume conductor.⁷⁸ In a theoretical point source representation of distributed sources, the double-layer sources over a closed surface (atria) can be reformulated with a Taylor series expansion representing an infinite sum of current multipole sources. However, the nature of higher-order terms, *i.e.* the m -th order moments of the multipole expansion varying inversely with r^{m+1} , r the distance between the source and the observation point, justifies the practicability of describing the physical source as a single dipole inside the thorax responsible for the potential distribution observed over the body surface. That is to say, the point source of dimension zero is physically meaningless for it would indicate an infinitely charged point current source inside the human body. The characterization of the electric cardiac dynamics is represented by the time course of a current dipole source. The interpretation of the body surface potentials as those expressed by the equivalent dipole source is called the vectorcardiogram (VCG).

The objective of this study was to design a VCG lead system dedicated to the analysis of atrial fibrillation. The motivation for using the vectorcardiogram for the analysis of AF relates to the fact that the chaotic nature of the electrocardiographic signals during AF so far has prevented the selection of spatio-temporal signal features that might be used in the classification of different types of AF.

This study aimed at designing an electrode configuration requiring at most 9 electrodes, the number involved in the standard 12-lead ECG, and its associated matrix of transfer coefficients. The work includes a thorough treatment of the methodology for the model-based design of limited lead systems, and highlights basic properties of the involved, required transfer matrices that so far seem to have escaped attention.

Atrial repolarization as observable during the PQ interval

2

2.1 Introduction

EVALUATING the electric activity of the heart through assessment of body surface potentials is the most commonly used, noninvasive approach for the diagnosis of cardiac arrhythmias. The current clinical interest in the electrical activity of the atria, with its focus on atrial fibrillation (AF), has revealed the relatively scarce knowledge that is available concerning the information content of P wave morphology. In the context of attempting to fill in various gaps existing in the understanding of such wave forms, the present work investigated the involvement of atrial repolarization process during the PQ interval. This process is usually assumed to coincide exclusively with, and thus be masked by, the QRST complex. Since the amplitudes of the atrial signals observed on the thorax are of the order of $100 \mu\text{V}$ and considerably lower during the PQ segment, special attention was given to the preprocessing of the data, in particular to the identification of the baseline. For this reason, the various steps taken are described in some detail.

2.2 Materials

Electrocardiograms, simultaneously recorded by using a 64-lead system, were taken from 75 healthy volunteers (57 males, 18 females). The recruitment aimed at including a wide range of ages and constitutional variables.

The data comprises the recordings of 50 subjects (42 males, 8 females) (database: DB1⁹³) observed using the "Nijmegen" lead system,^{37,39} and 25 subjects (15 males, 10 females) (database: DB2⁴¹) observed using the "Amsterdam" lead system.^{39,87} The main

statistics on the age of the subjects are shown in table 2.1. The full specification of the constitutional variables of the subjects in DB2 were documented in a previously published paper.¹⁰³

Physical examination of the subjects, including the measurement of blood pressure, analysis of the standard 12-lead ECG, echocardiography and anamnesis, revealed no trace of any cardiac disorder. No hypertensives were included; left atrial dimensions were within normal limits.

The electrodes in both systems are distributed over the entire surface of the thorax, with a higher electrode density in the pre-cordial region.³⁹ Both lead systems include the positions of the nine electrodes of the standard 12-lead ECG, as well as the seven electrodes of the Frank VCG²⁶ as subsets.

For the subjects in DB1, the 64 signals were recorded simultaneously at a sampling rate of 500 samples per second (sps) with $2 \mu\text{V}$ resolution, using a hardware high-pass filter at 0.05 Hz. The signals of the 25 subjects in DB2 were recorded with bandpass filter settings of 0.16-100 Hz and sampled at 1000 sps, with $0.7 \mu\text{V}$ resolution.⁴¹ The recordings were made with the subjects at rest in the supine position; the mean heart rate of the subjects was 61.9 ± 8 (mean \pm SD) beats per minute; range: (50-82), median: 62.

	Age statistics (year)		Number of subjects mean \pm SD (min, median, max)
	Male	Female	All
DB1	42 39.8 ± 15 (19.5, 41.3, 69.5)	8 43.0 ± 9.3 (27.4, 46.1, 54.1)	50 140.3 ± 14 (19.5, 42.6, 69.5)
DB2	15 40.3 ± 14 (26.0, 34.2, 64.9)	10 33.8 ± 12 (23.8, 29.1, 62.2)	25 37.7 ± 13 (23.8, 33.4, 64.9)
All	57 39.9 ± 15 (19.5, 35.7, 69.5)	18 37.9 ± 11.6 (23.8, 36.1, 62.2)	75 39.4 ± 14 (19.5, 36.1, 69.5)

Table 2.1 – Basic statistics on the age of the subjects studied, specified by gender and data base.

2.3 Methods

2.3.1 Definition of terms

The analysis of the atrial signals presented in this chapter relates to the entire depolarization and repolarization process of the atria. Because of this, rather than referring to signal components in individual leads, features were used that characterize the entire process. Their timing was extracted from the root-mean-square curve $RMS(t)$ computed from all recorded lead signals, after application of the zero-mean reference. By denoting the potential of any individual lead l by $V_l(t)$, the function $RMS(t)$ is defined as:

$$RMS(t) = \sqrt{\frac{1}{L} \sum_{\ell=1}^L V_{\ell}^2(t)}, \quad (2.1)$$

with L the number of leads. This function is positive only; it provides an overall view of the depolarization and repolarization processes of the entire heart, in a manner that is largely independent of the lead system used. An example of an RMS curve, computed from the 64-lead data of one subject, is displayed in figure 2.1. As is shown by the dashed trace in figure 2.1(a), it clearly identifies the onsets and endpoints of the P waves and QRS complexes of the subsequent beats. After application of the baseline correction described below (solid line) the quality of these markers is clearly enhanced.

Figure 2.1(b), an exploded view of the PQ interval of the RMS curve, is used to illustrate the definitions of the various terms used. The PQ interval is taken to be the interval between the timings t_{oP} and t_{oQ} , which denote the onset of atrial depolarization and that of ventricular depolarization, respectively. This interval is frequently, but imprecisely, referred to as the PR interval.⁶³ The maximum of the RMS curve is denoted by P_{apex} , its timing by $t_{P_{apex}}$. The timing of the maximum curvature of the down slope of the RMS curve following P_{apex} is taken to signify the end of atrial depolarization. It is a time instant similar to that of the J point; the point marking the end of the QRS complex and the beginning of the following part. This time instant is denoted by t_{Ja} . These time markers thus define the duration of the P wave as the interval between t_{oP} and t_{Ja} . Finally, the interval from t_{Ja} to t_{oQ} is referred to as the PQ segment.

2.3.2 Processing the signals

The signals that had been sampled at 500 sps were up-sampled to 1000 sps by means of spline interpolation. This clearly facilitated their subsequent analysis. From the data set, for each subject, episodes of 10 s were selected showing a stable baseline in all of the lead signals. In about 1% of all of the recorded signals this required a correction due to poor electrode contact. This correction was performed by using the method described by Oostendorp *et al.*⁷⁶

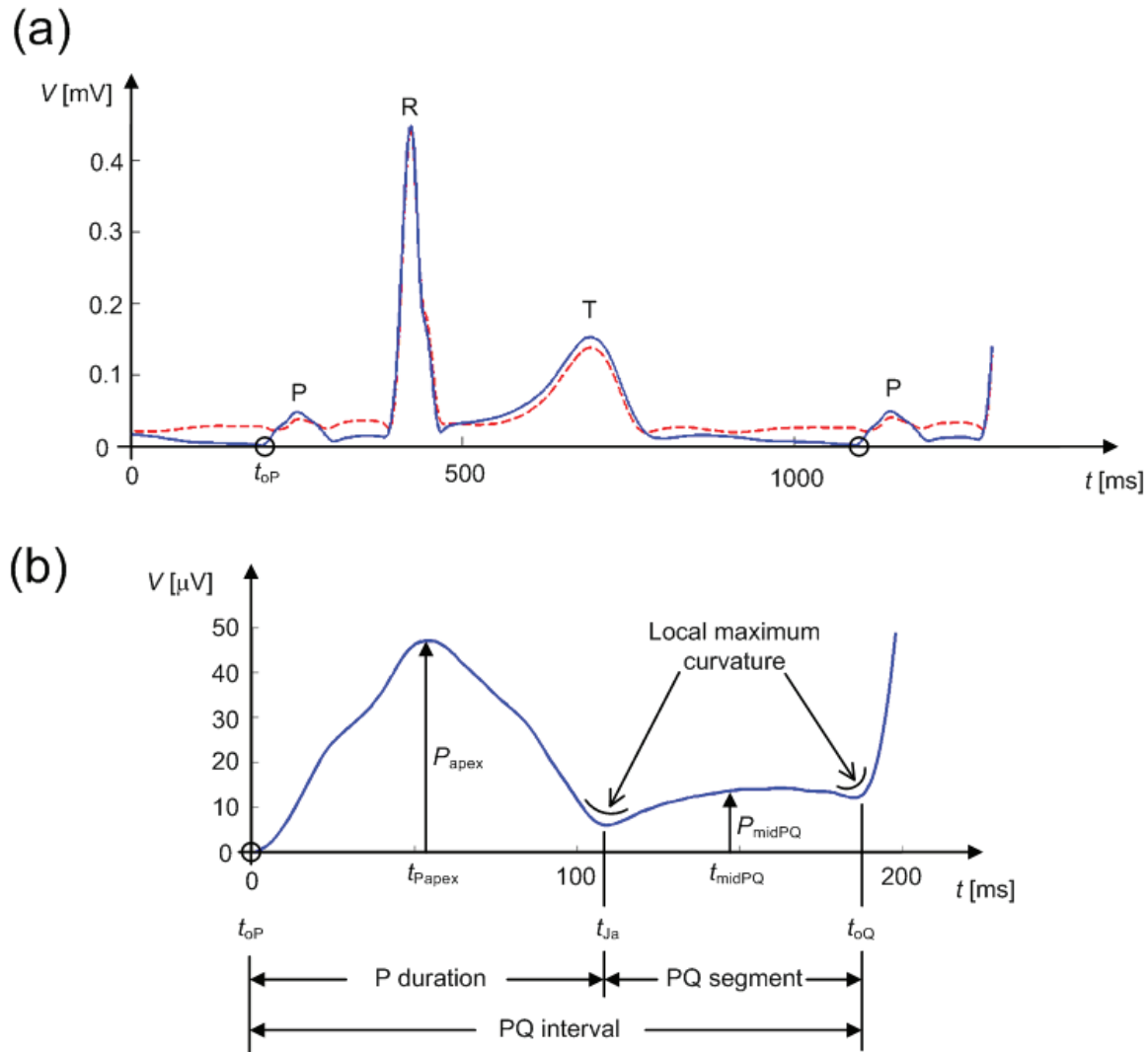


Figure 2.1 – RMS curves, derived from 64-lead data of one of the subjects, used for defining features and used in the various preprocessing steps. (a) Dashed line: RMS curve derived after a crude, initial baseline correction. Solid line: RMS curve after spline based baseline correction at the onsets (the circles) of the P waves in about 10 successive beats. (b) RMS curve of the PQ interval, with an indication of the definition of the terms used.

Baseline correction

The time instants of the onsets of the P wave, t_{oP} , in all subsequent beats, were identified automatically from the RMS curve. These time instants were taken as markers indicating the smallest involvement of the ventricular electrical activity in the data observed on the thorax. Note that “the end of the T wave”, estimated by whatever method, does not share this property. This poorly defined concept (“the end of the T wave”), supposedly characterizes the end of ventricular repolarization. The latter would mark the natural endpoint of any baseline correction. However, because such endpoints may be considerably

affected by the presence of U waves, we used the latest available point: the onset of the next P wave.

Based on the observed values at the time instants t_{oP} , a spline-based automatic baseline correction was performed, applied individually to all of the 64 signals of each subject.

Selection of PQ segments

In the signals obtained after baseline correction electric noise and muscle tremor artifacts were reduced by the application of a low-pass moving average filter taken over 20 samples, which has its first cut-off frequency at 50 Hz. The RMS curve of the filtered signals was used as an overall check of the previous processing steps. Next, this curve was used to identify the various timing makers described above. The onset of atrial depolarization was taken to be t_{oP} as identified during the baseline correction procedure. The end of the PQ interval, t_{oQ} , was taken to be the time instant of the maximal curvature of the RMS curve in the time interval preceding the fast upstroke of the QRS related part of the RMS curve. From the resulting PQ intervals, a single episode of the processed lead signals was used in the subsequent analysis. For each of the subjects this resulted in a data matrix Ψ of size $(64 \times NT)$, with NT the number of samples, typically being 170.

Selection of PQ segments

The XYZ components of the vectorcardiogram (VCG) \mathbf{V} were computed from the signals observed at the position of the seven Frank electrodes, by applying the coefficients of Frank's transfer matrix \mathbf{F} ,²⁶ hence $\mathbf{V} = \mathbf{F}\Psi$. Matrix \mathbf{V} has size $(3 \times NT)$; its three rows represent the signals $X(t)$, $Y(t)$, $Z(t)$ of the vectorcardiogram.

2.3.3 Extracted features

The following features were extracted from the PQ segments.

From the RMS curve:

The following features were selected from the RMS curve (See figure 2.1(b)).

PQ duration:	$PQdur = t_{oQ} - t_{oP}$
P wave duration:	$Pdur = t_{Ja} - t_{oP}$
Duration PQ segment:	$PQseg = t_{oQ} - t_{Ja}$
Timing of apex:	t_{Papex}
Amplitude of the apex:	$P_{apex} = RMS(t = t_{Papex})$
Timing mid-PQ:	$t_{midPQ} = (t_{Ja} + t_{oQ})/2$
Amplitude halfway the PQ segment:	$P_{midPQ} = RMS(t = t_{midPQ})$

The choice of mid-PQ identifies a point in time where the depolarization of the atria may be considered as complete, while also well clear of the onset of depolarization of the ventricles.

From the 64-lead signals:

For each subject, the leads were identified showing the maximal (positive) and the minimal (negative) potential values at $t = t_{\text{Papex}}$. The corresponding, observed extremes are denoted by P_{apex}^+ and P_{apex}^- , respectively. Similarly, the lead positions showing extreme potential values at $t = t_{\text{midPQ}}$ were identified, as well as the corresponding extremes P_{midPQ}^+ and P_{midPQ}^- .

From the VCG

The $X(t)$, $Y(t)$, $Z(t)$ components of the VCG were used to construct the signal $M(t)$ describing the time course of the spatial magnitude of the (P wave) vector: $M(t) = \sqrt{X^2(t) + Y^2(t) + Z^2(t)}$. The azimuth, elevation and magnitude values of the vector at $t = t_{\text{Papex}}$ as well as at $t = t_{\text{midPQ}}$ were added to the list of features. The azimuth and elevation were the conventional angles as used in vectorcardiography, φ and θ as shown in figure 2.3c, respectively.

2.3.4 Statistics

When possible, the observed features will be documented by their (mean \pm SD) values, as well as their range. However, some of the features have the nature of directional data.⁶⁶ These are the locations of the leads exhibiting extreme potential values and the vector directions at the time instants $t = t_{\text{Papex}}$ and $t = t_{\text{midPQ}}$.

Distribution of leads showing extreme potential values

The locations of leads showing extreme potential values were mapped on a standard geometry derived from the magnetic resonance imaging of the thorax of a male subject. The surface was discretized by a triangular mesh comprising 364 nodes and 724 triangles. The nodes included the coordinates of the 64 leads of both the Amsterdam and the Nijmegen lead system. The number of times any individual node was identified as locating, say, P_{apex}^+ , was counted, resulting in lead specific values N_l ($0 \leq N_l \leq 75$). Because of the two different lead systems involved and the relatively low number of subjects (75), the method for displaying the distribution of these values over the thorax was not immediately obvious. We based the method used here on Parzen estimation (see Chapt. VI of⁶⁸) now usually referred to as the Kernel Density Estimation (KDE).⁸⁰ It involves estimating a continuous

density function from observed (discrete) data. To this end, an assumed basic density function (kernel) is centered at each observed data point and the estimated density is found by adding up the contributions of all of the resulting kernel functions. For our application to a closed surface, the kernel function chosen was the Gaussian function:

$$f(d; \sigma) = \frac{1}{\sqrt{2\pi}\sigma} e^{-\frac{1}{2}(d/\sigma)^2}, \quad (2.2)$$

with d the distance between an observed data point and the position where the function needs to be evaluated, and σ a parameter setting the shape of the kernel, which influences the spatial smoothness of the final result. The distance variable used was taken over the surface between any lead position showing an extreme potential value and any of the other nodes specifying the thorax geometry. The distances were computed by means of the shortest path algorithm applied to the individual edge lengths of the triangles.¹⁰⁸ The integral of the resulting density function over the entire surface was forced to be one. The resulting density function was studied by plotting its isofunction lines. The latter form demarcation lines for areas encompassing a given percentile of the observations, with increasing number of observations being enclosed as their contained area increases. The shape parameter was increased until individual “islands” around individual lead positions were no longer found.

Directional statistics

By their nature, the orientations of vectors in 3D space constitute directional data. The statistical handling of such data has been discussed extensively in the literature.^{66,97} In the electrocardiographic literature, for the problem in hand, two statistics have been adopted from the general literature: the prevalent direction and the spatial precision.²² These are measures similar to the mean and standard deviation of single variates, respectively. By denoting the intersection of any vector \vec{V} with a unit sphere by its components (x_i, y_i, z_i) , the prevalent direction is that of the vector $\bar{x} + \bar{y} + \bar{z}$, with the bars denoting the mean of the variables. The spatial precision is $\sqrt{\bar{x}^2 + \bar{y}^2 + \bar{z}^2}$, a variable having a range of [0,1]; where 0 corresponds to a distribution randomly, uniformly scattered over a sphere, and 1 to the situation in which all samples are concentrated at the same coordinates. These statistics are used in the results section, where appropriate. However, as will be shown, the vectors around the prevalent direction are by no means distributed axially around this direction. Hence, the various statistical tests designed for this kind of problem cannot be applied. Instead, density functions will be shown, drawn on a unit sphere, the kernel function now being the von Mises distribution function⁶⁶

$$M(\theta; \kappa) = p_\kappa e^{\kappa \cos(\theta)}, \quad (2.3)$$

with θ the angle between the two vectors specifying the observed vector direction and any other point on the unit sphere, κ a shape parameter, and p_κ a normalizing parameter.

Durations and timings [ms]	mean \pm SD (min, median, max)
PQ interval	170 \pm 24 (122, 168, 285)
P duration	113 \pm 24 (80, 113, 147)
PQ segment	57 \pm 23 (10, 54, 176)
t_{Papex}	70 \pm 13 (45, 72, 118)
t_{midPQ}	146 \pm 16 (113, 148, 201)

Table 2.2 – Basic statistics of timings and durations of 73 healthy subjects, derived from their RMS curves. Definitions as indicated in figure 2.1b.

2.4 Results

When inspecting the raw ECG data, two cases in DB1 showed an insufficient signal to noise ratio in view of the low level P wave potentials. In DB2 one case was noted in which the data were recorded during a period of P wave inversion. These three cases were excluded from the subsequent statistical analyses; their exclusion did not produce any significantly different change in any of the statistics.

2.4.1 From the RMS curve

The PQ intervals and the P wave durations were found to have the same orders of magnitude as those previously presented in, *e.g.*,^{23,74}. However, in contrast to the results of those studies, no gender differences were observed in our data. An overview of the statistics of the features derived from the RMS curve is shown in table 2.2.

2.4.2 From the 64-lead signals:

The observed locations of extreme potential values are displayed in figure 2.2 by means of density maps drawn on the anterior thorax. The shape parameter κ of the Gaussian kernel used for the KDE was 8 cm. The black dots represent the locations of the nine electrodes of a standard 12-lead ECG. At $t = t_{\text{Papex}}$, the extreme positive potentials were observed in the region below the V2 lead position (figure 2.2b); the accompanying extreme negative values were observed in the upper right chest. At $t = t_{\text{midPQ}}$, approximately the same

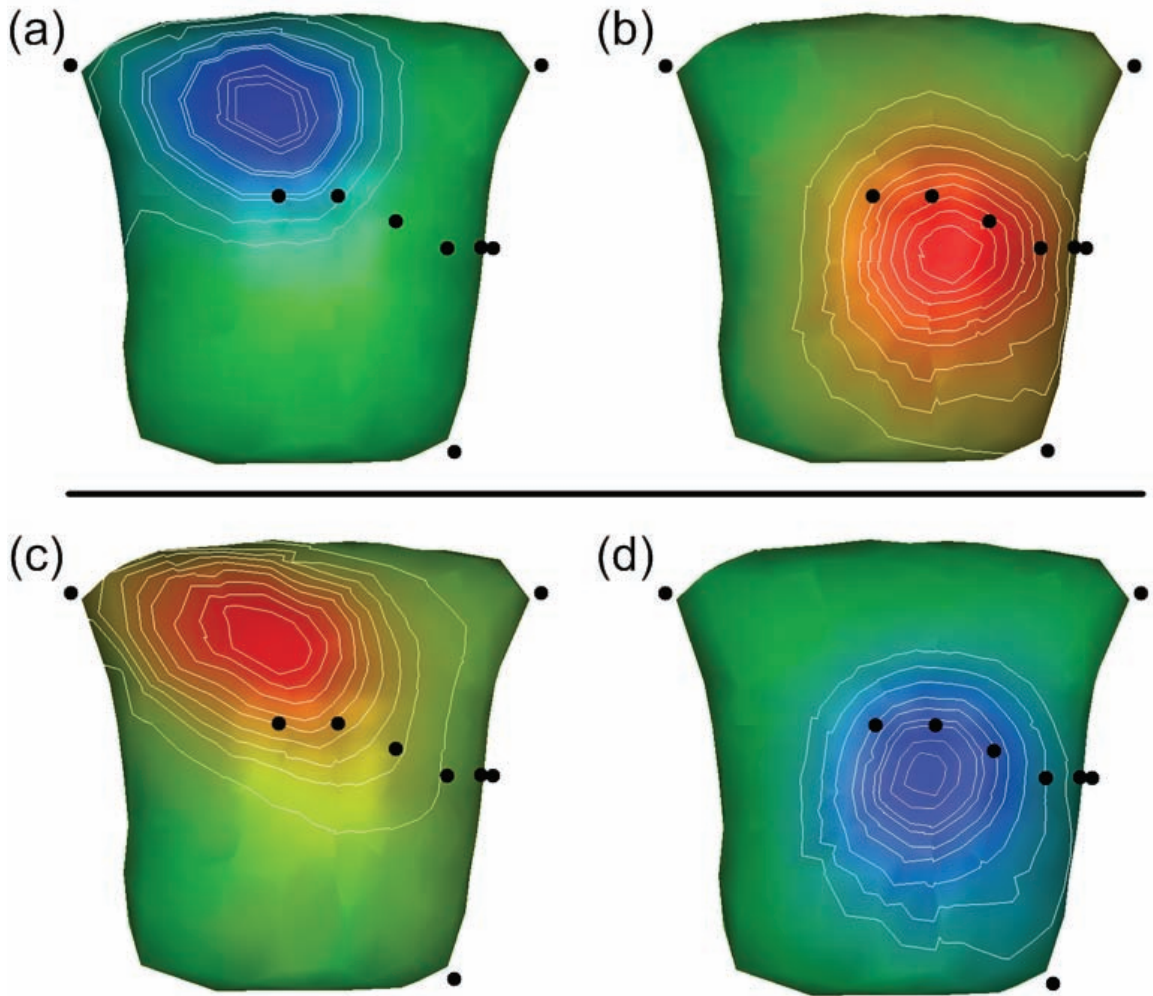


Figure 2.2 – Estimated densities of the location of the extreme potential values as observed in the 64-lead signals of 73 healthy subjects. The black dots indicate the locations of the nine electrodes of the standard 12-lead ECG. Successive contour lines are drawn at increments of 10% of the total number of observations. (a) Location of extreme negative values at $t = t_{\text{Papex}}$, (b) Location of extreme positive potentials at $t = t_{\text{Papex}}$. (c) Location of extreme positive potentials at $t = t_{\text{midPQ}}$, (d) Location of extreme negative potentials at $t = t_{\text{midPQ}}$

regions were found, now for extremes having a reversed polarity. These extreme potential values, observed at the respective time instants, are documented in table 2.3.

2.4.3 From the VCG

In figure 2.3 the directions of the observed dipole source vectors at $t = t_{\text{Papex}}$ and $t = t_{\text{midPQ}}$ are shown, plotted on a unit sphere by means of their estimated density. The shape parameter of the von Mises density function, a dimensionless factor, was set at 50. The corresponding vector magnitudes and directions are presented in table 2.4. The

Potentials [μV]	mean \pm SD (min, median, max)	
	t_{Papex}	t_{midPQ}
Extreme positive value	55 ± 17 (22, 53, 133)	36 ± 13 (8, 35, 70)
Extreme negative value	-93 ± 33 (-189, -93, -34)	-33 ± 13 (-76, -31, -16)
Max difference	148 ± 45 (70, 147, 288)	69 ± 23 (25, 68, 138)

Table 2.3 – Basic statistics of the extreme potentials of 73 healthy subjects as observed on the 64 leads at times $t = t_{\text{Papex}}$, the timing of the apex of the RMS curve, and $t = t_{\text{midPQ}}$, the timing of the middle of the PQ segment. (see figure 2.1b)

axes labeling used was set according to the standard VCG display convention shown in figure 2.3c.^{22?} Figure 2.3a shows a main dipole vector at $t = t_{\text{Papex}}$ that is directed from the back of the right shoulder to the left leg. As shown in figure 2.3b, at $t = t_{\text{midPQ}}$ the main vector showed an approximately reverse direction. The spatial orientation of *Papex* presented in the literature²³ for males is indicated by a black cross in figure 2.3a, which lies within the 20% density contour. An example of the vector data of one subject during the PQ interval (187 ms) is presented in figure 2.4. Like shown in this figure, the vector loops during the P wave revealed maximal values of the spatial magnitude $M(t)$ at time instants that were close to t_{Papex} . In other subjects, the clear majority of the loops in the horizontal plane (88%) had counter-clockwise orientations, like the one in figure 2.4a. A similar result was found in the left sagittal plane: 92% of the loops having a counter-clockwise orientation such as the one in figure 2.4d. By contrast, in the frontal plane the orientation of the loop was less uniform: 28% revealed a clockwise orientation like the one in figure 2.4c. Because of the onset of ventricular depolarization, the vector loops related to the atrial T waves could not be followed to their conclusion. However, those parts visible, as shown in figure 2.4, generally showed directions that were opposite to those of the mean vectors during the P wave. The magnitudes following t_{midPQ} tended towards lower values.

2.5 Discussion

The characteristics of the observed P waves are in agreement with those previously described in the literature.¹⁹ To these characteristics, owing to some dedicated preprocessing steps of the signals like an appropriate baseline correction, the description of a substantial involvement of atrial repolarization during the PQ segment could be added. The analysis

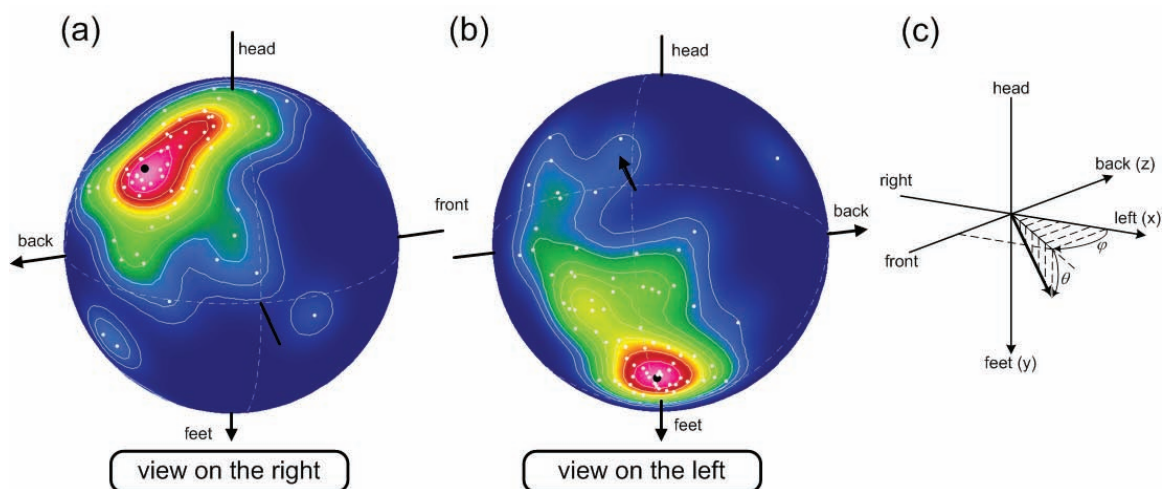


Figure 2.3 – Directional representation of the dipole source orientations. (a) Dipole vector directions during atrial depolarization at $t = t_{\text{Papex}}$. The white dots indicate the individual vector directions of 73 healthy subjects. The color map is the estimated continuous density. Increments of 10% between successive density lines. The large black dot indicates the position of the mode of the density and the cross is the direction presented in the literature.²² (b) As in figure 2.3a, but now during repolarization at $t = t_{\text{midPQ}}$. (c) Definition of the vector axes and the vector angles: azimuth and elevation .

Vector data		
	t_{Papex}	t_{midPQ}
Vector magnitude [μV]	96 ± 32 (40, 92, 209)	30 ± 14 (5, 30, 86)
Prevalent direction [deg]	$\varphi = 9; \theta = 50$	$\varphi = -132; \theta = -45$
Spatial precision	0.84	0.75
Angle of corresponding dispersion cone [deg]	33	41
Angle between the prevalent directions at the two time instants [deg]		135
Spatial precision		0.9
Angle of corresponding dispersion cone [deg]		26

Table 2.4 – Basic statistics of the vector data at times $t = t_{\text{Papex}}$, the timing of the apex of the RMS curve and $t = t_{\text{midPQ}}$, the timing of the middle of the PQ segment. The azimuth φ and elevation θ angles of the vectors are as defined in figure 2.3.

of low level ECG potentials demands great care, as was realized right from the start in the earlier studies on P waves, the PQ segment, the STT segment and the U wave.⁸⁹ The use of the RMS curve, in particular when applied to signals referred to zero-mean and supported

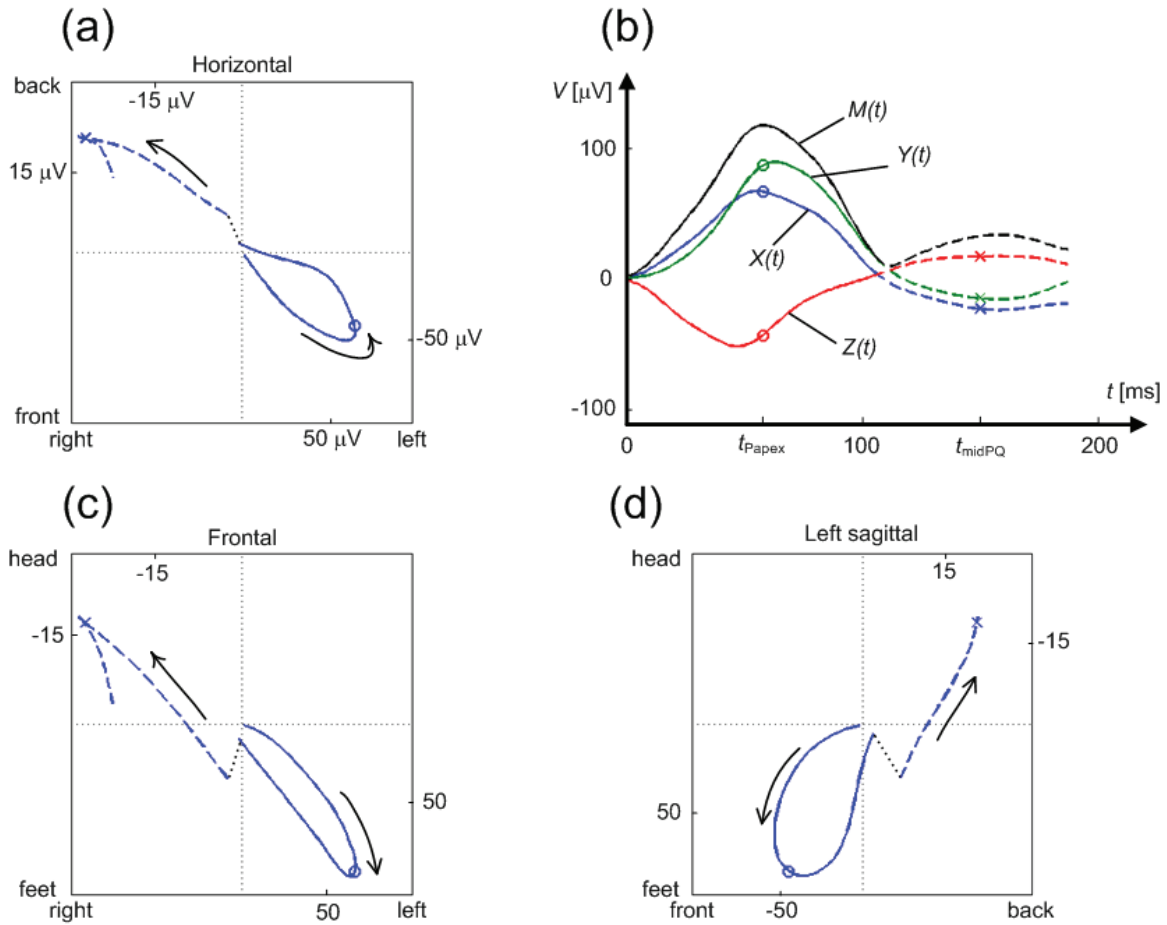


Figure 2.4 – Example of the vector data during the PQ interval (duration 187 ms) in one of the subjects. The trajectory of the vector displayed in three planes: (a) horizontal, (c) frontal, and (d) left sagittal. The solid line is used during the duration of the P wave, whereas the dashed line represents the PQ segment, drawn to a different amplitude scale. The corresponding amplitude scales are expressed in μV . The circles indicate the instant of $t = t_{\text{Papex}}$, the crosses indicate $t = t_{\text{midPQ}}$. (b) The vector magnitude $M(t)$ and its components $X(t)$, $Y(t)$, and $Z(t)$. The PQ segment is shown in dashed lines, drawn to the same scale.

by a spline-based baseline correction, provided a clear view of the overall timing of the depolarization and repolarization processes of the heart as observable from the ECG. This was used previously for the analysis of the low-level potentials by Mervis.⁶⁹ By comparing their defining equations it can be seen that, apart from a scaling factor, the $RMS(t)$ curve may be viewed as a generalization of the spatial magnitude function $M(t)$ used in vectorcardiography.

2.5.1 Locations of extreme potentials

During the P wave, the locations of the extreme positive and negative surface potentials were observed in regions not included in the standard 12-lead system (figure 2.2a, b).^{19,69}

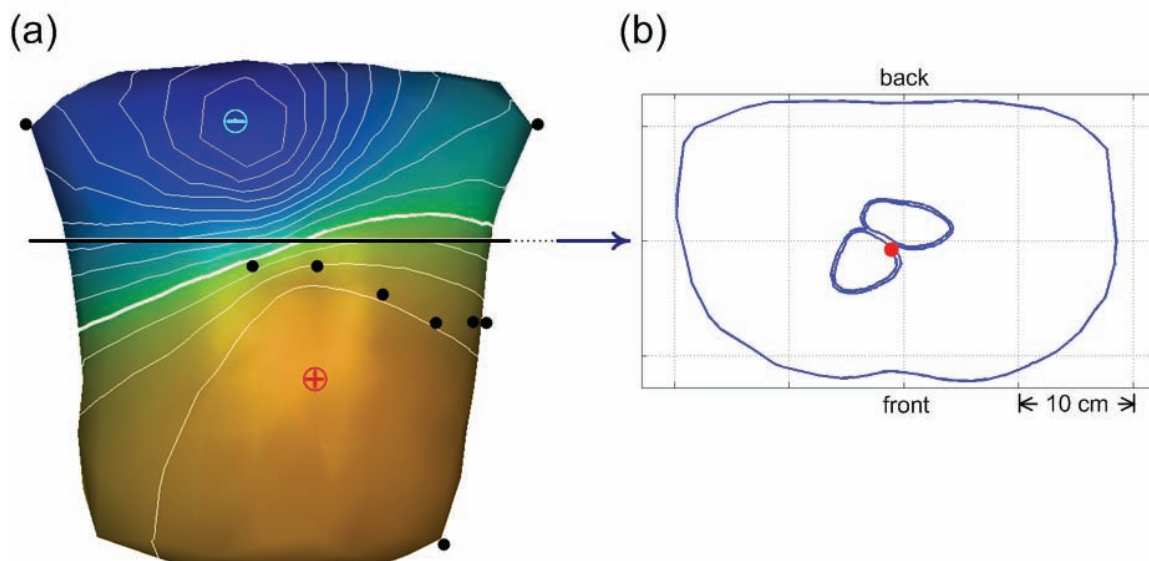


Figure 2.5 – (a) Body surface map of the potential generated by a dipole with magnitude proportional to the mean vector at $t = t_{\text{Papex}}$ (top row of table 2.4) and having the corresponding prevalent direction (second row of table 2.4) located inside a homogeneous, thorax shaped volume conductor. (b) Location of the dipole (heavy dot) indicated in a cross-section of the thorax. The heavy dots indicate the locations of the electrodes of the standard 12-lead ECG. The level of the cross-section is at the center of gravity of the myocardial mass of the atria, whose outline is indicated. The level is indicated by the heavy black line in figure (a). Isopotential lines in figure (a) drawn at $10 \mu\text{V}$ intervals, with the heavy line denoting zero with respect to the zero mean thorax potential reference.

This suggests that better lead positions may be found for monitoring and analyzing atrial signals. This idea is currently investigated in our group. Preliminary results of the analysis of AF signals have corroborated this hypothesis.⁴⁷ Approximately the same locations were identified for the extremes at $t = t_{\text{midPQ}}$. The locations are similar to those previously reported in the literature.

As an aside we note that these locations also correspond to the efficacious positions for the application of defibrillation paddles.^{3,35} This should come as no surprise in view of Helmholtz's theorem of reciprocity (see, *e.g.*,⁷⁷): when the electric source and the field point coordinates are interchanged, the resulting potential remains the same. In other words, in order to transfer electric energy to the heart with the highest efficiency, one must apply the power source at the locations where the heart's electric activity is expressed most strongly. ...*Similia similibus curentur**.

The orientation of the line connecting the regions of extreme potential values, *e.g.* those connecting the minima shown in figure 2.2a to the maxima shown in figure 2.2b,

*In 1899, the principle of similars was diluted by changing the indicative to a subjunctive. *Similia similibus curantur* became *curentur*.⁸¹ The weakening of the principle, in the English translation, is even clearer: 'like is cured by like' becomes 'let like be cured by like' whereby it is diminished from a supposed 'law of nature' to a 'method of treating disease'.

may seem to be at odds with the corresponding vector directions, *e.g.* the one shown in figure 2.3a. This apparent discrepancy is explained by the fact that the center of gravity of the atrial myocardial tissue is located at a slightly anterior position inside the thorax. This is illustrated in figure 2.5b. Figure 2.5 represents the body surface potentials generated by a current dipole representing the dominant vector at $t = t_{\text{Papex}}$ (top row of table 2.4) having the corresponding prevalent direction (second row of table 2.4) located inside a homogeneous volume conductor. The thorax geometry (the same as in figure 2.2) is that of one of the subjects, derived from magnetic resonance imaging of the subject (in DB2).⁴¹ The potential distribution was computed by using our dedicated Boundary Element Method software.⁷⁵ Note that locations of the extremes are similar to those shown in figure 2.2a and 2.2b and that the ratio of the absolute values of the extreme potentials shown in figure 2.5 is similar to what can be derived from the left column of table 2.3.

2.5.2 Involvement of atrial repolarization

Our observations during the PQ segment confirm that, although the temporal behavior of the individual signals is rather flat, a clear spatial, almost stationary distribution is present, and hence the PQ segment is not electrically silent.^{19,69} Currently, this fact is rarely acknowledged. During the Computers in Cardiology 2005 meeting in Lyon, the only presentations in which this fact was discussed came from our group (www.lausanneheart.ch). In other presentations, invariably, PQ segments coinciding with the baseline were shown, probably, but incorrectly, caused by starting the application of the baseline correction at the onset of ventricular depolarization. The almost reverse direction of the vector at $t = t_{\text{midPQ}}$ with respect to that at $t = t_{\text{Papex}}$ (figure 2.3) suggests discordant atrial T waves, as do the observed locations of the extreme potentials. This in turn suggests a small dispersion of the action potential durations of atrial myocytes.¹⁰² Usually, the PQ interval is not long enough to reach the end of atrial repolarization. However, the observations at $t = t_{\text{midPQ}}$, with subsequent diminishing vector magnitudes, indicated that the major expression of atrial repolarization may well be on its return at the normal timing of the onset of QRS. The results of a recent, model based analysis of atrial repolarization suggest that action potential durations of atrial myocytes are much shorter than those resulting from the commonly used Courtemanche model.¹⁶ In fact they are likely to be more in agreement with those of the working atrial myocardium.²⁹ A consequence of this would be that the ECG signals throughout the PQ interval are affected by repolarization processes.⁹⁸

2.6 Limitations

This study was prompted during the setting up of a model aimed at supporting the analysis of ECG signals during AF. The data for the full validation of such a model is not available, and as a first step the model was tested in an application to the normal P wave. It is here that the interest in the PQ segment arose. The signals during the PQ segment of the healthy subject studied showed clear,⁹⁸ non-isoelectric potentials, and we were interested

to see whether this might be due to a recording artifact. The results from the analysis of the combined data available from two previous studies, as well as results from the literature are discussed. The focus here was on the quantification of potential magnitude during the PQ segment of healthy subjects for which some reference data were available from the literature on body surface potential maps and VCGs. No effects of a multitude of various other possible factors or pathology were studied. The derived model is currently used for the analysis of the simultaneous presence and superposition of atrial depolarization and atrial repolarization, or atrial repolarization and ventricular depolarization, both during normal activation and during AF. In addition, it is used to establish which chamber is contributing to which portions of atrial repolarization on the body surface. This can only be accomplished by relating the surface events to what is going on electrophysiologically in the heart at the same time. The model includes sophisticated elements for modeling the myocardial sources, linked to electrophysiology as well as of the biophysics of linking sources to body surface potentials. The results of the application of this model, extending those already shown in⁹⁸, will be presented at a later stage.

2.7 Conclusion

This study confirms earlier reports that the PQ is not isoelectric. The time course of the potential distribution is very similar to that at the apex of the P wave, but for a reversed polarity and about 3-fold lower magnitude. The local potential extremes during this segment were found at positions not sampled by the standard leads, which implies that the positions of the standard leads are sub-optimal for studying the electric activity of the atria. The results demonstrate a significant involvement of atrial repolarization during the PQ interval, and essentially discordant “atrial T waves”, suggesting a small dispersion of atrial action potential durations. This study stresses the need for an appropriate signal processing of the (low-level) atrial ECG potentials and introduces some new methods for the directional statistics of the directions involved in the analysis of vectorcardiograms.

Adaptation of the standard 12-lead ECG system dedicated to the analysis of atrial fibrillation

3

3.1 Introduction

B EING the most commonly used tool for the non-invasive diagnosis of cardiac diseases, the standard 12-lead ECG measures the body surface potentials (BSP) as an expression of the electric state of the heart. Historically, the interest of electrocardiology has been focused on the electric activity of the ventricles: the nine electrodes of the 12-lead ECG were positioned on the thorax in order to follow the global depolarization and repolarization of the ventricles.¹ It is therefore likely that the information content available from these electrodes may not be optimal for studying atrial activity and, in particular, not if the interest is focused on the diagnosis of atrial fibrillation (AF).

A clearer view of atrial activity may be gleaned from the method of body surface potential mapping (BSPM). This was in fact performed right after the early introduction of this method.^{19,89} These studies have not led to any adaptation of the 12-lead system that is used clinically. Moreover, this method so far has not been applied to the analysis of AF. The more recent study of SippensGroenewegen *et al.*⁸⁶ reported on the analysis of BSPMs for the localization of the atrial foci responsible for atrial tachycardia, but the general problem of extracting information from the ECG for the classification of different types of AF was not addressed.

The current interest in morbidity and mortality related to AF has prompted the work presented in this chapter, aimed at designing a lead system dedicated to the extraction of information about the atrial electric activity during AF. In view of its ultimate clinical application and the highly limited availability of BSPM equipment in the clinic, the design

was restricted to the incorporation of just nine electrodes, the number of electrodes involved in the recording of the standard 12-lead ECG. In this way, standard, available ECG recording equipment could be used.

Another design constraint formulated in advance was that the electrode positions of the adapted lead system should be anchored as much as possible to those of the standard leads. This would reduce the complexity of lead placement in the clinic and reduce the possibility of lead misplacement, a problem even encountered frequently in the 'standard' positioning of the nine electrodes.³⁸ In an early, heuristic implementation of this constraint, the extremity electrodes VR, VL and VF were left in place, as were the electrodes V1 and V2.⁴⁷ Following the recording of an ECG at the 'normal' 12-lead electrode locations, the electrodes sensing V3-V6 were, sequentially, repositioned in a counterclockwise fashion, around those of V1 and V2 (figure 3.1). The positions chosen were inspired by their close proximity to the atria. By including the extremity electrodes, the commonly used Wilson Central Terminal (WCT) as the potential reference for the observed signals could be retained. This lead system dedicated to the recording of atrial signals, denoted in this paper as the ACG (atriocardiogram) lead system, is currently being tested in the clinic. At the present time up to 120 recordings on AF patients have been documented. For each of these, both the 12-lead ECG and the ACG-lead signals have been stored. No difficulties were encountered in the clinical implementation of this procedure.

A preliminary analysis of the clinical data comparing the AF signals derived from both lead systems suggested that, indeed, the adapted lead positions would provide a clearer view on AF. This prompted us to investigate the optimal lead positions for replacing 4 of the 6 precordial electrodes. The method for finding this optimum and the results obtained are discussed in this chapter. This search demands the availability of body surface potentials during AF over the entire thorax. Since no such data are available, we used as an alternative the AF signals generated by a previously developed biophysical model. The model includes the descriptions of the active electric sources during AF, as well as their expression on the thorax. It has recently been shown to generate AF signals that are in full qualitative agreement with those observed clinically.⁵¹ An attractive feature of using simulated data is that it permits the analysis of AF signals that are completely free of any ventricular involvement.

After describing the materials and methods employed, the results will be shown of a comparison between the standard 12-lead system, the ACG-lead system and the lead positions found to be optimal. The latter will be referred to as the OACG-lead system.

3.2 Materials and methods

3.2.1 Simulated atrial fibrillation

Body surface potentials of AF were simulated using a biophysical model of the human atria and thorax. The computation requires the specification of the atrial electric sources as

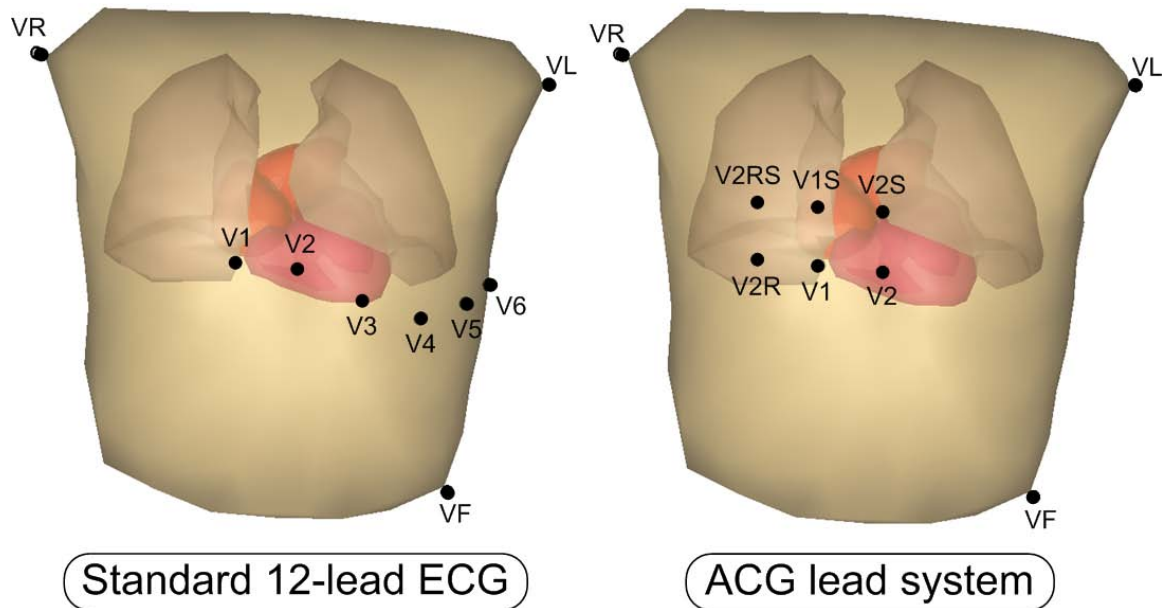


Figure 3.1 – Display of the biophysical model used in this study and two of the lead systems studied. The geometries shown are those of the thorax, the lungs, the atria, the ventricles and the blood-filled cardiac cavities. The black dots indicate the positions of the electrodes. (a) The standard 12-lead ECG. (b) The ACG (atriocardiogram) lead system.

well as that of the volume conductor that governs the transfer from source elements to the potentials at the observation points. The geometry of these models was derived from an MRI dataset taken from a healthy subject and discretized as triangulated surfaces.¹⁰⁴

A thick-walled 3D model of atria was developed, which consists of 800,000 units encapsulated in a triangular mesh (1297 nodes) representing both the epicardial and endocardial surface.⁵¹ The formulation of the membrane kinetics of the units was based on the Courtemanche et al. model of human atrial myocyte.¹⁶ The propagation of the electrical impulse within the atrial myocardium was simulated using a reaction-diffusion system (in the monodomain framework).³⁶

Eleven different episodes of AF were generated using this model. Heterogeneities in action potential duration were introduced by changing the local electrophysiological properties of the cells, as described previously.^{51–53,105} Simulated AF was initiated through rapid pacing in the left atrial appendage. After the pacing protocol was stopped, a time-interval of 10 seconds during AF was extracted for subsequent analysis. These 11 episodes differ by the arrhythmogenic substrate that was created in order to make the model vulnerable to AF. As a result, the dynamics of the depolarization waves, the number of wavelets and their wavelength were different, as is documented in table 3.1.

AF No.	number of wavelets	average wavelength [cm]	dominant frequency [Hz]
1	1 - 3	6.2 ± 2.7	2.5, 4.0
2	1 - 3	6.2 ± 2.3	6.6
3	1 - 4	5.7 ± 2.7	6.8
4	1 - 4	5.9 ± 3.3	6.9
5	1 - 4	5.6 ± 3.2	6.9
6	3 - 7	7.7 ± 3.9	3.7, 6.8
7	1 - 3	7.3 ± 4.0	4.4, 7.1
8	1 - 4	7.2 ± 3.8	4.1, 7.0
9	1 - 4	7.6 ± 3.9	3.9, 6.7
10	3 - 6	3.1 ± 0.1	11.0
11	2 - 4	8.0 ± 3.9	4.7

Table 3.1 – *The specifications of the 11 episodes of AF simulated by the biophysical model of the human atria. The dynamics characteristics of the simulations are specified by the number of wavelets counted on the surface of the atria, their wavelengths (mean \pm SD) as well as the dominant frequency measured on endocardial electrograms.*

3.2.2 Equivalent source strength

The equivalent current source representation of the electric activity of the entire ensemble of 800,000 atrial units used was the equivalent double layer (EDL). This method justifies the representation of the electric activity within the atrial myocardium by double layer sources on the surface bounding it (endocardium and epicardium). In its numerical implementation 2590 small triangular elements were used, which formed the basis of a time varying (non-uniform) double layer. The local source strength at the 1297 vertices (nodes) of the triangles was assigned to be proportional to the time course of the transmembrane potential simulated at the nearest atrial unit. This equivalent source can be represented by a matrix, \mathbf{S} , whose element $s_{n,t}$ is the source strength at node n at time instant t .¹⁰⁴

3.2.3 Computation of body surface potentials

The transfer from the EDL source to the body surface was calculated by means of the *boundary element method* (BEM), applied to a volume conductor model of the thorax including the inhomogeneous conduction properties of the lungs and cardiac cavities.^{45,98,101} The transfer is represented by matrix \mathbf{A} . Each row of \mathbf{A} is the contribution of all the source elements to one observation point on the body surface, and each column is the contribution of one source element to all the observation points of the body surface. The resulting body surface potentials Ψ are computed as

$$\Psi = \mathbf{A}\mathbf{S} \quad (3.1)$$

Geometries of the thorax and the ventricles

The thorax model used in the previous simulation of AF signals¹⁰⁴ was a surface based on the MR images of a healthy male subject; its body surface is specified by 300 nodes that are distributed over the entire thorax surface. This geometry was used during developing the optimization procedure. In addition, the geometries of the thorax, lungs and ventricles were obtained from 25 (healthy) subjects documented during a previous study.⁴¹ The database included the geometries of 15 males and 10 females, constituting a substantial range in thorax morphologies and variations of heart position and orientation, which made it suitable for testing the various lead systems. Each surface representing the thorax geometry was specified by 642 nodes (the vertices of the involved triangles). The single, above mentioned model of the atria was fitted into the individual thorax geometries, in order to match size, location and orientation of the ventricular cavities and the lungs of the individual subjects. This was, unfortunately, required since the original study was dedicated to ventricular activity only, and atrial geometry having sufficient accuracy was not available. The transfer matrix \mathbf{A} (642×1297) was computed for each subject, while taking into account the inhomogeneous conduction properties of lungs and atrial and ventricular, blood-filled cavities.

3.2.4 Simulated body surface potentials

Each of the 11 simulated episodes of AF lasted 10 s, with a time resolution of 1 ms, resulting in 11 variants of matrix \mathbf{S} . These were used as test signals for the evaluation of the lead systems. The resulting body surface potentials were computed using equation 3.1, separately applied to all of the individual transfer matrices \mathbf{A} . The nodes of the thorax geometries involved contained the standard locations of the 12-lead ECG as a subset. As a consequence, the computed matrix of simulated body surface potentials, Ψ , contained the standard leads as subsets. In order to suppress the effect of discretization noise resulting from the finite number of EDL source elements, a low pass moving averaging filter over 20 samples, with its first cutoff frequency at 50 Hz, was applied to the signals at the body surface.

In every observation (or recording) based on a limited number of electrodes, the potentials represent a spatially sampled version of the entire body surface potential distribution. In the case of the simulated AF sequences, Ψ is computed at all L possible electrode positions, that is, all nodes on the surface of the thorax model. For T samples ($T = 10,000$) Ψ has a dimension of ($L \times T$): the potentials at the dedicated nine electrode positions of the standard 12-lead ECG are denoted as Ψ_{ECG} of dimension ($9 \times T$). An example of the lead V1 signal during simulated AF is presented in figure 3.2, a signal completely free of ventricular involvement. The realism of the simulated signal can be judged by comparing

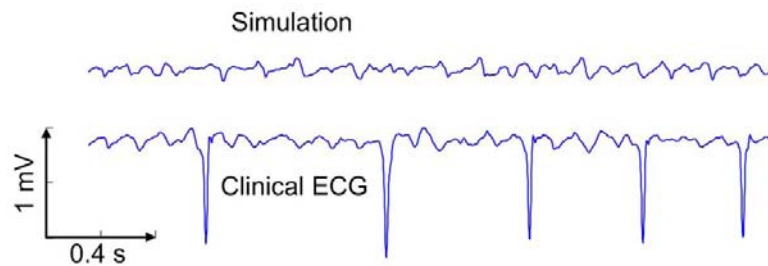


Figure 3.2 – Example of the ECG of lead V1 during AF. Top panel: one of the simulated episodes of AF observed at the position of the V1 electrode. It corresponds to the simulation No. 6 presented in table 3.1. Bottom panel: a clinical record of a patient during AF

it to an example of a clinical lead V1 signal during AF.

3.2.5 Information content

Currently, the use of body surface potentials for classifying different types of AF is largely a terra incognita. As a consequence, no obvious, clinically based criterion exists that can be used to optimize the locations of surface electrodes. Here, we used a criterion derived from the standard, general theory of signal analysis: the method of principal component analysis. The latter was performed by computing the singular value decomposition (SVD) of the data matrix representing the observed signals.

Singular Value Decomposition

The SVD of any real matrix Ψ results in the product of three matrices:

$$\Psi = \mathbf{U}\mathbf{\Sigma}\mathbf{V}^T. \quad (3.2)$$

The columns of matrix \mathbf{V} are the so-called principal signals identified in the data. The relevance of their contribution is expressed by the respective singular values σ_i ($= \Sigma_{i,j}$) of the data matrix, on the main diagonal of matrix $\mathbf{\Sigma}$ resulting from the decomposition, all of which are non-negative. The decomposition produces the singular values in decreasing order of magnitude: $\sigma_1 \geq \sigma_2 \geq \dots \geq \sigma_k > 0$. The principal signal corresponding to the largest value, σ_1 , is the 'most principal' among the identified principal signals. The largest index of the non-zero singular values, k , reveals the rank of the data matrix. This rank indicates the maximum number of independent signals that are present in the observed data. For a matrix having dimension ($L \times T$), its rank is at most equal to the minimum between L and T .

Optimization criterion α

The optimization criterion used in this study was the maximization of $\alpha_k = \sigma_k/\sigma_1$, the ratio of the smallest to the largest singular value. Provided between matrices of the same rank, the one with the largest α_k can be considered to carry the most information in terms of the complexity of the signal dynamics, this value can be used as a criterion for the information content of a data set. For the data matrices derived from the simulated AF signals at nine electrode positions we have, with $M = 9$ and $T = 10,000$, $k \leq 9 (= M < T)$, and in fact $k = 8$ since the nine electrode positions imply a reference, and so the number of independent signals (potential differences) can be at most eight. Accordingly, we used $\alpha_8 = \sigma_8/\sigma_1$, with larger values of α taken to indicate a data set containing more significant information.

As stated, the number of independent signals is at most eight. With $T = 10,000$, any numerical analysis is likely to reveal a rank $k = 8$, but the number of signals that are significant to the problem addressed may even be lower due to the possible inclusion of non-related noise-terms or other artifacts. In this simulation study, as stated also, some discretization noise was involved, resulting from the finite number of EDL source elements. To make sure that indeed $k = 8$, we used the minimum description length (MDL) estimate of the number of independent signal components contained in the data matrix.^{4,40,94,95} As documented in the results section, this justified using $k = 8$ as the effective rank of the data and, hence, using α_8 .

3.2.6 Search methods

The optimal electrode positions were determined in the following way. As is motivated in the Introduction section, we decided to leave five out of the nine electrodes of the standard 12-lead ECG in place. These were the three limb leads, VR, VL and VF, as well as two precordial leads, V1 and V4. The choice of V1 is obvious in that it is the closest to the atria of all possible positions. Lead V4 was selected since, among leads V2 to V6, its AF signal revealed the smallest correlation with that of lead V1,⁵¹ thus providing the maximally independent view on AF. The locations for the remaining four electrodes were selected from all remaining 295 (=300-5) nodes on the thorax at which the AF signals were simulated. The following two procedures were used.

Sequential search

Starting with the set of initial $L = 5$ electrodes, the value of the optimization criterion α_L was computed for $L + 1$ electrode positions: the previous set of $L = 5$ plus one selected from the remaining $300 - L$ positions. This was done for all of the remaining positions; the one selected was the one yielding the highest value of α_L . Upon adding the selected electrode position to the set, L was increased by one, and the procedure was iterated until the total number of electrodes in the set reached 9. The procedure was applied separately to all 11 episodes of AF.

Exhaustive search

The procedure of the sequential search does not guarantee the optimal selection of the four additional electrode locations from the 295 possible locations. The theoretical optimum can only be found by the exhaustive search of all combinations of 4 positions out of 295 ones. This requires about 3.1×10^8 evaluations of α_8 , which would take about five years to compute. Instead, a limited subset of 64 positions was used, that of the Nijmegen lead system.^{37,39} The latter subset has previously been shown to contain all information contained in the ECG, albeit not documented for signals during AF.⁹⁴ The computation time required for the exhaustive search based on 4 out of 61 possible electrode locations was three days for the about 5.2×10^5 combinations involved. The electrode positions yielding the highest value of α_8 were considered as the best set.

3.2.7 Evaluation Method

The lead system, OACG, resulting from the search methods, is presented in the results section. This system was found from the thorax, electrode positions, volume conductor and heart configuration of a single subject. Its performance is documented by comparing the resulting α_8 values found for the 11 AF episodes with the corresponding α_8 values found from the standard electrode positions.

In an independent evaluation, the same procedure was carried out by applying the OACG leads to each of the 25 other thoraxes, and comparing the α_8 values for each of the 11 AF episodes when using the electrodes of the new lead system as well as those of the standard leads.

3.3 Results

3.3.1 Number of independent signals

The MDL functions were computed for the data matrices of the body surface potentials of all eleven AF episodes. The location of the minimum in such functions estimate the number of independent signals contained in the data matrices.⁴¹ This was done for the data matrices of all $L = 300$ electrode positions, Ψ_{300} as well as for Ψ_{64} the data at the $L = 64$ electrode positions used in the exhaustive search. The mean values and the standard deviations are presented in figure 3.3. The number of independent signals found for Ψ_{300} was 58 (figure 3.3a), while for Ψ_{64} it was estimated as 16 (figure 3.3b). Both values are higher than the value of the rank, $k = 8$, thus justifying the use of k in the analysis.

3.3.2 The new lead system

The search procedure identified four disjunct thorax regions for the localization of the four electrodes. Those identified by the sequential search and the exhaustive search were similar

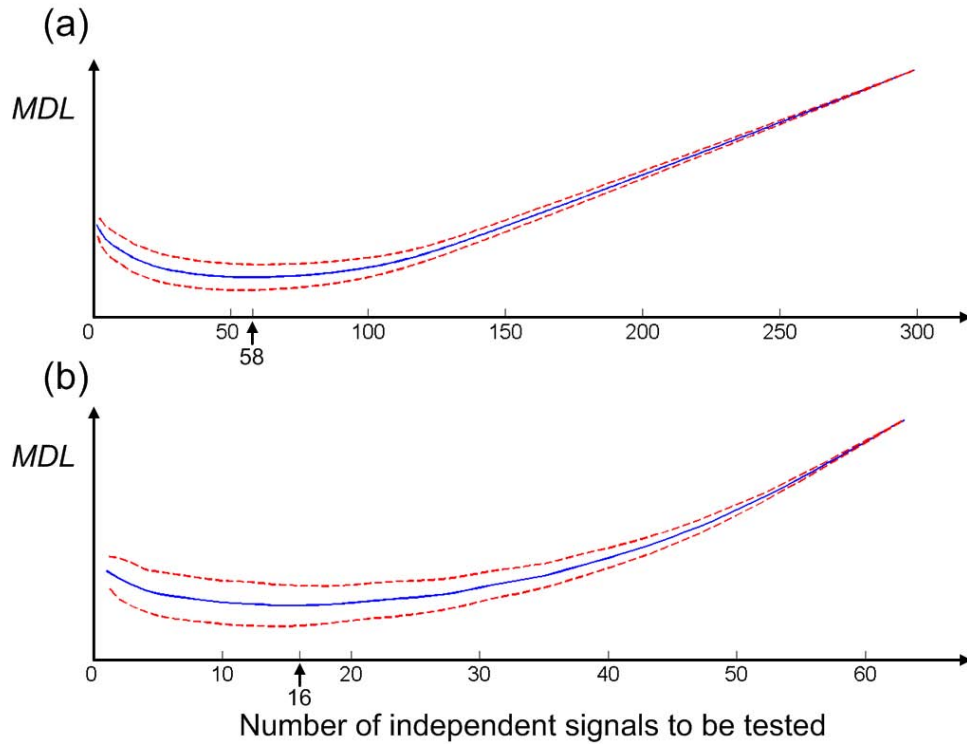


Figure 3.3 – MDL functions computed from the body surface potentials of the reference thorax. The solid line is the mean of the values of all 11 episodes of simulated AF. The dashed lines are the upper and lower bounds of the standard deviation. (a) Based on body surface potentials simulated at all 300 nodes. (b) Based on the subset of the signals of 64 leads.

and the locations found for different AF episodes were pooled.

Based on these pooled results, a new electrode configuration was chosen, the one shown in figure 3.4: the OACG lead system. One electrode, V1S (V1 superior), is placed one inter costal space above the V1 electrode position. The second, V2RS, is placed at the right of the V1S, at the same height. Note that these two positions are also included in the ACG lead system mentioned in the Introduction. The third one is positioned just below the left clavicle as VLC. The last one, V1P (P=posterior) is the one on the back just behind the atria at the same level as V1.

The performance of the lead systems

The spectra of the normalized singular values of data matrices (signals) observed with the three lead systems are presented in figure 3.5. In fact, their normalized values, α_m are shown. These values provide a quantitative view about the information content of the signals. A clear difference between the values related to the standard 12-lead ECG and those related to the other two lead systems may be observed. Beyond $m = 3$, the spectra of ACG and OACG lie constantly above that of the standard 12-lead ECG.⁴⁷ Moreover, the first four values share more or less the same range between ACG and OACG, whereas for

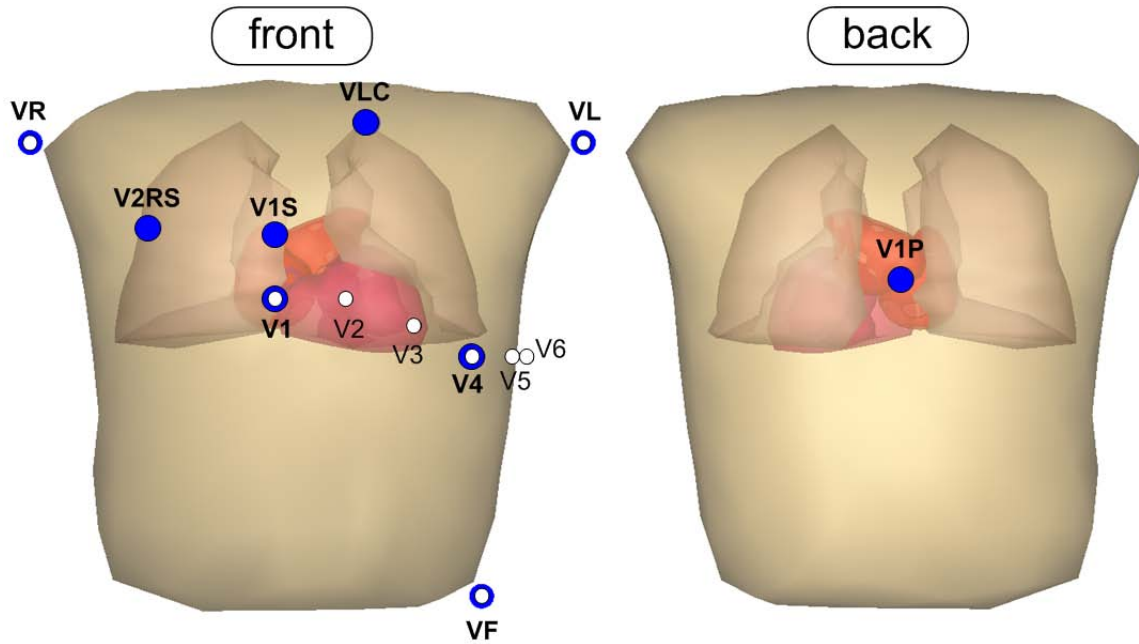


Figure 3.4 – The proposed OACG lead system. The white dots indicate the standard 12-lead ECG electrode positions. The larger, heavy dots are the electrode locations of the proposed lead system.

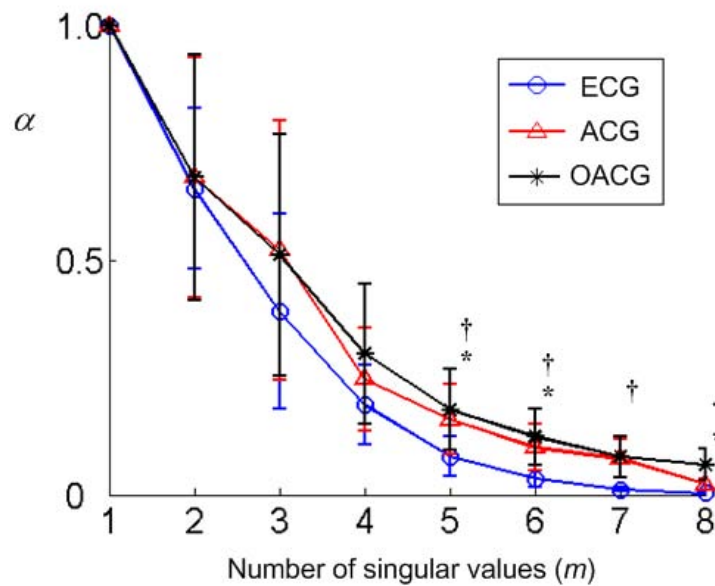


Figure 3.5 – The distributions of m values derived from different lead systems, computed on the 11 simulations of AF, shown as mean \pm SD. The significance values (paired t -test) are presented by the markers: †: ECG vs OACG lead system, $p < 0.001$. *: ACG vs OACG lead system, $p < 0.01$.

the last four, those of OACG are higher ($p < 0.01$). Especially for the last one, α_8 , that of the OACG lead system yielded a twenty-fold larger value compared to that of the standard 12-lead ECG, and three-fold larger than the ACG.

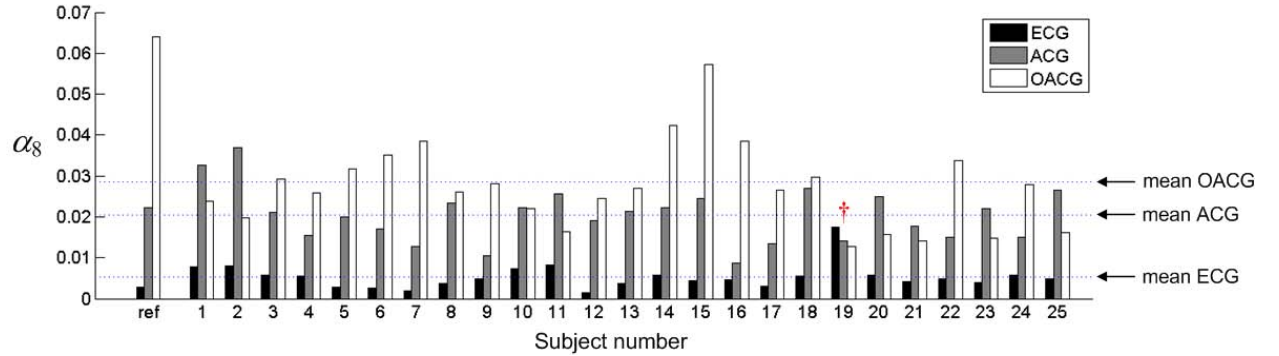


Figure 3.6 – The mean values of the optimization criterion α_8 computed on all simulated AF for each of the 25 thoraxes. The values at the left are those of the reference thorax on which the eleven AF episodes were simulated for the search methods. Detailed statistics are listed in table 3.2. Except for the case indicated by a dagger (\dagger) (outlier, subject 19), the significance value of the paired t -test was $p < 0.001$ between the distributions of ECG and OACG. The dotted horizontal lines represent the mean levels found for the three lead systems.

3.3.3 Evaluation of OACG

Figure 3.6 presents the criterion α_8 calculated from the body surface potentials of AF episodes computed with 25 different thorax geometries. With one exception, the α_8 values as found for the OACG lead system were higher than those for the standard 12-lead ECG. The mean value for the 25 cases yielded a five-fold larger value for the proposed lead system vis-a-vis the standard ECG. Note that for the reference thorax used in the search process, this ratio was 20-fold larger. No difference according to gender was observed.

3.4 Discussion

The MDL function revealed the presence of almost 60 independent signals⁴⁰ in the entire set of 300 body surface potentials of simulated AF, reflecting the high complexity of the underlying dynamics of the signals. The observation that the subset of 64 selected electrodes gave rise to 16 independent signals indicates the difficulty of capturing the full electric activity of the atria even with this large number of electrodes. It is therefore impossible to retrieve the entire information contained in body surface potential during AF by applying only nine electrodes. Within the constraint of applying just 9 electrodes, the higher 8 values for the proposed lead system suggest that it extracts a larger amount of information than those of the standard 12-lead system.

The identified electrode V1S of the OACG lead system, the one above V1, coincides with the location of the lead S of the EASI lead system;²¹ the one on the back at the level of the atria is near the lead M of the Frank’s vector lead system.²⁶ The non-dipolar nature of the ECG during AF demands a more complete three-dimensional capture of information around the thorax, thus necessitating a lead on the back. The four electrode positions found

	ECG	ACG	OACG
ref	0.29 (0.17, 0.37)	2.23 (1.35, 3.09)	6.41 (3.07, 9.08)
1	0.79 (0.42, 1.01)	3.27 (1.14, 5.11)	2.39 (0.74, 3.34)
2	0.81 (0.39, 1.15)	3.69 (1.25, 5.55)	1.98 (1.22, 2.46)
3	0.57 (0.31, 0.79)	2.12 (1.04, 2.82)	2.93 (1.37, 4.36)
4	0.55 (0.25, 0.69)	1.55 (0.68, 2.01)	2.58 (0.94, 3.45)
5	0.28 (0.17, 0.38)	1.99 (1.28, 2.53)	3.16 (1.75, 4.19)
6	0.27 (0.15, 0.39)	1.71 (0.79, 2.34)	3.50 (1.55, 4.87)
7	0.20 (0.16, 0.24)	1.28 (0.58, 1.85)	3.84 (2.72, 5.01)
8	0.38 (0.27, 0.51)	2.33 (1.14, 3.26)	2.61 (0.95, 3.59)
9	0.49 (0.41, 0.62)	1.04 (0.45, 1.54)	2.80 (1.72, 3.90)
10	0.74 (0.52, 1.02)	2.23 (1.03, 3.14)	2.21 (1.31, 2.98)
11	0.83 (0.49, 1.15)	2.55 (0.87, 3.98)	1.63 (0.75, 2.16)
12	0.15 (0.07, 0.21)	1.90 (0.80, 2.42)	2.44 (1.14, 3.30)
13	0.38 (0.22, 0.49)	2.14 (1.02, 2.87)	2.70 (0.90, 3.67)
14	0.57 (0.26, 0.78)	2.21 (1.33, 2.72)	4.23 (2.39, 5.53)
15	0.43 (0.22, 0.60)	2.44 (1.08, 3.30)	5.72 (1.59, 8.50)
16	0.45 (0.28, 0.57)	0.87 (0.44, 1.14)	3.86 (2.35, 5.08)
17	0.31 (0.13, 0.43)	1.33 (0.56, 1.80)	2.66 (1.19, 3.66)
18	0.56 (0.25, 0.81)	2.70 (1.12, 3.66)	2.96 (1.04, 4.14)
19	1.75 (0.77, 2.45)	1.41 (0.75, 2.04)	1.28 (0.48, 1.60)
20	0.59 (0.24, 0.88)	2.50 (1.22, 3.67)	1.56 (0.61, 2.11)
21	0.42 (0.21, 0.61)	1.77 (0.80, 2.50)	1.42 (0.47, 1.98)
22	0.48 (0.32, 0.65)	1.51 (0.69, 2.07)	3.36 (1.50, 4.67)
23	0.39 (0.19, 0.54)	2.20 (1.05, 2.78)	1.49 (0.57, 1.91)
24	0.57 (0.34, 0.80)	1.51 (0.56, 2.26)	2.78 (1.34, 3.73)
25	0.49 (0.35, 0.67)	2.66 (1.31, 3.40)	1.61 (1.10, 2.00)

Table 3.2 – *The values of α_8 for all simulated AF for each of the 25 thoraxes. The columns present the lead systems used and the rows are the subjects. The first row is that of the reference thorax on which the eleven AF episodes were simulated for the searching methods. The values indicated are the mean and the interquartile range (25%, 75%), all divided by 100.*

demonstrated a robust nature. During the search procedure, if we included one (or two, or three) of them as the initial condition and searched for the remaining ones, the other optimal positions invariably showed up in the remaining of the four identified regions and, thus, the total configuration remained the same.

The evaluation of the OACG lead system applied to the 25 different thorax geometries and their conductive properties showed a clear and consistent advantage of the proposed lead system with respect to the information content of AF compared with that of the

standard 12-lead system. There seemed to be one clear outlier (Subject 19, figure 3.6). However, inspection of geometries involved revealed that this related to the geometry of a very thin male, for whom the heart position was found to be much lower than normal, and the electrode positions documented for all of the standard leads were above the level of the atria.

3.5 Limitations

Although different types of AF were simulated, there is only one type of atrial geometry on which the transmembrane potentials are computed. Matching individual atrial morphologies would be preferable for the AF simulations in all 25 thorax geometries, but hard to implement in practice.

The novel positions were sought for just four of the nine electrodes of the standard 12-lead system. Because of the initial objective to be easily applicable in clinical practice, at least half of the total number was fixed to standard positions used in the clinical practice. A free search for all of nine electrode positions may yield an even better performance. The same applies to the use of a larger number of electrodes, as is done in body surface mapping procedures.

A limitation of this study has been the lack of clinical body surface potential signals recorded during AF. The use of extended lead systems, such as the 64-lead system mentioned, has been shown to be very effective, and necessary, in the computation of the cardiac generator. However, it is questionable at the present moment whether the complexity of the generator of AF signals would allow inverse computation of the same quality.

3.6 Conclusion

The locations of the electrodes of the standard 12-lead system were shown to be clearly suboptimal in terms of information content of atrial electric activity. The proposed adaptation, OACG lead system, provides more information. Its electrode locations are anchored to those of the electrodes of the standard leads. Three of the four new electrode locations are above the level of V1, one is on the back at the level of V1. Recordings may be made by using the standard equipment available in the clinic.

The OACG lead system is currently evaluated in a clinical study of ECGs recorded during AF. As in the study reported here, the results will be compared to those obtained with the standard 12-lead ECG as well as those of the ACG electrode placement. Initial results so far have confirmed the superiority of the OACG electrode montage. They will be presented in the next chapter.

Performance of lead systems dedicated to atrial fibrillation: application to clinical data

4

4.1 Introduction

THE recent veer of trend in cardiology and, as presented in the previous chapter, our current interest in the search for a classification of different types of atrial fibrillation (AF) by its underlying etiology prompted us to search for methods that would optimize the extraction of information on this complex phenomenon from signals observed on the body surface. The types of problems to be addressed include **a)** the optimum selection of electrode locations, **b)** the cancellation of the involvement of ventricular activity in the observed signals and **c)** the determination of a measure of the overall complexity of the AF signals. These three elements have been studied in our group, based on a biophysical model of the genesis of atrial signals during AF and of the volume conduction properties of the body tissues. Details of the design procedure involved in the selection of the optimal electrode positions are described in chapter 3. This chapter reports on the results of an evaluation of the performance of the novel lead system, the OACG lead system, in its application to signals recorded from AF patients. This evaluation depends critically on the quality of the other elements: cancellation of the ventricular activity and identification of a complexity measure. All three elements will be summarized in the methods section. The motivation for the attention devoted to these elements is as follows.

Lead systems

The method of body surface potential mapping (BSPM) provides the most complete view on the atrial activity (AA).^{19,89} However, the required recording equipment is not generally available in the clinic. This method has not been applied in the analysis of AF so far. In fact, the general problem of extracting information from the ECG for study of AF study has never been addressed to the extent of our knowledge. It is for this reason that we concentrated on the optimized locations of the 9 electrodes sensing the signals of the standard 12-lead ECG. The standard 12-lead ECG remains the most commonly used tool with well-defined equipment and protocol.² Since the interest of electrocardiology has been historically focused on the electric activity of the ventricles, the information content available from the signals observed from these electrodes is likely not to be optimal for studying atrial activity, in particular during AF. This hypothesis was shown to be true in a simulation study presented in the previous chapter using a biophysical model of the human atria and thorax.⁴⁸ The novel lead systems ACG (atrial cardiogram)⁴⁷ and OACG (optimized atrial electrocardiogram)⁴⁹ were the resulting heuristic and optimized lead systems, respectively.

Extracting atrial signals

The analysis of AF from observed ECG signals demands a high quality suppression of the contribution of the electrical activity of the ventricles to the observed signals. Several, dedicated methods have been reported in the literature.^{59,88,91} The method used in this work was a refinement of those published previously, which allowed us to perform our analysis on data that showed almost imperceptible ventricular involvement.

Complexity measure

At this moment, even when atrial signals during AF are available that are free of ventricular involvement, it is not clear which would be the appropriate features to extract for classification of the disease. In our study we used a complexity index derived from the singular value decomposition, performing the principal component analysis, of the data. Features of this type have been previously introduced in the analysis of ECG data.⁹⁶ The aforementioned three elements discussed are the main ingredients used in the evaluation of the performance of the ACG and OACG lead system.

4.2 Methods

4.2.1 Lead systems

The three montages of 9 electrodes for recording the ECG data during AF were that of the standard 12-lead ECG, of a heuristically defined configuration (ACG) and of an optimized variant (OACG). The montages of the lead systems are presented in figure 4.1.

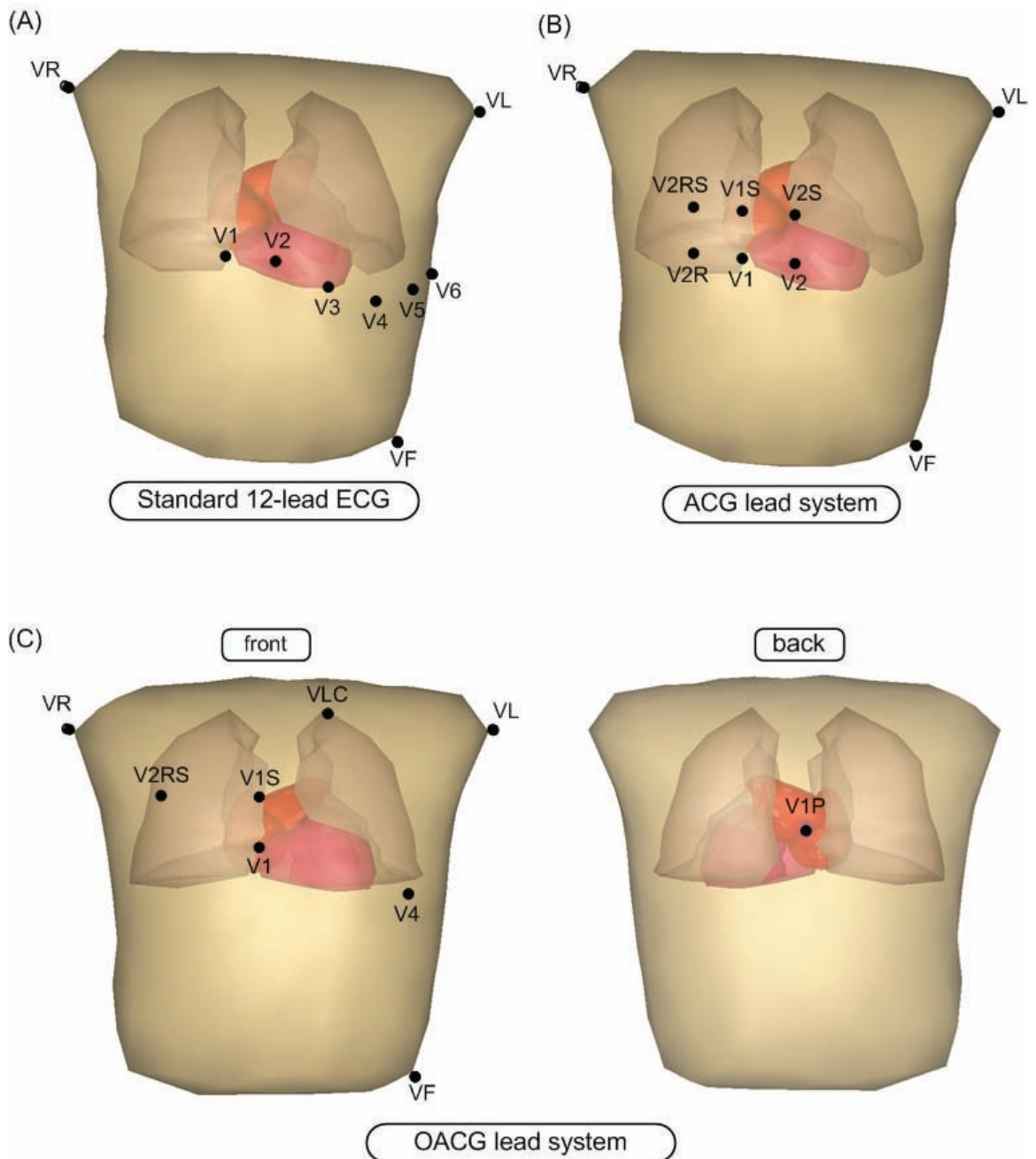


Figure 4.1 – The locations of the electrodes used by the lead systems. (A) The standard 12-lead ECG. (B) The ACG (atriocardiogram) lead system. (C) The OACG (optimized ACG) lead system.

The ACG lead system

The ACG lead system is a new configuration of the standard 12-lead ECG by moving 4 of the 9 electrodes to their dedicated positions as also described in chapter 3. The aim in the design of this lead system was based on the motivation to position the precordial leads closer to the atria. In view of its clinical application, another important point in the design

was to anchor the electrode locations as much as possible to those of the standard ECG. The three limb leads, VR, VL and VF were left in their original configurations so as to preserve the Wilson Central Terminal (WCT) reference. The positions of leads V1 and V2 lead positions were also maintained due to their proximity to the atria. In this way, more than the half, that is 5 out of the 9 electrodes, are anchored to the locations of the standard 12-lead ECG. The 4 remaining precordial leads, V3 to V6 were moved counterclockwise around the lead positions of V1 and V2 thus forming a 2×3 grid overlying the atria as presented in Fig. 1b. The V3 electrode is placed above the V2 electrode position as V2S (superior), V4 above V1 as V1S, V5 to the right of V1S as V2RS (right superior) and V6 to the right of the V1 lead position as V2R (right).⁴⁷

The OACG lead system

The OACG lead system is optimal with respect to the extraction of information content of AF, using the standard ECG equipment of 9 electrodes. The detail of its design process is described in the previous chapter. The basis of its design is similar to that which grounded the ACG lead system: to anchor at least the half of the electrodes to their standard position. Here, VR, VL, VF as well as V1 and V4 were left in the original locations. The three limb leads were chosen for the same reason as described above, to maintain the WCT reference used in clinical practice. The V1 is the closest to the atria, and V4 was selected according to a precedent observation that the potentials observed at this location had the smallest correlation with those of lead V1 during AF,⁵¹ thus providing the maximally independent view on AF. By using simulated episodes of AF generated with a biophysical model of the human atria and thorax, the remaining four electrodes, originally used as V2, V3, V5 and V6, were repositioned on the surface of the thorax so as to maximize the information extraction. The 4 electrodes were relocated by being added one by one to the initial 5 electrodes so that the measure of information content α_k , as introduced below, is maximized at each addition.⁴⁹ The electrode positions of the OACG lead system is presented in figure 4.1c.

4.2.2 Clinical AF signals

The clinical signals were taken from patients admitted in the ER showing symptoms of AF. The recordings were performed consecutively with the standard 12-lead ECG, the ACG and the OACG montage, each for a period of 5 minutes. The sampling rate was 500 sps. The recordings were documented with the patient data including the identification of the patient, basic constitutional variables, the diagnosis, anamnesis, history of admission and drug therapy. It is still an ongoing study and, indeed, there is only a limited number of clinical signals available for the OACG lead system so far. Recording using the standard ECG and ACG started years ago, while the OACG lead system has just been introduced.

From the database, 66 recordings of 5 minutes were selected that showed stable AF episodes without major artifacts. They were taken from 32 patients, of whom 30 patients

	male (15)	female (17)	total (32)
age [years]	72.9 ± 9.6 (67, 73, 82)	77.4 ± 16.7 (71, 83, 88)	75.4 ± 14.1 (67, 79, 85)
height [cm]	173.1 ± 7.4 (169, 174, 180)	165.1 ± 7.2 (160, 165, 170)	168.5 ± 8.3 (160, 168.5, 174)
weight [kg]	81.2 ± 11.4 (72, 80, 88)	64.7 ± 12.1 (56, 63, 71)	71.8 ± 14.3 (62, 70.5, 80)

Table 4.1 – *Basic statistics of the 30 patients. There are 13 male patients and 17 female patients. The values are given as the mean \pm standard deviation and the interquartile values (25 percentile, median, 75 percentile) of the distribution.*

with recordings using the standard 12-lead ECG and ACG, and 2 patients with all three lead systems including the OACG. The main statistics of the subjects are shown in Table 4.1.

4.2.3 VA cancellation

The cancellation of the ventricular contributions to the observed signals was carried out as follows.

The signals were preprocessed with a baseline correction (cubic spline interpolation anchored on the onsets of the QRS complexes) and a low pass filter with a cutoff frequency at 50 Hz. The dominant T wave⁹⁹ has been introduced as a means to characterize the general similar shape of the T waves in different leads. It was also shown that an individual T wave could be represented by a linear combination of the dominant T wave and its time derivatives.¹⁰⁰ Based on those observations, the T wave of each cardiac cycle was estimated using the dominant T wave and its first and second derivatives. The dominant T wave was obtained by fitting an analytical function (multiplication of two logistic functions) to the first principal component computed on the ST-T segment. The U wave was estimated by fitting a Gaussian function to the same first principal component. These estimated repolarization waves were weighted and subtracted from the original signal.

The method adopted for the AA over each QRS complex was the following. In contrast to a standard *subtraction* method, it estimates directly the atrial components over each QRS complex based on the cleaned up segments that precede and follow the complex. The AA over these two segments is estimated by a finite sum of sinusoid functions. Each sinusoid is described as a weighted sum of sine and cosine functions with the same frequency. The 50 frequencies for the set of sinusoids were uniformly distributed between 0 and 10 Hz. The weights related to the sine and cosine functions of the set were optimized over the two cleaned up segments on all leads in a least squares sense.³¹ The interval over the QRS complex was defined as the AA estimate. This procedure can be seen as an extrapolation

of the atrial contribution over the regions of the ventricular one.

A low pass filter was applied at the end of this process to smooth the difference of levels between estimated AAs located before, during and after the QRS complex.

Each of the selected 66 recordings therefore became a 5-minute sequence on each individual lead of atrial activity only.

The above presented VA cancellation methodology was designed, implemented and tested by Mathieu Lemay for the NAF project and his Thesis work.

4.2.4 The complexity index

The measure used to evaluate the information content in the recording of AA is based on standard and general theory of signal processing: the singular value decomposition (SVD).

The signals recorded by each lead system are observations of potential differences using 9 electrodes. The body surface potentials observed at the corresponding electrode positions can be therefore represented by a data matrix Ψ of size $(9 \times T)$, with T the number of samples in time. Application of SVD to this data matrix yields 8 singular values since the 9 electrode positions imply a reference, and so the number of independent signals (potential differences) can be at most 8. The decomposition produces the singular values in decreasing order of magnitude: $\sigma_1 \geq \sigma_2 \geq \dots \geq \sigma_k > 0$. The principal signal (*conf.* chapter 3, equation 3.2) corresponding to the largest value, σ_1 , is the ‘*most principal*’ among the identified principal signals.

The measure of information content used in this study is the ratio of the smallest to the largest singular value, $\alpha_8 = \sigma_8/\sigma_1$, with larger values of α_8 indicating a data set containing more significant information. Provided the number of independent signals available in the entire body surface potentials of atrial activity is higher than the rank of the data matrix,^{40,49} the use of α_8 is justified in that this value does not include significant information of non-related noise terms or other artifacts.

The behavior of the α_8 measure was studied as a function of time during the 5-minute episode of recording. This was necessary since the recordings using different lead systems were effectuated consecutively and not simultaneously. The stable behavior of signal dynamics had to be evaluated first in order to compare the complexity index between signals of the same patient. Each data matrix of atrial fibrillation was subdivided in segments of 10 seconds, thus providing 30 blocks for each of the lead systems in every patient. In this way, the temporal behavior of the complexity index can also be studied. The time window of 10 seconds was chosen to have a reasonable compromise between accuracy and the need for local stationarity. The α_8 value was studied for each 10-second segment over the entire 5-minute episodes, while the first and the last segment were systematically discarded because these segments contained large artifacts due to the recording procedures.

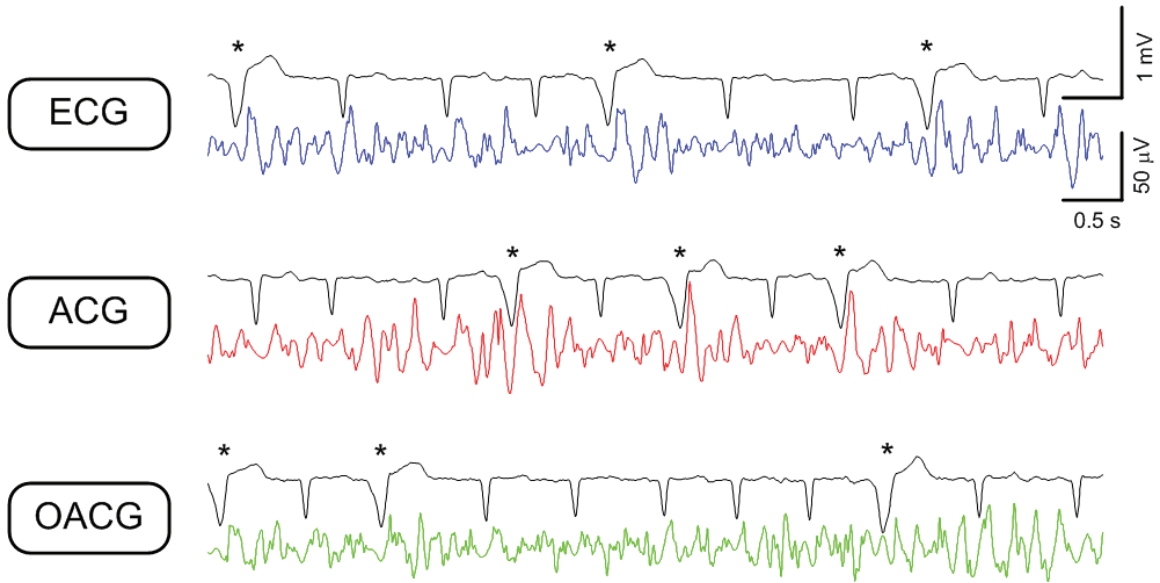


Figure 4.2 – Example of QRST cancellation of the signals observed on the V1 lead position. For each lead system mentioned on the left, the top signal is the original body surface potential (atrial and ventricular activity), while the bottom part is the separated atrial activity after application of the VA cancellation method. The two traces are drawn at different scales. The asterisks indicate the ectopic beats.

4.3 Results

4.3.1 VA cancellation

An example of VA cancellation is presented in figure 4.2 for lead V1, an electrode position that is common to all lead systems. The episodes of AF come from the same patient, in a sequential recording using the three lead systems. Although the original recordings seem to exhibit the same type of stable AF wave forms, the separated AA signals look different. The difference comes from the VA cancellation method using body surface potentials observed at different locations on the thorax. One prominent observation is that just after an ectopic beat, marked by an asterisk in figure 4.2, the VA cancellation applied to the signals of the standard ECG and ACG montage leaves a residual artifact, while with OACG it is inhibited. The amplitude of the AA signals available from the OACG lead systems is the most constant when compared to those from the standard ECG and ACG.

4.3.2 The complexity index

The normalized singular values

An example of α_8 as a function of time during a 5-minute sequence is presented in figure 4.3. Each marker indicates the α_8 value for the corresponding 10-second segment. The stability of the values over time measured as the standard deviation normalized by the mean value

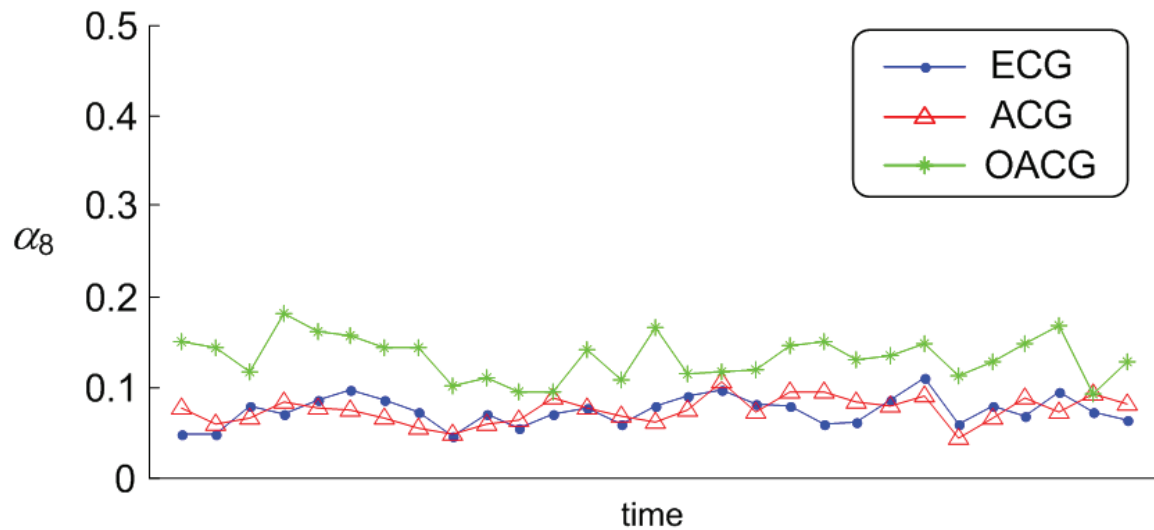


Figure 4.3 – The variation of α_8 as a function of time for each lead system. An example taken on the 5-minute episodes recorded on the same patient. Each marker represents the 8 value for the corresponding 10-second segment.

was respectively 0.24, 0.23 and 0.22 for the standard ECG, ACG and OACG in that patient. Although limited to the cases of only 2 patients, the α_8 of OACG signals lied constantly higher than the two others. The values showed a stable behavior of the same order of magnitude in the signals from all patients.

The spectra of the normalized singular values α_k for the three lead systems computed on all patients are shown in figure 4.4. The singular values for the OACG lied constantly above those of the ECG, and each paired distribution of singular value α_k ($k = 2, \dots, 8$) had a significance value $p < 0.005$ in the paired double-sided t -test. The difference becomes even clearer for the smallest singular values, where the mean exhibited a 2.23-fold higher value for the α_8 of the OACG compared to that of the standard ECG and 1.78-fold compared to the ACG. The ACG showed a 1.25-fold higher value than that of the standard ECG.

Paired statistics of α_8

The statistics of α_8 for each patient are shown in figure 4.5. The bar diagram and the error bars show the mean \pm the standard deviation of the distribution of α_8 over 5 minutes for each subject and each lead system. For the comparison of the standard ECG and ACG, except for 5 patients indicated by a †, the significance between each pair of distribution was $p < 0.05$ (figure 4.5a). The mean value among the patients of the ratio between the average α_8 for ACG over that of the ECG was 1.34. For the 2 patients for whom recordings with all three lead systems are available, the comparison is shown in figure 4.5b. Here, the mean α_8 values were even more significantly different in all cases between the OACG and the other two lead systems ($p < 10e-10$), and indicated constantly higher values for the OACG lead system (1.82-fold higher).

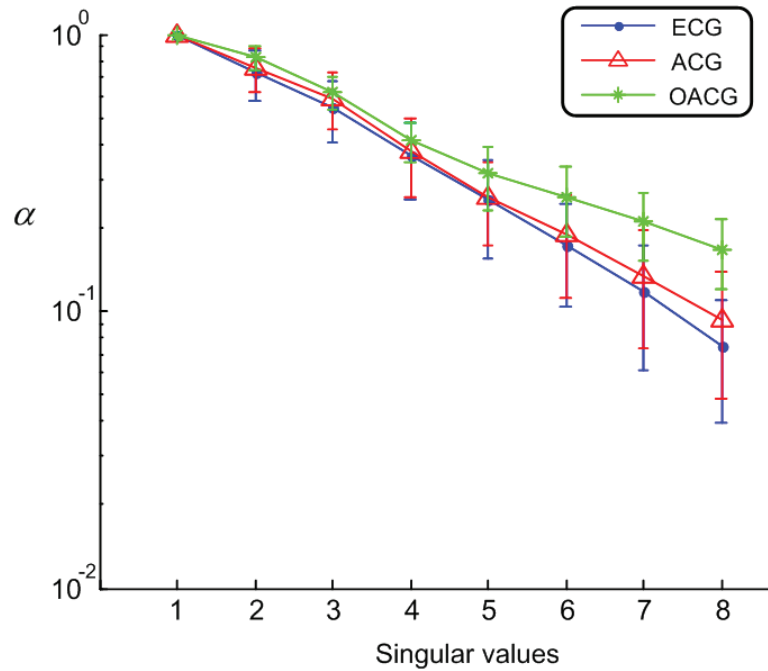


Figure 4.4 – Singular value spectrum of the data matrices. The values are normalized with respect to the first (largest) one. The markers are the mean values of the pooled data of all patients and all segments of 10 seconds. The error bars are the standard deviations of the distributions.

4.4 Discussion

Results on VA cancellation demonstrated the global superiority of the OACG lead system under visual inspection with regard to cancellation artifacts. Interestingly, for the common leads in the three systems, such as V1 in figure 4.2, a better enhancement of AA in OACG compared to the standard ECG or ACG was observed. This is due to the VA cancellation processing the entire data matrix simultaneously, and thus considering the global information content available from all 9 leads. That is, the capture of higher information of AF from the body surface potentials improves the estimation of AA from the body surface potential signals in its entirety.

For the clinical episodes of AF in which the AA was dissociated from VA, the spectrum of the singular values showed a consistently higher value for the OACG lead system compared to the standard ECG and ACG. This suggests that the signals observed at the locations of the OACG electrodes carry a higher complexity of dynamics, *i.e.* extra information content, with regard to the standard ECG lead system while using the same number of electrodes and more than half of which is anchored to the initial position.

In the paired statistics of the α_8 value of the ECG and ACG studied in each individual patient, more than 2/3 of the cases showed a higher value for the ACG with significant difference. The ratio of the α_8 value derived by the signals of ACG to those of the ECG in a paired comparison showed a non negligible advantage of the ACG (1.34-fold in average).

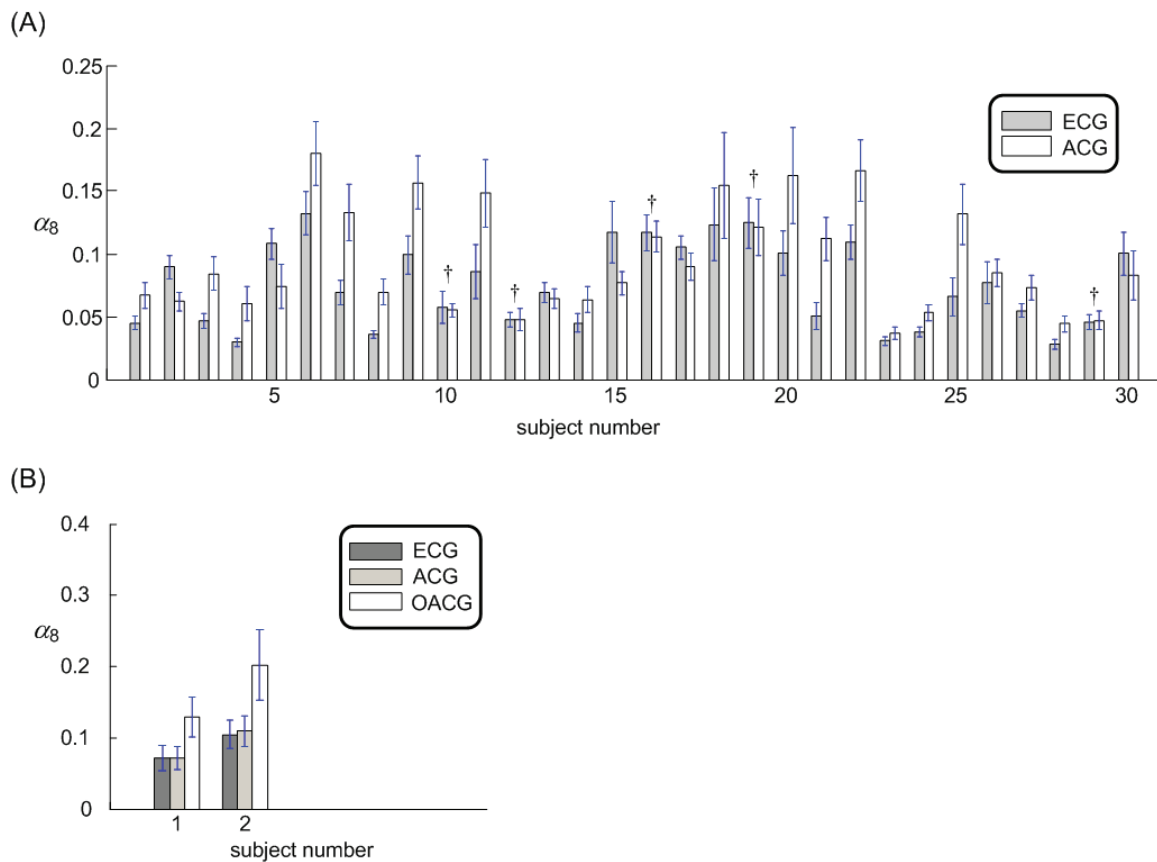


Figure 4.5 – Paired statistics of α_8 for all subjects. The bar diagram is the mean value with the error bars indicating the standard deviation of the distribution during the 5-minute recording in segments of 10 seconds. **(A)** Diagram for ECG vs ACG in 30 patients. The † are the cases in which the paired t-test between the respective distribution was not significant ($p > 0.05$). **(B)** Diagram for ECG, ACG and OACG.

Although with a very limited number of clinical signals, the OACG consistently displayed better performance with a 1.82-fold higher value of α_8 . The prominent superiority of the OACG lead system in this study is a good sign toward confirmation of the advantage and necessity of having at least one electrode in the back, should we aim at studying AF in depth with limited number of electrodes and constraints on their general positions.

4.5 Limitations

One drawback of the presented study is the lack of simultaneous recordings using the standard ECG, ACG and OACG. The signals were recorded in a consecutive manner with a length of 5 minutes each. The stability of all episodes needed to be verified in order to treat them as originating from stable atrial fibrillation dynamics from the same patient. In order to refer to the information content during evolution of AF, a simultaneous recording with multiple lead systems is required. However, the recording method used in this study

and the results on the stationarity presented justify the use of the OACG lead system in the clinical practice for the diagnosis of AF, to be used consecutively after a standard recording procedure using the standard 12-lead ECG material.

4.6 Conclusion

Using a limited number of 9 electrodes in order to capture the AA during AF, the lead locations of the standard ECG were shown to be clearly suboptimal for analyzing AF from clinical signals. The information content of the AA in terms of singular values of the data matrix exhibited a higher value for the recorded signals using the OACG lead system. The augmented information content by the OACG lead system improved the performance of the VA cancellation that uses the entire data of body surface potentials acquired by the 9 electrodes.

Special thanks

All clinical signals used in the study presented in this chapter were recorded by Ms. Véronique Prudent, an experienced nurse assigned to this project at the Lausanne University Hospital Center, the division of cardiology. I express my appreciation and gratitude to the care that has been taken in the application of the new lead systems and for the recordings of the clinical signals from the patients. I know it wasn't always easy.

Also shall I give an address of great thanks to all the patients suffering from AF who were admitted in the ER of the Lausanne University Hospital Center and who always accepted with good grace the extra recordings for our project.

Vectorcardiographic lead systems for the characterization of atrial fibrillation

5

5.1 Introduction

ONE of the methods used for the interpretation of the time course of the potentials observed on the body surface is the vectorcardiogram (VCG). It estimates a compact representation of the cardiac electric generator: the equivalent current dipole. The restriction involved permits the analysis of the spatio-temporal aspects of the cardiac generator based on the time courses of the three dipole components, the signals $X(t)$, $Y(t)$ and $Z(t)$, or visualized by means of vector loops. These aspects are less easily discernable in plots of the standard 12-lead ECG. Currently interest in the VCG seems to have waned. The motivation for using the VCG for the analysis of atrial fibrillation (AF) relates to the fact that the apparent chaotic nature of the ECG signals during AF has so far prevented the selection of signal features that might be used in the classification of different types of AF. Up until now, efforts have concentrated on the spectral analysis of ECGs, but spatio-temporal types of analysis remain to be developed. The more important, clinical motivation for studying this topic is the increasing incidence of AF with age, alongside the steady increase in the average age of the population.

This study aimed at designing an electrode configuration using a limited number of electrodes and associated transfer coefficients dedicated to characterizing atrial fibrillation (AF). The combination of both is referred to as the lead system. The electrode configurations studied were restricted to variations of existing lead systems. In this way the ultimate clinical application of any new lead system is facilitated. The design of the lead systems was based on body surface potentials generated during episodes of 10 different types of atrial

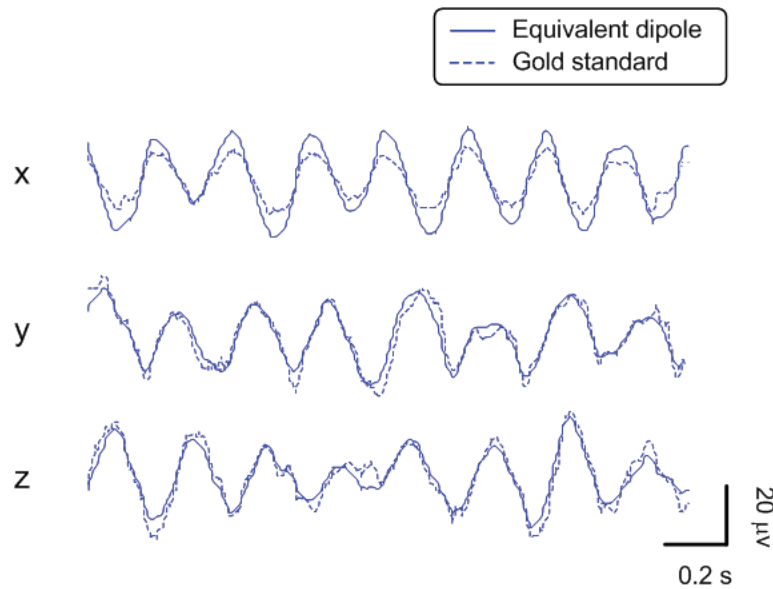


Figure 5.1 – Dipole components during atrial fibrillation. Solid lines show the equivalent dipole components, dotted lines those of the gold standard derived from the Gabor-Nelson equations. The axes are those of the standard VCG protocol pointed toward the left (x), foot (y), and to the back (z).

fibrillation (AF) simulated by a previously developed and validated biophysical model. The model of the thorax includes the inhomogeneous conductive properties of the lungs as well as the atrial and ventricular blood-filled cavities. It allowed us to proceed to the analysis of body surface potentials and atrial dipole signals entirely free of any involvement of the electric activity of the ventricles. The testing of the performance of the various lead systems was based on a collection of 25 different volume conductor models, with the relevant geometry derived from individual MRI data. For each subject, the entire procedure was carried out separately based on its geometry (*design stage*); the resulting lead systems were tested in their application to the thorax models of the other 24 subjects (*evaluation stage*).

In order to describe the definition of VCG, a general discussion on designing vector lead systems is presented first in this chapter; it also introduces the various notations used. Next, the material used in the study is documented, as well as the methods employed. Finally, the results are presented, including a full analysis of the application of the proposed system in its application to individual thorax geometries. Since the design is based on simulated AF, various intermediate illustrations of the different steps taken are included to justify their use.

5.2 Designing VCG lead systems

Vectorcardiographic lead systems may be designed by using either statistical or model-based methods. Examples of both methods may be found in recent publications on this

topic.^{25,43,62} The best known lead system is the one designed by Frank, which represents the initial, essential, model based approach.²⁶ This section summarizes the model based type of approach and its background. It is the method used in the present study. It stresses some aspects involved that so far have not received adequate attention.

The vectorcardiogram is an estimate of the equivalent current dipole $\vec{D}(t)$ representing, to a first order approximation, the spatial distribution throughout the myocardium of the time course of the currents generated at the membranes of all cardiac myocytes. Being a vector in 3D space, the spatio-temporal nature of the current dipole may be fully characterized by the time courses of its 3 components $D_x(t)$, $D_y(t)$, $D_z(t)$. An example of these components derived from the electric activity of the atria during AF, as described in the methods section, is shown in figure 5.1. The three components of the potentials of the VCG, $V_x(t)$, $V_y(t)$, and $V_z(t)$ that estimate the dipole are, ideally, directly proportional to the dipole components. The estimation of the current dipole on the basis of observed body surface potentials constitutes a so-called inverse problem. Its solution demands the specification of a volume conduction model of the thorax, and in particular of the surface bounding the medium: the body surface.

When a single dipole current source is placed inside the thorax model, the potential $\phi_\ell(t)$ generated at electrode l on the surface of the thorax is a weighted sum of the potentials that the three individual dipole components generate separately. The three weighting coefficients for electrode l , $w(\ell, x)$, $w(\ell, y)$ and $w(\ell, z)$, depend on the distance between the location of the electrode and that of the dipole, as well as on the overall nature of the volume conductor. Accordingly, for a time-varying dipole strength the potential $\phi_\ell(t)$ at electrode l reads

$$\phi_\ell(t) = w(\ell, x) D_x(t) + w(\ell, y) D_y(t) + w(\ell, z) D_z(t). \quad (5.1)$$

This expression may be interpreted as a scalar product of two vectors: the dipole vector and a vector with elements $w(\ell, x)$, $w(\ell, y)$ and $w(\ell, z)$. Correspondingly, the latter is referred to as the lead vector at the position of electrode.⁴²

When treating the collection of potentials observed at L electrode positions and sampled at T time instants, equation 5.1 can be conveniently expressed by the matrix multiplication

$$\mathbf{\Phi} = \mathbf{W} \mathbf{D}, \quad (5.2)$$

in which $\mathbf{\Phi}$ is the matrix of observed potentials (size: $L \times T$), \mathbf{W} the matrix (size: $L \times 3$) comprising all lead vectors at the L electrode locations considered and \mathbf{D} the matrix of instantaneous dipole strengths (size: $3 \times T$). Matrix \mathbf{W} represents the so-called forward transfer matrix of the involved forward problem.

The volume conductor model implied in the VCG is a homogeneous one, bounded by the body surface. In the work of Frank²⁶ the forward transfer coefficients were based on measured potential differences on the surface of a thorax shaped tank containing a fluid with homogeneous electric conductivity. A physical current dipole was placed inside the tank in the ventricular region. Based on these measurements, a set of seven electrodes was selected heuristically, with positions that were, likewise heuristically, chosen on the thorax,

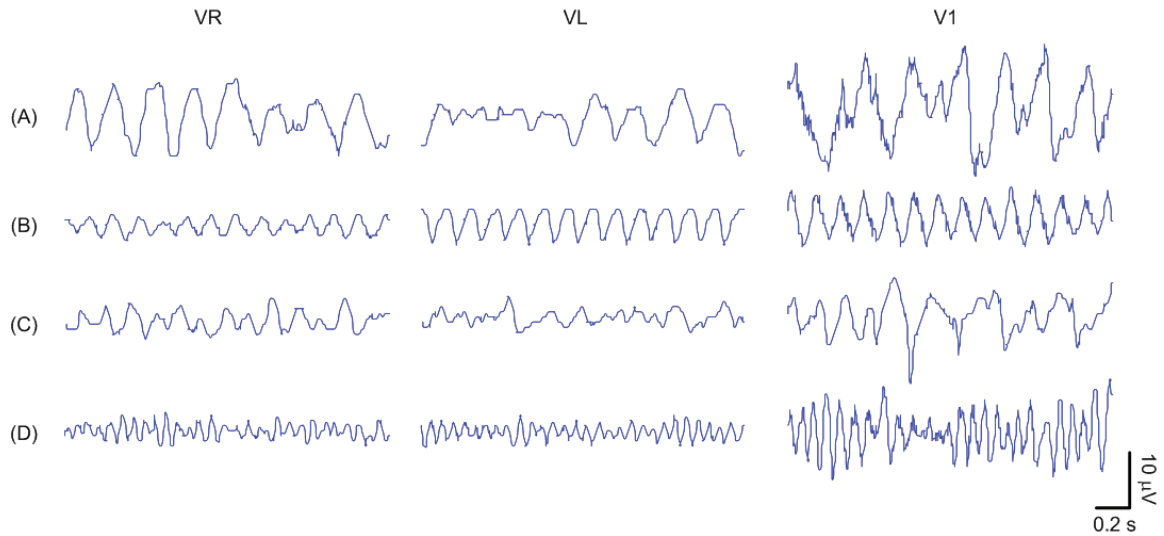


Figure 5.2 – Examples of simulated AF as visible in the ECG. (A) to (D) are four of the ten AF variants used in this study. The columns are leads VR, VL and V1; variant (A) is the same as the one showed in figure 5.1.

	A	C	E	F	H	I	M
x	0.61	0.171	0	0	0	-0.781	0
y	0	0	0	0.655	-1	0	0.345
z	0.133	-0.231	-0.374	0	0	-0.264	0.736

Table 5.1 – The original transfer coefficients proposed by Frank.

five of them selected at a transverse cross-section at the level of the ventricles (figure 5.3d). Based on the analysis of the measured lead vectors, Frank proposed a matrix of transfer coefficients for estimating \mathbf{D} on the basis of the potentials at the seven electrode locations (table 5.1).

The matrix was implemented by a resistive network. The signals observed at the three outputs of the resistive network have become the standard for the VCG. The procedure may be expressed by the matrix multiplication

$$\mathbf{D} = \mathbf{T} \Phi, \quad (5.3)$$

in which Φ is the matrix of observed potentials at the seven electrode locations (size: $7 \times T$) and \mathbf{T} the matrix (size: 3×7) for deriving the dipole estimate from a limited set of observed potentials. Note that the resistive network was connected directly to all electrodes sensing the actual potential. Since the mean of the potential as such on the thorax is unrelated to internal current source strength, Frank's matrix satisfies the required property that the

sum of the elements of each row be zero. Expressed in matrix/vector notation

$$\mathbf{T} \mathbf{e} = \mathbf{0}, \quad (5.4)$$

in which \mathbf{e} is a column vector with all its L elements equal to one. This property should be a condition in all expressions for deriving a dipole estimate from a limited set of observed potentials. Over the years, the VCG derived from the Frank electrodes and the corresponding matrix has become to be regarded as the gold standard in vectorcardiography. However, this has unfortunately led to the situation that several recent efforts have been directed toward deriving, *i.e.*, approximating Frank's based derivation of the dipole strength (VCG) from alternative, limited electrode configurations rather than deriving the dipole estimate itself.

Recent advances in computer-based modeling of the volume conduction properties of the thorax, and the numerical handling of the solution of systems of equations have provided accurate methods^{33,75} for designing and testing different configurations of electrodes and their corresponding (inverse) transfer matrices. These are the methods applied in this paper.

For any configuration of electrodes, the associated transfer matrix \mathbf{T} may be computed as follows. Based on an assumed dipole source matrix \mathbf{D}_{ref} and on the involved forward transfer \mathbf{W} , a set of reference potentials is computed as

$$\Phi_{\text{ref}} = \mathbf{W} \mathbf{D}_{\text{ref}}, \quad (5.5)$$

as in equation 5.2. Next, the required transfer matrix \mathbf{T} is computed as the one that minimizes the sum of the squared differences between all elements of the reference source \mathbf{D}_{ref} and those of its estimate

$$\mathbf{D}_{\text{est}} = \mathbf{T} \Phi_{\text{ref}}. \quad (5.6)$$

The linear constraint equation 5.4 needs to be included in the solving of this problem. This is implemented by using the zero-mean version of the potentials:

$$\Psi = \Phi_{\text{ref}} - \frac{1}{L} \mathbf{E} \Phi_{\text{ref}}, \quad (5.7)$$

with \mathbf{E} a square matrix (size: $L \times L$) having unit elements only. Based on this zero-mean version of the potentials, the desired transfer \mathbf{T} is found to be

$$\mathbf{T} = \mathbf{D}_{\text{ref}} \Psi^{\dagger} (\Psi \Psi^{\dagger})^{\ddagger}, \quad (5.8)$$

with \ddagger denoting the pseudo inverse of a matrix. The quality of the entire procedure, *viz.*, of the selection of the number of electrodes and of the computed associated transfer \mathbf{T} , may be quantified by taking measures of the matrix of residual differences, $\mathbf{R} = \mathbf{D}_{\text{ref}} - \mathbf{T} \Phi_{\text{ref}}$, either as such or when compared with the elements of the reference source \mathbf{D}_{ref} .

If, like when using the Frank leads and its associated transfer matrix \mathbf{T} , the VCG is derived from a limited number of observed signals, the estimated dipole vector will produce errors if applied to dipole locations and/or thorax geometries other than the one used in the

design procedure. The redundancy in using seven electrodes, as in Frank's system (four are sufficient if design and application relate to the same dipole location and thorax geometry) aimed at reducing the errors in applications of the 'one lead system fits all' type. Being aimed at finding the dipole vector related to ventricular activity, Frank's system cannot be considered as the gold standard when designing alternative lead systems focusing on the atrial VCG during AF.

The gold standard used in the present study is the one based on the Gabor-Nelson equations.²⁸ Based on a specified geometry of S_b , the surface bounding the thorax, a full description of the potential field on the thorax ϕ and a homogeneous conductivity of its interior, these equations yield the unique identification of the dipole vector \vec{D} as

$$\vec{D} = \sigma \int_{S_b} \phi \, d\vec{S} \quad (5.9)$$

irrespective of its location. This makes it ideally suited for serving as the gold standard in designing new vector lead systems, as was done in this study. In its application to discretized, sampled data, the Gabor-Nelson equations read

$$\mathbf{D}_{GN} = \sigma \mathbf{S}_b \Phi, \quad (5.10)$$

with \mathbf{S}_b the matrix (size: $3 \times L$) of the matrix of the body surface normals at the positions sampling the potential field. Since $\int_{S_b} d\vec{S} = 0$ for any closed surface, condition of equation 5.4 is automatically satisfied. The accuracy of this numerical estimate of the exact expression of equation 5.9 increases with the number of observation points. Simulated body surface potentials during AF at all $L = 642$ nodes of the triangulated torso boundaries were used in this study.

5.3 Materials and Methods

5.3.1 Geometries of the human thorax

The thorax models used were based on the MR images of 25 healthy subjects. These were collected in a previous study⁴¹ and included the specification of the geometries of the thorax boundaries, lungs and ventricles of 15 males and 10 females. The data comprise a substantial range of thorax morphologies and variations of heart position and orientation. Each surface representing the thorax geometry was specified by 642 nodes as the vertices of a dense triangulation. The nodes contained the locations of the electrodes of the 12-lead ECG as well as those of the Frank lead system as subsets. The measure used for the characterization of overall thorax morphology was derived from the ponderal index.^{58,60} By introducing the mean density ρ of body tissues into the definition of the ponderal index, a dimensionless shape factor was derived

$$PI = \frac{\sqrt[3]{m/\rho}}{h}, \quad (5.11)$$

with m and h denoting body mass and height of the subjects, respectively. For the 25 subjects the mean ponderal index value was $PI = 0.24 \pm 0.01$ (mean \pm SD), with range: [0.22, 0.26]. A single (male, mesomorphic) subject was selected with $PI = 0.24$, the value of the median. This reference subject will be referred to as subject RS. The results derived for this subject are used during the illustration of the various steps of the design procedure. However, as documented in the Evaluation section, the entire procedure was performed by taking each of the geometries separately in the design procedure, followed by an evaluation based on each of the remaining 24 geometries.

5.3.2 Model of the human atria

A thick-walled 3D model of the human atrial myocardium was derived from MRI data of a healthy subject.¹⁰⁴ Its numerical implementation comprised 2590 triangular elements (1297 vertices), representing both the epicardial and endocardial surface.

The geometry of the atrial model was fitted to the individual geometries of the subjects, aiming at matching size, location and orientation of the atria with reference to the ventricles and the lungs.

5.3.3 Simulated atrial fibrillation

The study required the body surface potentials over the entire surface of the thorax. Since no such data are available, the alternative used was to generate the episodes of atrial activity by a previously developed biophysical model.

Full source description

Ten different variants of AF were generated by means of the biophysical model. To this end, heterogeneities in action potential duration were introduced by changing the local electrophysiological properties of the cells, as described previously.^{36,105}

The model of atrial morphology comprised 800,000 coupled units. The propagation of the electrical activation was derived from a reaction-diffusion system (in the monodomain framework). For each of the units, the membrane kinetics was based on the Courtemanche et al. model of human atrial myocytes.¹⁶ AF was initiated through rapid pacing in the left atrium appendage. During AF, after the pacing protocol was stopped, the data during a time interval of 10 seconds were extracted for subsequent analysis. The AF signals produced by the model have shown to be in full qualitative agreement with those observed clinically.⁵¹ The 10 variants of AF were found to differ, depending on the arrhythmogenic substrate that was used in order to make the model vulnerable to AF. The differences showed up in the dynamics of the depolarization waves, the number of wavelets and their wavelength.⁵³

The electrical activity of the entire ensemble of 800,000 units was represented by the equivalent double layer (EDL).^{30,104} This expresses the electric activity within the atrial myocardium by a double layer source on the surface bounding the atria (endocardium and

epicardium: 1297 nodes), the local strength of which is proportional to the time course of the local transmembrane potential, $V_m(t)$. The numerical representation of the double layer is the source matrix \mathbf{S} (size: $1297 \times 10,000$), whose element $s(n, t)$ is the source strength at node n of the atrial surface at time instant t within the 10 s episode, sampled at 1000 sps.¹⁰⁴

The equivalent dipole

The equivalent dipole representation of the source matrix \mathbf{S} is computed with

$$\vec{D}_{\text{eq}}(t) = \sigma \int_{S_a} V_m(t) d\vec{S}. \quad (5.12)$$

This expression is similar to 5.10, but here the integration is carried out over the bounding surface of the atria (epicardium and endocardium) and the integral is the local transmembrane potential. An example of this equivalent dipole components is shown by the solid lines in figure 5.1.

5.3.4 Body Surface Potentials during AF

Body surface potentials generated by atrial electric activity depend on the magnitude and nature of the electric sources as well as on the properties of the volume conductor that governs the transfer from source elements to the potentials at the observation points. In this study, the transfer from the double layer sources \mathbf{S} to the potentials on the body surface was computed by means of the boundary element method (BEM).³³ The result is described by a linear transfer, which is represented by a matrix \mathbf{A} , (size: 642×1297). It accounts for the major effects of the conductive properties of the body tissues: those of the lungs and cardiac cavities. Each row of \mathbf{A} is the contribution of all the source elements to a field point on the body surface (electrode position), and each column is the contribution of one source element to all the field points on the body surface. The resulting body surface potentials Ψ are computed as

$$\Psi = \mathbf{A}\mathbf{S}. \quad (5.13)$$

A total of $T = 10,000$ body surface potential maps (10 seconds of simulated AF sampled at 1000 sps) were computed and documented at each of the 642 locations over the surface of the thorax; has size $(642 \times T)$. Individual transfer matrices \mathbf{A}_i ($i = 1, \dots, 25$) were computed for all 25 volume conductor models. For each variant j , ($j = 1, \dots, 10$) of the different types of simulated AF, the potential was computed, resulting in the 250 potential matrices $\Psi_{i,j} = \mathbf{A}_i\mathbf{S}_j$.

A low-pass moving averaging filtering over 20 samples, having a first cutoff frequency at 50 Hz, was applied to all signals. This preprocessing was necessary in order to suppress the effect of discretization noise of the simulation. Examples of the variants of the simulated

AF are presented in figure 5.2. The variant shown in (the top) row (A) was used in all various steps of the design procedure.

5.3.5 Design of the Lead Systems

The gold standard

The framework of vectorcardiography implies a single current dipole as the source, placed inside a homogeneous volume conductor. The gold standard in this study is the equivalent dipole estimated by the Gabor-Nelson equations 5.10 as discussed above,

$$\mathbf{D}_{\text{GN}} = \mathbf{S}_b \boldsymbol{\Psi}, \quad (5.14)$$

with \mathbf{S}_b , the matrix of body surface normals, and $\boldsymbol{\Psi}$, the matrix of simulated body surface potentials during AF. In spite of the implied homogeneity, the Gabor-Nelson estimate proved to come close to the ‘true’ equivalent dipole computed by using equation 5.12. This can be seen by comparing the Gabor-Nelson based estimate, shown in figure 5.1 by the dotted lines, with the solid line for the ‘true’ equivalent dipole.

Electrode configurations

Six different electrode montages were studied, namely the ones shown in figure 5.3, drawn on the thorax of subject RS. These are those of: (A) the Frank lead system as well as a modified version of it, (B) the result of a search procedure, (C) the standard 12-lead ECG, (D) the ACG lead system⁴⁷ and (E) the OACG lead system.⁴⁹

The modified Frank lead system, (A2), is a heuristic adaptation of Frank’s electrodes, (A1), in which the electrodes in the horizontal plane, *i.e.* A, C, E, I, and M, are moved up by one intercostal space.

(B), is the result of search procedure described in a subsequent section.

The ACG lead system, (D), is a montage that was conceived heuristically so as to increase the information content of the ECG on atrial electric activity; it is currently tested in clinical applications. It uses the same number of electrodes, 9, as used for the standard 12-lead ECG and has 5 of its electrodes, VR, VL, VF, V1 and V2 anchored to their standard positions.

The OACG (Optimized ACG) montage (E) is a lead system aimed at maximizing the information extraction of atrial fibrillation, also anchored to some of the locations used in the standard 12-lead ECG. The locations of four electrodes were optimized, while leaving the remaining 5 electrodes, VR, VL, VF, V1 and V4 in place. The reason for including V1 and V4 is that, among the six precordial leads, their signals showed the lowest correlation during AF, thus promising maximal independent information on AF.

The optimal electrode configuration would be the one using all 642 electrode positions. A less demanding electrode configuration is that of the 64 electrodes used in Body Surface

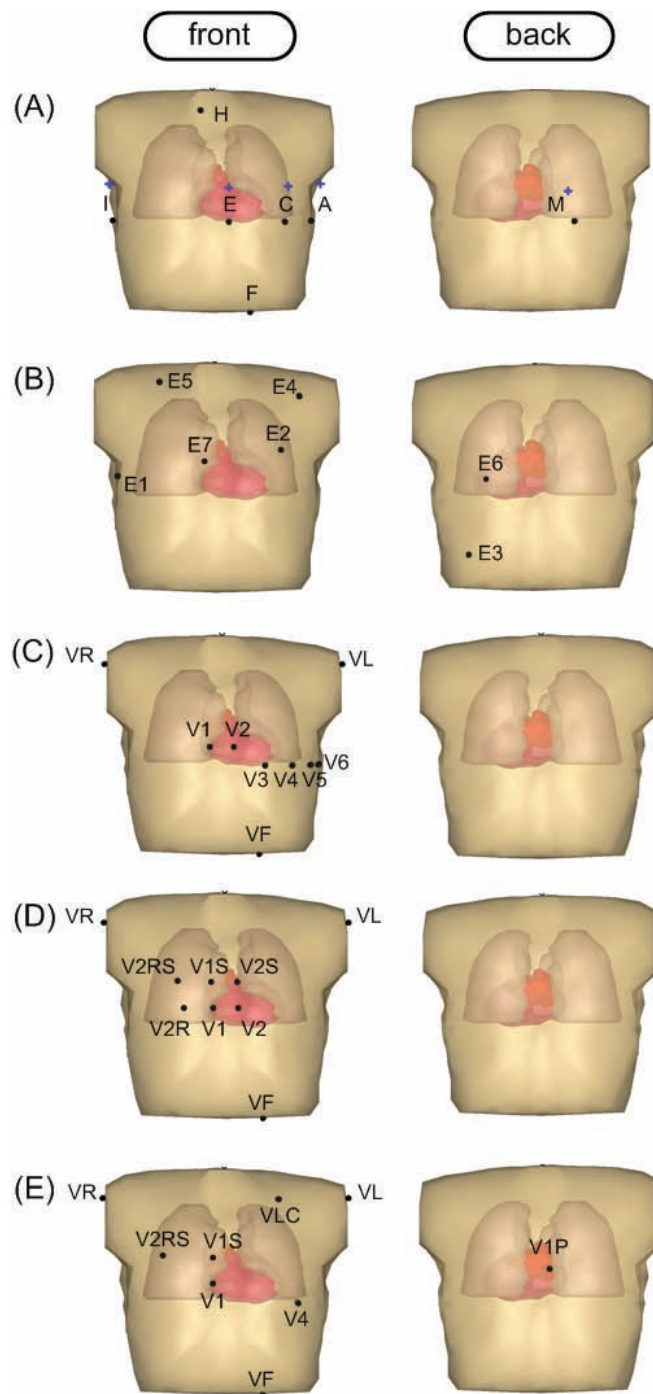


Figure 5.3 – The electrode montages studied, displayed on the biophysical model of the human thorax. The geometries shown are those of the thorax, the lungs, the atria, the ventricles and the blood-filled cardiac cavities. The black dots indicate the positions of the electrodes. (A) The Frank lead system and the modified Frank lead system. The modified one has the five electrodes of the horizontal plane shifted one intercostal space up to the level of the atria. (B) The optimized 7-electrode lead system. (C) The standard 12-lead ECG system. (D) The ACG lead system. (E) The OACG lead system.

Potential Mapping (BSPM) systems.^{37,86} To test the quality of the resulting estimate, the potentials at all 642 nodes on the thorax were derived from an interpolation procedure based on the surface Laplacian.⁷⁶ The equivalent dipole estimate was derived from the Gabor-Nelson equations applied to these interpolated data.

Dedicated transfer coefficient

For all 6 electrode montages shown in figure 5.3, dedicated transfer coefficients were computed, aimed at the analysis of AF signals. These were computed as $\mathbf{T} = \mathbf{D}_{\text{GN}} \Psi^t (\Psi \Psi^t)^\sharp$, as in equation 5.8, here with \mathbf{D}_{GN} and Ψ as in equation 5.13. Based on these matrices, the VCG type estimate of the dipole vector of an AF episode was

$$\mathbf{D}_{\text{est}} = \mathbf{T} \Psi_{i,j}. \quad (5.15)$$

In all of the various applications, matrix \mathbf{T} was scaled so that the sum of the squares of all elements of matrix \mathbf{D}_{est} was the same as that of the corresponding elements derived from the Frank lead system.

Performance Measure

The performance of the lead systems was quantified by the relative RMS difference, RD , defined as

$$RD = \frac{\|\mathbf{D}_{\text{GN}} - \mathbf{D}_{\text{est}}\|_{\text{F}}}{\|\mathbf{D}_{\text{GN}}\|_{\text{F}}}, \quad (5.16)$$

in which \mathbf{D}_{GN} and \mathbf{D}_{est} are the reference (*gold standard*) and the estimated dipole, respectively, and $\|\cdot\|_{\text{F}}$ is the Frobenius norm operator.

Searching for the optimal seven

The best lead system based on k electrodes positioned freely over the whole surface of the thorax (642 possible positions) would be the one that produces the lowest value of RD . For $k = 7$, the number of electrodes used by Frank, an exhaustive search for the optimal seven out of the 642 nodes on thorax would require over 8.6×10^{15} evaluations, taking more than 500,000 years of computation time. Instead, we performed a two-stage exhaustive search among a uniformly sub-sampled version of the 642 nodes on the thorax, comprising 162 nodes. This reduced the computation time to just two days. The initial four leads required for any vector lead system were selected exhaustively from the subset of 162 nodes. After accepting these four electrode positions, another three electrode locations were identified by an exhaustive search among the remaining $162 - 4 = 158$ locations.

5.3.6 Evaluation Method

The design of the transfer coefficients was based on the data of the reference subject (subject RS). The performance of each lead system was quantified by the RD values resulting from

their application to all 10 AF signals, for each of which the potential distributions $\Psi_{i,j}$ on all 24 thoraxes was simulated.

In addition, for each subject, the entire procedure was carried out separately based on his or her geometry (design stage) and the resulting lead systems were evaluated in their application to the thorax geometries of the other 24 subjects.

5.4 Results

5.4.1 Evaluation of the gold standard

The derivation of the Gabor-Nelson equations assumes a homogeneous volume conductor. However, different body tissues have different conductivity values, and the major ones of such inhomogeneities were included in the forward transfer used for computing the potentials Ψ by means of equation 5.13. Because of this it is not self-evident that the Gabor-Nelson estimate, \mathbf{D}_{GN} , would come close to the equivalent dipole \mathbf{D}_{eq} . The evaluation of this aspect yielded the following results.

The time courses of the equivalent dipole components of the atrial sources during AF, computed on the basis of equation 5.12, and their estimates used as the gold standard derived from the Gabor-Nelson equations, equation 5.14, were found to be very similar, as shown in figure 5.1. The correlation coefficients of the paired vector components of the X, Y, Z signals shown were 0.98, 0.96 and 0.96, respectively; the corresponding RD values were 0.43, 0.31 and 0.34. Similar values were found for all other episodes and all 10 different variants of simulated AF studied. Based on the observed similarity, the Gabor-Nelson based estimate was accepted as the gold standard in this research.

The computation of the Gabor-Nelson based estimate requires the full potential distribution on the thorax as well as the individual thorax geometry to be known (equation 5.14). As in the Frank system, the lead systems documented in this paper involve just a crude sampling of the potential distribution on the thorax, and, moreover, are aimed at applications that ignore individual thorax geometry, the “one lead system fits all” principle. Before presenting the results pertaining to these limited lead systems, the consistency and quality of the design procedure is documented here. First, a single matrix of transfer coefficients and resulting \mathbf{D}_{est} was computed based on the geometry of subject RS. The resulting RD value was 0.018 (left solid bar in figure 5.4; first row, first column of table 5.4). Next, this matrix was tested in its application to the potentials of all remaining 24 subjects. The mean of the RD values found was 0.052 (left open bar in figure 5.4; left column of table 5.4). This demonstrates that if the full potential distribution is available, the use of a single matrix is acceptable. Next, in a similar fashion, the effect of reducing the number of electrodes to 64, the number involved in some of the body surface potentials mapping systems, was studied. The results are listed in columns 2 and 3 of table 5.4 and the corresponding bars are indicated in figure 5.4. The results of two different procedures are shown. In the first one, the potentials at all 642 nodes were derived from the 64 nodes of the BSPM configuration

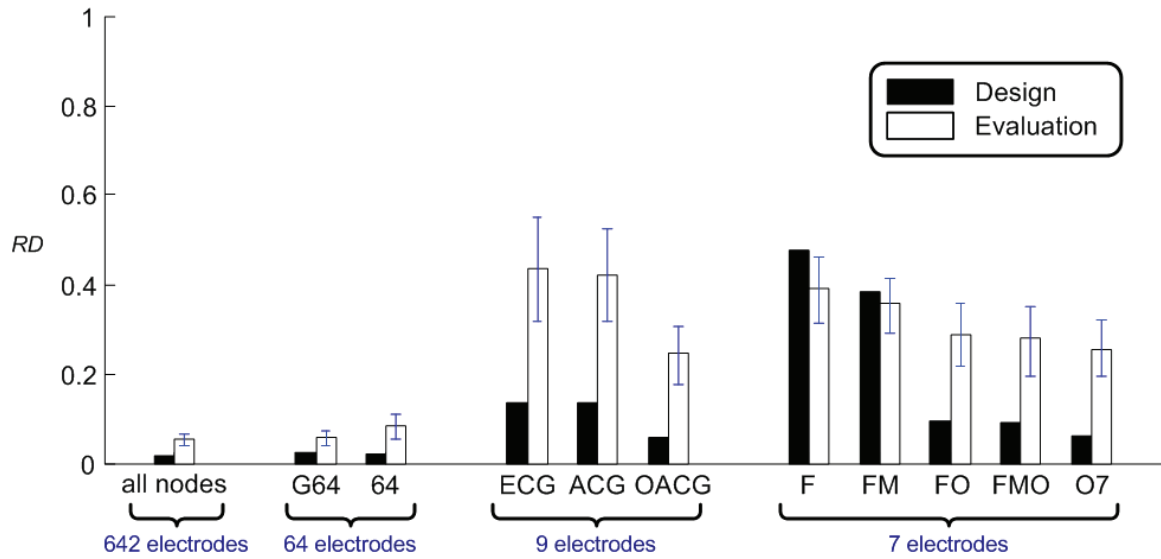


Figure 5.4 – The performance of the lead systems expressed as the relative RMS differences RD between the estimated and the gold standard dipole components. The black bars relate to the RD value for subject RS, the final residual of the designing stage. The white bars are the mean values for the single, dedicated transfer coefficients tested on all 10 variants of AF, each of which computed on 24 different models of the thorax. The error bars are the interquartile ranges.

by means of the surface Laplacian based interpolation method. The estimate employed the individual thorax geometries. In the second procedure, a single transfer matrix was derived, based on the thorax geometry of subject RS.

5.4.2 Dedicated transfer coefficients

The matrices of the transfer coefficients derived from equation 5.8, based on the geometry of subject RS and dedicated to the various electrode montages shown in figure 5.3, are presented in table 5.2 and 5.3. The first three matrices involve seven electrodes, as in Frank’s system. The first one of these relates to the standard electrode positions of the Frank system, now dedicated to the atrial VCG during AF (figure 5.3A, dots). The second relates to the situation where the electrodes in the transverse plane have been moved up one intercostal space (figure 5.3A, crosses). The third relates to the locations identified in the two-stage exhaustive search.

The final three matrices involve 9 electrodes, as in the standard 12 lead-ECG. The first of these relates to the positions of the standard electrodes, figure 5.3C, the second to the ACG configuration (figure 5.3D) and the final one to the OACG configuration (figure 5.3E). Note that all of these satisfy the constraint expressed by equation 5.4: the sum of all row elements is zero.

Dedicated Frank							
	A	C	E	F	H	I	M
x	0.5467	0.7668	-0.4318	-0.1912	-0.0427	-0.7199	0.0722
y	-0.6354	-0.1003	-0.0403	1.7631	-0.4820	-0.1703	-0.3348
z	0.9500	-0.2713	-0.7001	-0.7633	-0.3951	0.3269	0.8528

Dedicated Frank Modified							
	A*	C*	E*	F	H	I*	M*
x	0.6274	0.3511	-0.2957	0.1204	0.0003	-0.5066	-0.2969
y	-0.5729	0.2302	-0.0401	1.0745	-0.4662	-0.2259	0.0005
z	0.6772	-0.1290	-0.6769	-0.1088	-0.2849	0.0497	0.4727

Dedicated Optimized 7-electrode							
	E1	E2	E3	E4	E5	E6	E7
x	-0.9253	-0.0529	0.4072	0.6444	-0.1913	0.0312	0.0867
y	0.5279	-0.1142	0.8528	-0.3255	-0.9214	-0.0795	0.0599
z	0.5489	-0.3543	-0.3258	-0.0200	-0.0656	0.7012	-0.4845

Table 5.2 – *The transfer coefficients adapted for the described lead systems using 7 electrodes. The rows refer to the orthogonal dipole components; the columns to the electrodes of the montages. The directions are those of the standard VCG protocol, pointed toward the left (x), foot (y), and to the back (z). When applied to measured potentials, the unit of the estimated dipole components have been scaled so as to be the same as in the original Frank VCG system [mV].*

5.4.3 The optimal 7-electrode montage

The locations of the electrodes found by means of the two-stage, exhaustive search are shown in figure 5.3B. The electrodes E1 – E4 are the initial four electrodes, and E5 – E7 are the three ones added in the second stage of the search. This configuration relates to the optimal positions found for the reference subject RS. When the same search was performed on the ECG and geometries of the other 24 subjects, the precise locations found showed substantial individual differences. However, the main features of the patterns were similar, demanding at least one electrode on the back.

Dedicated ECG									
	V1	V2	V3	V4	V5	V6	VR	VL	VF
x	-0.1945	0.0328	0.0597	0.2633	0.3079	0.3973	-0.6119	0.3392	-0.5938
y	0.3386	-0.1329	-0.0555	-0.2779	-0.1318	0.4412	-0.5936	-0.8563	1.2681
z	0.1033	-0.0113	-0.5413	-1.1370	-1.0640	0.6810	-0.1587	0.4030	1.7249

Dedicated ACG									
	V1	V2	V2S	V1S	V2RS	V2R	VR	VL	VF
x	-0.2483	0.3510	-0.1903	0.2569	0.1121	-0.2534	-0.9206	0.8212	0.0715
y	-0.0185	0.0289	-0.1464	-0.1793	0.1096	0.3355	-0.7433	-0.4629	1.0764
z	1.1642	-0.4857	-0.9338	0.9926	-1.6420	-1.2647	1.2878	0.2036	0.6778

Dedicated OACG									
	V1	V4	V1P	V1S	V2RS	VLC	VR	VL	VF
x	-0.1411	0.3008	-0.0691	0.1543	-0.2259	-0.2070	-0.5909	0.8909	-0.1121
y	-0.0048	0.4656	0.0356	-0.1315	0.0222	-0.5756	-0.2472	-0.2971	0.7327
z	-0.1967	-0.1670	0.4971	-0.3913	0.1565	-0.5180	0.0343	0.7033	-0.1182

Table 5.3 – *The transfer coefficients adapted for the described lead systems using 9 electrodes. The rows refer to the orthogonal dipole components; the columns to the electrodes of the montages. The directions are those of the standard VCG protocol, pointed toward the left (x), foot (y), and to the back (z). When applied to measured potentials, the unit of the estimated dipole components have been scaled so as to be the same as in the original Frank VCG system [mV].*

5.4.4 Performance

The RD values found for the various lead systems are presented in figure 5.4, with their corresponding numerical values as documented in table 5.4. The RD values are derived from the pooled data of all 10 variants of AF, computed over the entire 10 s intervals. The solid bars in figure 5.4 represent the RD values based on the data of subject RS (design set), for which the various transfer coefficients are documented in Table 5.2. The open bars represent the RD values resulting from the application of the respective transfer coefficients to the signals of the 24 remaining subjects.

	642	G64	64	ECG	ACG	OACG	F	FM	Fd	FMd	O7
Desn.	0.018	0.024	0.020	0.134	0.137	0.059	0.474	0.383	0.095	0.090	0.061
Eval.											
mean	0.052	0.056	0.083	0.430	0.413	0.242	0.390	0.355	0.282	0.278	0.249
25%	0.017	0.016	0.032	0.117	0.115	0.073	0.077	0.066	0.076	0.086	0.061
75%	0.013	0.016	0.026	0.119	0.106	0.063	0.071	0.058	0.071	0.069	0.068

Table 5.4 – Numerical values of the results depicted in figure 5.4. The performance of the lead systems expressed by the relative difference between the estimated and the gold standard dipole components. The values are specified as mean the interquartile range.

5.4.5 Validation

The RD values found for the various lead systems as documented in the preceding sub-section were based on the geometry of the reference subject RS. The latter geometry was selected as the median of a spectrum ranging from lean to obese morphology. Even so, this choice may be biased when comparing the qualities of the respective lead systems. To study this, the entire design and evaluation procedure was repeated by taking each of the individual geometries as the reference, and documenting the performance of the application of the individual transfer coefficients to all remaining 24 subjects. The results are presented in a similar way as in the preceding sub-section: a bar diagram in figure 5.5 and corresponding numerical values as documented in table 5.5. The solid bars represent the RD values of the design stage of each of the 24 subjects. The open bars relate to the evaluation stage for these respectively designed lead systems: the means of the performances resulting from selecting each of lead systems and applying them to the remaining 24 subjects.

5.5 Discussion

The analysis presented in this paper emphasizes the fact that the VCG should be viewed as the result of an inverse procedure aimed at estimating the equivalent current dipole of cardiac electric activity. Like in all other types of inverse procedures,^{15,17,18,34,46,67,71,82} the accuracy of the estimate deteriorates if **1**) fewer electrodes are sampling the potential field, **2**) modeling errors are involved (inhomogeneity is discarded), or, **3**) a standard, non-tailored geometry of the volume conductor is used, the “one set of transfer coefficient serves all” principle. All of these points are reflected in the increase in the RD values shown in table 5.4 and 5.4. Even in the tailored design the results shown by the solid bars, the RD increased. This is even more noticeable when reducing the number of electrodes from 9, as in the standard 12-lead system, to 7, as in Frank’s lead system.

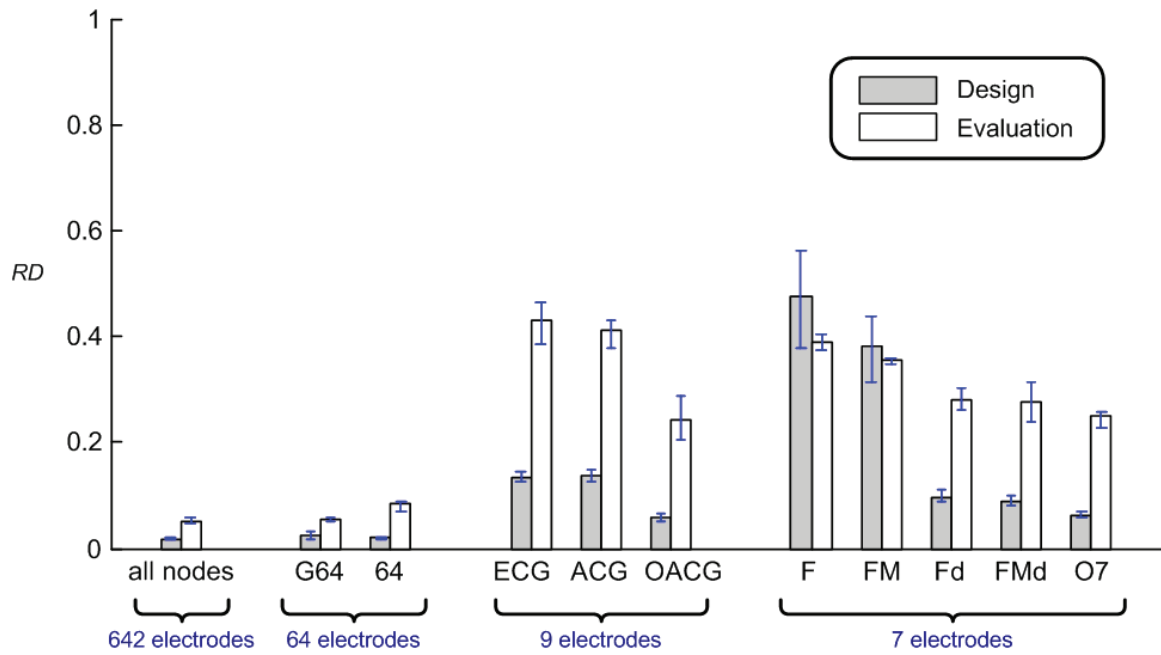


Figure 5.5 – The deviations of the estimation performance. The bars are those of figure 5.4. The error bars on the gray bars relate to the RD values of the 24 subjects during the design stage. The error bars on the white bars are the ranges of the mean RD for each new transfer coefficients and lead system designed on the individual thorax model applied to the remaining 24 models. They represent the mean \pm interquartile range

	642	G64	64	ECG	ACG	OACG	F	FM	Fd	FMd	O7
Desn.											
mean	0.018	0.024	0.020	0.134	0.137	0.059	0.474	0.383	0.095	0.090	0.061
25%	0.001	0.005	0.002	0.010	0.010	0.007	0.095	0.068	0.008	0.009	0.002
75%	0.001	0.008	0.002	0.011	0.013	0.008	0.088	0.054	0.015	0.010	0.007
Eval.											
mean	0.053	0.057	0.085	0.295	0.397	0.224	0.391	0.356	0.315	0.273	0.193
25%	0.005	0.005	0.012	0.044	0.034	0.037	0.016	0.009	0.020	0.040	0.021
75%	0.005	0.004	0.006	0.033	0.016	0.048	0.014	0.006	0.022	0.035	0.010

Table 5.5 – Numerical values of the results depicted in figure 5.5. The deviations of the mean RD performance for each new transfer coefficients and lead system designed on the individual thorax model applied to the remaining 24 models. The values are given as the mean \pm the interquartile range.

The analysis used the Gabor-Nelson based estimate as the gold standard. This proved to yield time courses of the components of the derived dipole that came close to those of the

equivalent dipole (figure 5.1). In particular, the wave forms were very similar (high correlation coefficients). The relatively high RD values may be attributed to the inhomogeneities of the conductivity. This was confirmed by recomputing the Gabor-Nelson estimate, now based on the potentials simulated for a homogeneous thorax. Here all three correlation coefficients increased to values higher than 0.99 and the corresponding RD values decreased to values below 0.016.

The various transfer matrices dedicated to the various electrode montages studied were derived while including the constraint of zero row sums, equation 5.4. As a consequence, the transfer matrix may be applied to the potentials at the electrodes, irrespective of the potential reference, be it WCT, zero mean, or any of the electrodes involved. In the latter situation, the potential values at the electrode chosen as the reference will be included in the computation (equation 5.15) as a zero vector.

Of the 7-electrode systems studied, the optimal 7-lead system (optimal 7) had the lowest RD values. However, compared to the modified (shifted) version with dedicated transfer coefficients, the difference was not found to be significant ($p = 0.18$). Moreover, when repeating the design procedure for the optimal 7, the electrode locations identified for different thorax geometries were never the same. This suggests that the montage of the shifted transverse electrodes, and its dedicated transfer coefficients are the optimal choice, since its locations are easily adapted from the traditional locations introduced by Frank. Note that, (figure 5.4), with the shifted electrode positions and dedicated transfer coefficients, the RD values decreased significantly ($p = 0.004$).

Among the montages involving nine electrodes, the lead system OACG yielded the smallest RD values (figure 5.4; table 5.4), values that were smaller than those of the optimal 7. This demonstrates that transfer coefficients for the estimation of the VCG on the basis of the signals of the 9 electrodes of the 12-lead ECG should be derived in the straightforward manner using the methods presented in this paper, rather than by adapting previously published estimates based on fewer electrodes. When applied to the 4 electrode positions of the so-called EASI lead system (not treated here), the performance RD values for subject RS increased by a factor of 3.7 with respect to those of the modified, dedicated Frank lead system.

Among the adapted lead systems, there is a considerable difference between the ones that have at least one electrode on the back (Frank, OACG, Optimized 7-electrodes) and those without (ECG, ACG). This means that the distributed nature of the atrial electric activity during AF demands a more complete three-dimensional capture of information around the thorax, thus necessitating at least one electrode placed on the back.

The result found from the additional evaluation, based on the other 24 thorax geometries were essentially the same as the ones found in subject RS. However, for all OACG lead systems designed on each of the 24 thoraxes, the spread of the interquartile range of the RD values, when tested on all other thoraxes, was found to be larger than that by using the dedicated transfer coefficients of the subject RS. In other words, the lead system designed on this mesomorphic subject was the most robust at the evaluation stage. This also justifies

the selection and evaluation of the various lead systems specified by the transfer coefficients documented in table 5.2 and 5.3.

5.6 Limitations

A single biophysical model of human atria was fitted to the available, MRI based geometry of the ventricles of all subjects. However, within the framework of the present study, this did facilitate the study of the volume conduction properties of the different thorax models as such, since it avoided the effect of the additional variability on that of the simulated potentials. The simulation of the body surface potentials accounted for the inhomogeneities due to lungs and cavities only. Possible effects of other inhomogeneities, like those of bone, fat and major vessels, as well as that of the anisotropic properties of skeletal muscle, were ignored. The model used has previously been found to yield highly realistic atrial signals.¹⁰⁴

During AF, no clinical body surface potential distributions over the entire thorax during AF were available. We are currently developing a method to separate the atrial and ventricular contributions to the 12-lead ECG, recorded in a clinical study of AF both from the traditional electrode locations and the other electrode montages discussed in this chapter. These data will be used in a comparison of the performance in clinical applications of the lead systems discussed.

5.7 Conclusion

The methodology required for a model-based design of leads systems dedicated to the analysis of the VCG during AF was discussed.

The estimate of the equivalent dipole derived from the Frank lead system was shown to be suboptimal in the estimation of the VCG during AF. Among the various lead systems studied for this purpose, the superior one was the OACG system, an electrode montage which includes five of the traditional electrode positions: VR, VL, VF, V1 and V4, and four additional locations. The inclusion of at least one electrode on the back, at the level of V1, proved to be essential for a limited lead system aimed at observing the dipolar activity of the atria during AF.

Conclusions

6

6.1 Achievements

THE surge of interest that can be witnessed today regarding atrial arrhythmias justifies the initiative of the Lausanne Heart group and its persistent commitment to the understanding and analysis of atrial fibrillation.

The principal contribution of the work presented in this thesis lies in the design of a novel lead system dedicated to the analysis of atrial fibrillation and evaluation of its performances with clinical and simulated signals. The main contributions of these studies as mentioned in the previous chapters are as follows.

6.1.1 Chapter 2

Atrial repolarization as observable during the PQ interval

In this chapter, the objective was to find the involvement of atrial repolarization in the body surface potentials, a process that was so far considered to be entirely masked by the ventricular components, the QRS complex.

Electrocardiograms of 73 healthy subjects were recorded using 64-lead systems. The data analysis focused on the PQ intervals, while devoting special attention to the low-amplitude signals during the PQ segment: the segment from the end of the P wave till onset QRS. The data were analyzed by inspecting body surface potential maps and the *XYZ* signals of the vectorcardiogram.

The results demonstrated a significant involvement of atrial repolarization during the

PQ interval. It confirmed the presence of the essentially discordant “atrial T waves”, which are visible on the body surface potentials when appropriate signal processing procedures of low-level signals are applied. The observation suggests a small dispersion of atrial action potential duration as well as its much shorter duration than what is used in common cellular models.

The local potential extremes during the depolarization and repolarization were found at positions not sampled by the standard 12-lead ECG, implying the sub-optimality of this standard lead system for studying the electric activity of the atria.

A method was introduced for the handling of the directional statistics over an arbitrary shaped surface involved in the analysis of vectorcardiograms.

6.1.2 Chapter 3

Adaptation of the standard 12-lead ECG system dedicated to the analysis of atrial fibrillation

This chapter presented the design process of a new lead system aimed at optimizing the information extraction of atrial fibrillation, and its evaluation using the biophysical model of the human atria and thorax.

The location of 4 of the 6 precordial electrodes was optimized while leaving the remaining 5 of the 9 electrodes of the standard 12-lead system in place. The analysis was based on episodes of 11 different variants of AF simulated with a biophysical model of the atria positioned inside an inhomogeneous thorax. The optimization criterion used was derived from the singular value decomposition of the data matrices.

While maintaining VR, VL, VF, V1 and V4, the 4 new electrode positions increased the ratio of the eighth to the first singular values of the data matrices of the new configuration about five-fold compared to that of the conventional electrode positions. The locations of the electrodes of the standard 12-lead system were shown to be clearly suboptimal, while the proposed adaptation, the *OACG lead system*, provides more information on the atrial electric activity during fibrillation. Its electrode locations are anchored to those of the electrodes of the standard leads and can be used in clinical practice using the standard equipment.

The adapted lead system produces a more complete view on AF compared to that of the conventional the standard 12-lead system.

6.1.3 Chapter 4

Performance of a lead system dedicated to atrial fibrillation: application to clinical data

The OACG lead system was designed and evaluated in chapter 3 in a biophysical-model study by comparing its performance to those of the standard 12-lead ECG and the previous-

ly designed ACG lead system. This chapter presented the application of the lead systems to the clinical data. The database comprised the recordings of 32 patients during AF, of which 30 patients from whom data with the standard ECG and ACG were recorded, and 2 patients from whom data with all three lead systems were documented.

Clinical recordings of AF are perturbed by the ventricular components. In order to dissociate the atrial contribution, a VA cancellation method was applied to each of the signals providing 5-minute sequences of uncontaminated AF episodes.

A complexity index, defined as the optimization criterion in chapter 3, was computed for the AF signals. The stationarity of this value was studied by segmenting the 5-minute sequence into segments of 10 seconds.

Signals recorded with the OACG lead system allowed for an enhancement of AA through application of the VA cancellation method. The results showed a clear superiority of the OACG lead system under visual inspection with respect to the cancellation of the artifacts.

Within the limitation of the small number of recordings, signals observed with the OACG lead system provided constantly larger values of the normalized singular values and the complexity index compared to those with the standard ECG and ACG. The ACG exhibited a 1.34-fold larger value in the paired statistics of α_8 with respect to the standard ECG, while the OACG lead system presented a 1.82-fold improvement.

The application of the OACG lead system to patients in AF admitted to the hospital emergency room have experienced no problem so far. The original intention of leaving 5 of the 9 electrodes anchored to the conventional positions made the adaptation of recording smooth, and, notably, the inclusion of one electrode on the back showed no difficulty in its application.

6.1.4 Chapter 5

Vectorcardiographic lead systems for the characterization of atrial fibrillation

For the vectorcardiographic representation of the electric dynamics generated by the atria, the objective of this study was to design a VCG lead system dedicated to the analysis of atrial fibrillation.

Body surface potentials during atrial fibrillation were simulated by using a biophysical model of the human atria and thorax. The XYZ components of the equivalent dipole were derived from the Gabor-Nelson equations. These served as the gold standard while searching for methods for the derivation of the vectorcardiogram from a limited number of electrode positions and their transfer coefficients. Six electrode configurations and dedicated matrices were tested using 10 different episodes of simulated AF and 25 different thorax models.

The methodology required for a model-based design of leads systems dedicated to the

analysis of the VCG during AF was discussed, notably the gold standard using the Gabor-Nelson equations as the reference dipole components was substantiated.

The estimates of the equivalent dipole derived from the Frank lead system and the standard 12-lead ECG system were shown to be suboptimal in the estimation of the VCG during AF. An adaptation of the 9 electrodes of the standard ECG, the OACG lead system, reduced the RMS-based relative estimation error by 40 % compared to the conventional Frank lead system and its original transfer coefficients. Significantly, the recent trend of ‘*derived*’ lead systems for computing the VCG is severely questioned.

The inclusion of at least one electrode on the back, at the level of V1, proved to be essential for a limited lead system aimed at observing the dipolar activity of the atria during AF.

6.1.5 Answers to the questions

Q: What can we see of atrial electric activity on the body surface?

A: The two principal features of the atrial activity, depolarization *and* repolarization, can be observed on the body surface potentials. In a normal cardiac cycle, depolarization was observed from the onset of the activation followed by the repolarization as potential extremes of opposite polarity at locations not covered by the standard 12-lead ECG lead system. The VCG representation at the time instants of the extreme potentials showed opposite directions. This signifies a small dispersion of the APD value of atrial cardiomyocytes.

Q: Can we learn more about atrial fibrillation from body surface potentials?

A: Yes. In all observations presented so far using both the simulated AF episodes and clinical recordings during AF, the standard 12-lead system was clearly suboptimal for the information content of AF that is available from the entire body surface potentials.

Q: How can we capture the information more effectively?

A: Within the limitation of clinical practice and current equipment using nine electrodes, the proposed OACG lead system offers an augmented capture of information of atrial activity during AF as well as a higher precision in the equivalent dipole estimation. One of the crucial issues is to have an electrode on the back of the thorax so as to catch the complex three-dimensional dynamics of AF.

6.2 Perspective

The entire study carried out by the Lausanne Heart group is advancing day by day. At its dawn, the concept of a biophysical model of the human atria manifesting propagation of

atrial fibrillation was constructed and tested on simple geometries and with elementary electrochemical kinetics.⁵ The use of a more realistic geometry and incorporation of elaborate mechanisms led to a recognition of the model in the medical field.⁵⁰ Concerning practical aspects, the model has been used in the investigation into possible therapies for atrial arrhythmias, such as radio frequency ablation or drug therapy, treatments which cannot be easily tested in the clinic due to its invasiveness.²⁰

The momentum of these activities fed the current study in which theoretical, practical and clinical aspects entwine and evolve in synergy; the development of the model by including fast conducting bundles and histological pathologies, the volume conductor aspects like those treated in this thesis in the expression of the electric source on the surface, and finally the classification of clinical AF signals using ventricular activity cancellation and feature extraction from ECG recordings.

As one may say, the results are never final.¹⁴ In a never-ending search for the best lead system, the inhomogeneity of the biophysical model can be enhanced by including the liver or fatty tissue such as the mammae. The differences of conductivity in these tissues are non-negligible and their effect supposedly large. The effect of the position of the atria inside the thorax needs as well be investigated as it is most essential in the framework of electric volume conduction.

The design of the OACG lead system was limited by self-imposed constraints. The possibility of other types of adaptation of the standard ECG, such as an added “12+n”-lead system or the optimization of the three limb leads, are potential topics that can be investigated by using the methods developed in this thesis.

Concerning chapter 4, the collection of clinical data of atrial fibrillation using the OACG lead system is in progress. The evaluation process will be repeated once a statistically sufficient number of recordings is attained.

The design and evaluation process of the new lead system are shown in detail in this thesis. The impact of the OACG lead system in terms of practical application is yet to be tested. For instance, classification and identification of atrial fibrillation types with respect to its etiology through feature extraction of body surface potentials is an interesting topic. The next milestone of this study would be the search for actual features in body surface potentials such as the bias of vector direction or the distribution of potential extremes during atrial fibrillation. These are studies that can be tested with more precision using the OACG lead system.

Bibliography

- [1] Committee of the american heart association for the standardization of precordial leads. supplementary report. *Am Heart J* 15 (1938), 235–239.
- [2] Report of committee on electrocardiography, american heart association. recommendations for standardization of leads and of specifications for instruments in electrocardiography and vectorcardiography. *Circulation* 35, 3 (1967), 583–602.
- [3] Consensus report: International guidelines 2000 for CPR and ECC, part 4: The automated external defibrillator: Key link in the chain of survival. resuscitation 2000;46:73-91. Tech. rep., 2000.
- [4] AKAIKE, H. A new look at statistical model identification. *IEEE Trans Auto Control* 19 (1974), 716–723.
- [5] BLANC, O. *A computer model of human atrial arrhythmias*. PhD thesis, Swiss Federal Institute of Technology Lausanne, 2002.
- [6] BRAHMS, J. *Ein deutsches Requiem*. Schneider, Basel, 1869. Nach Worten der heiligen Schrift, für Soli, Chor und Orchester, op. 45 aufgeführt vom Basler Gesangverein in der Kirche zu St. Martin, Mittwoch 24. März 1869.
- [7] CALVIN, J. *Joannis Calvini Commentarii in secundam Pauli epistolam ad Corinthios*. Jo. Gerard, Genevæ, 1548.
- [8] CALVIN, J. VII Election and Predestination. In *Calvin: commentaries*, J. Haroutunian, Ed., new ed., vol. 23 of *The Library of Christian classics*. Westminster Press, Philadelphia, 1979.
- [9] CAMUS, A. *L'étranger*. Gallimard, Paris, 1942.
- [10] CAMUS, A. *La peste*. Gallimard, Paris, 1947.
- [11] CAMUS, A. *La chute*. Gallimard, Paris, 1956.
- [12] CARROLL, L., AND TENNIEL, J. *Alice's adventures in Wonderland*. Macmillan, London, 1865.

-
- [13] CHUNG, M. K. Current clinical issues in atrial fibrillation. *Cleve Clin J Med* 70 Suppl 3 (2003), S6–11.
- [14] CLAUSEWITZ, K. v. *Vom Kriege*. Dümmlers Verlag, Berlin, 1832.
- [15] COLLI-FRANZONE, P. C., GUERRI, L., TACCARDI, B., AND VIGANOTTI, C. *The direct and inverse potential problems in electrocardiology. Numerical aspects of some regularization methods and application to data collected in dog heart experiments*. I.A.N.-C.N.R., Pavia, 1979.
- [16] COURTEMANCHE, M., RAMIREZ, R. J., AND NATTEL, S. Ionic mechanisms underlying human atrial action potential properties: insights from a mathematical model. *Am J Physiol* 275, 1 Pt 2 (1998), H301–21.
- [17] CUPPEN, J. J. M. *A Numerical Solution of the Inverse Problem of Electrocardiography*. University of Amsterdam, Amsterdam, The Netherlands, 1983. Ph.D. Thesis.
- [18] CUPPEN, J. J. M., AND VAN OOSTEROM, A. Model studies with the inversely calculated isochrones of ventricular depolarization. *IEEE Trans Biomed Eng BME-31* (1984), 652–659.
- [19] DAMBROGGI, L., MUSSO, E., AND TACCARDI, B. Body-surface mapping. In *Comprehensive electrocardiology, volume II*, P. W. Macfarlane and T. D. V. Lawrie, Eds. Pergamon Press, Oxford, 1989, pp. 1015–1049.
- [20] DANG, L. *An investigation into therapies for atrial arrhythmias using a biophysical model of the human atria*. PhD thesis, Swiss Federal Institute of Technology Lausanne, 2005.
- [21] DOWER, G. E., YAKUSH, A., NAZZAL, S. B., JUTZY, R. V., AND RUIZ, C. E. Deriving the 12-lead electrocardiogram from four EASI electrodes. *J Electrocardiol* 21 Suppl (1988), S182–7.
- [22] DOWNS, T. D., AND LIEBMAN, J. Statistical methods for vectorcardiographic directions. *IEEE Trans Biomed Eng* 16, 1 (1969), 87–94.
- [23] DRAPER, H. W., PEFFER, C. J., STALLMANN, F. W., LITTMANN, D., AND PIPBERGER, H. V. The corrected orthogonal electrocardiogram and vectorcardiogram in 510 normal men (Frank lead system). *Circulation* 30 (1964), 853–64.
- [24] EINTHOVEN, W. Die galvanometrische Registrierung des menschlichen Elektrokardiogramms, zugleich eine Beurtheilung der Anwendung des Capillarelektrometers in der Physiologie. *Pflügers Archiv für die Gesamte Physiologie des Menschen und der Tiere* 99, 472–480 (1903).
- [25] FEILD, D. Q., FELDMAN, C. L., AND HORACEK, B. M. Improved EASI coefficients: their derivation, values, and performance. *J Electrocardiol* 35 (2002), S23–S33.

- [26] FRANK, E. An accurate, clinically practical system for spatial vectorcardiography. *Circulation* 13, 5 (1956), 737–749.
- [27] FUSTER, V., RYDEN, L. E., ASINGER, R. W., CANNOM, D. S., CRIJNS, H. J., FRYE, R. L., HALPERIN, J. L., KAY, G. N., KLEIN, W. W., LEVY, S., MCNAMARA, R. L., PRYSTOWSKY, E. N., WANN, L. S., WYSE, D. G., GIBBONS, R. J., ANTMAN, E. M., ALPERT, J. S., FAXON, D. P., FUSTER, V., GREGORATOS, G., HIRATZKA, L. F., JACOBS, A. K., RUSSELL, R. O., SMITH, S. C., J., KLEIN, W. W., ALONSO-GARCIA, A., BLOMSTROM-LUNDQVIST, C., DE BACKER, G., FLATHER, M., HRADEC, J., OTO, A., PARKHOMENKO, A., SILBER, S., AND TORBICKI, A. ACC/AHA/ESC guidelines for the management of patients with atrial fibrillation: Executive summary a report of the American College of Cardiology/American Heart Association Task Force on Practice Guidelines and the European Society of Cardiology Committee for Practice Guidelines and Policy Conferences (committee to develop guidelines for the management of patients with atrial fibrillation) developed in collaboration with the North American Society of Pacing and Electrophysiology. *Circulation* 104, 17 (2001), 2118–50.
- [28] GABOR, D., AND NELSON, C. V. The determination of the resultant dipole of the heart from measurements on the body surface. *J Appl Phys* 25 (1956), 413–416.
- [29] GELBAND, H., BUSH, H. L., ROSEN, M. R., MYERBURG, R. J., AND HOFFMAN, B. F. Electrophysiologic properties of isolated preparations of human atrial myocardium. *Circ Res* 30, 3 (1972), 293–300.
- [30] GESELOWITZ, D. B. The concept of an equivalent cardiac generator. *Biomed Sci Instrum* 25 (1963), 325–30.
- [31] GOLUB, G. H., AND VAN LOAN, C. F. *Matrix computations*, 2nd ed. ed. John Hopkins University Press, 1989.
- [32] GRAY, H., AND LEWIS, W. H. *Anatomy of the human body*, 20th ed. Lea and Febiger, Philadelphia ; New York, 1918.
- [33] GULRAJANI, R. M. *Bioelectricity and Biomagnetism*. John Wiley and Sons, New York, 1998.
- [34] GULRAJANI, R. M., ROBERGE, F. A., AND SAVARD, P. The inverse problem of electrocardiography. In *Comprehensive Electrocardiology*, P. W. Marfarlane and T. D. Veitch Lawrie, Eds., vol. I. Pergamon Press, Oxford, 1989, pp. 237–288.
- [35] HEAMES, R. M., SADO, D., AND DEAKIN, C. D. Do doctors position defibrillation paddles correctly? observational study. *Bmj* 322, 7299 (2001), 1393–4.
- [36] HENRIQUEZ, C. S., AND PAPAZOGLU, A. A. Using computer models to understand the roles of tissue structure and membrane dynamics in arrhythmogenesis. *Proc IEEE* 84, 3 (1996), 334–354.

-
- [37] HERINGA, A., UIJEN, G., AND VAN DAM, R. T. A 64-channel system for body surface potential mapping. In *Electrocardiology*, Z. Antalóczy and I. Préda, Eds. Academia Kiado, Budapest, 1981, pp. 297–301.
- [38] HERMAN, M. V., INGRAM, D. A., LEVY, J. A., COOK, J. R., AND ATHANS, R. J. Variability of electrocardiographic precordial lead placement: a method to improve accuracy and reliability. *Clin Cardiol* 14, 6 (1991), 469–476.
- [39] HOEKEMA, R., HUISKAMP, G. J., OOSTENDORP, T. F., UIJEN, G. J., AND VAN OOSTEROM, A. Lead system transformation for pooling of body surface map data: a surface Laplacian approach. *J Electrocardiol* 28, 4 (1995), 344–345.
- [40] HOEKEMA, R., UIJEN, G., AND VAN OOSTEROM, A. The number of independent signals in body surface maps. *Methods Inf Med* 38, 2 (1999), 119–124.
- [41] HOEKEMA, R., UIJEN, G. J., VAN ERNING, L., AND VAN OOSTEROM, A. Interindividual variability of multilead electrocardiographic recordings: influence of heart position. *J Electrocardiol* 32, 2 (1999), 137–48.
- [42] HORÁČEK, B. M. Lead theory. In *Comprehensive Electrocardiology*, P. W. Marfarlane and T. D. Veitch Lawrie, Eds., vol. I. Pergamon Press, Oxford, 1989, pp. 291–315. 10.
- [43] HORÁČEK, B. M., WARREN, J. W., FEILD, D. Q., AND L., F. C. Statistical and deterministic approaches to designing transformations of electrocardiographic leads. *J Electrocardiol* 35 (2002), S41–S52.
- [44] HUGO, V. *Les misérables*. A. Lacroix Verboeckhoven et Cie., Bruxelles, 1862.
- [45] HUISKAMP, G., AND VAN OOSTEROM, A. The depolarization sequence of the human heart surface computed from measured body surface potentials. *IEEE Trans Biomed Eng* 35, 12 (1998), 1047–58.
- [46] HUISKAMP, G. J. M., AND VAN OOSTEROM, A. Heart position and orientation in forward and inverse electrocardiography. *Med. Biol. Eng. and Comput.* 30 (1992), 613–620.
- [47] IHARA, Z., JACQUEMET, V., VESIN, J., AND VAN OOSTEROM, A. Adaptation of the ECGs standard 12-lead system focusing on atrial electrical activity. In *Computers in Cardiology* (2005), vol. 32, pp. 203–205.
- [48] IHARA, Z., VAN OOSTEROM, A., AND HOEKEMA, R. Atrial repolarization as observable during the PQ interval. *J Electrocardiol* 39, 3 (2006), 290–297.
- [49] IHARA, Z., VAN OOSTEROM, A., JACQUEMET, V., AND HOEKEMA, R. Adaptation of the standard 12-lead ECG system dedicated to the analysis of atrial fibrillation. *J Electrocardiol* accepted (2006).

-
- [50] JACQUEMET, V. *A biophysical model of atrial fibrillation and electrograms: formulation, validation and application*. PhD thesis, Swiss Federal Institute of Technology Lausanne, 2004.
- [51] JACQUEMET, V., VAN OOSTEROM, A., VESIN, J. M., AND KAPPENBERGER, L. A biophysical model approach supporting the analysis of electrocardiograms during atrial fibrillation. *IEEE Eng Med Biol Mag* (2006).
- [52] JACQUEMET, V., VIRAG, N., IHARA, Z., DANG, L., BLANC, O., ZOZOR, S., VESIN, J. M., KAPPENBERGER, L., AND HENRIQUEZ, C. Study of unipolar electrogram morphology in a computer model of atrial fibrillation. *J Cardiovasc Electrophysiol* 14, 10 Suppl (2003), S172–9.
- [53] JACQUEMET, V., VIRAG, N., AND KAPPENBERGER, L. Wavelength and vulnerability to atrial fibrillation: Insights from a computer model of human atria. *Europace* 7 Suppl 2 (2005), 83–92.
- [54] JUNG, C. G. The gifted child. In *The development of personality*, G. Adler and R. F. C. Hull, Eds., 2nd ed., vol. 17 of *The Collected Works of C.G. Jung*. Routledge, London, 1991.
- [55] JUNG, C. G. Problems of modern psychotherapy. In *The practice of psychotherapy : essays on the psychology of the transference and other subjects*, G. Adler and R. F. C. Hull, Eds., 2nd ed., vol. 16 of *The Collected Works of C.G. Jung*. Routledge, London, 1993.
- [56] KANT, I. *Die Metaphysik der Sitten*. F. Nicolovius, Königsberg, 1797.
- [57] KAPPENBERGER, L. Arrhythmia: a therapeutic dilemma. In *Computer simulation and experimental assessment of cardiac electrophysiology*, N. Virag, O. Blanc, and L. Kappenberger, Eds. Futura Publishing Co., Inc., New York, 2001, pp. 185–188.
- [58] KEYS, A., FIDANZA, F., KARVONEN, M. J., KIMURA, N., AND TAYLOR, H. L. Indices of relative weight and obesity. *J Chronic Dis* 25, 6 (1972), 329–43.
- [59] LEMAY, M., JACQUEMET, V., FORCLAZ, A., VESIN, J. M., AND KAPPENBERGER, L. Spatiotemporal QRST cancellation method using separate QRS and T-waves templates, 2005.
- [60] LIVI, R. L'indice ponderale o il rapporto tra la statura. *Atti Soc Romana Antrop* 5 (1897), 125–153.
- [61] LUTHER, M. *Biblia: das ist die gantze Heilige Schrift*. Hans Lufft, Wittemberg, 1534.
- [62] MACFARLANE, P. W. Lead systems. In *Comprehensive electrocardiology: Theory and Practice in Health and Disease*, P. W. Marfarlane and T. D. Veitch Lawrie, Eds., vol. 1. Pergamon Press, Oxford, 1989, p. 315.

-
- [63] MACFARLANE, P. W., AND VEITCH LAWRIE, T. D. Diagnostic criteria. In *Comprehensive electrocardiology: Theory and Practice in Health and Disease*, P. W. Macfarlane and T. D. Veitch Lawrie, Eds., vol. 3. Pergamon Press, Oxford, 1989, p. 1528.
- [64] MALMIVUO, J., AND PLONSEY, R. *Bioelectromagnetism*. Oxford University Press, New York, 1995.
- [65] MANN, M. *Heat*. Warner Bros., 1995.
- [66] MARDIA, K. V. *Statistics of directional data*. Academic Press, London, 1972.
- [67] MARTIN, R. O. *Inverse Electrocardiography*. Duke University, Duke, NC; USA, 1970. Ph.D. Thesis.
- [68] MEISEL, W. S. *Computer-oriented approaches to pattern recognition*. Academic Press, New York, 1972.
- [69] MIRVIS, D. M. Body surface distribution of electrical potential during atrial depolarization and repolarization. *Circulation* 62, 1 (1980), 167–173.
- [70] MITCHELL, M. *Gone with the wind*. Macmillan, New York, 1936.
- [71] MODRE, R., TILG, B., FISCHER, G., HANSER, F., MESSARZ, B., AND SEGERS, J. Atrial noninvasive activation mapping of paced rhythm data. *J Cardiovasc Electrophysiol* 13 (2003), 712–719.
- [72] NATTEL, S. New ideas about atrial fibrillation 50 years on. *Nature* 415, 6868 (2002), 219–226.
- [73] NATTEL, S., AND EHRLICH, J. R. Atrial fibrillation. In *Cardiac Electrophysiology: from Cell to Bedside*, D. P. Zipes and J. Jalife, Eds., 4 ed. Saunders, W. B., Philadelphia, 2004, pp. 512–523.
- [74] NEMATI, M., DOYLE, J. T., McCAUGHAN, D., DUNN, R. A., AND PIPBERGER, H. V. The orthogonal electrocardiogram in normal women. implications of sex differences in diagnostic electrocardiography. *Am Heart J* 95, 1 (1978), 12–21.
- [75] OOSTENDORP, T. F., AND VAN OOSTEROM, A. Source parameter estimation in inhomogeneous volume conductors of arbitrary shape. *IEEE Trans Biomed Eng* 36, 3 (1989), 382–91.
- [76] OOSTENDORP, T. F., VAN OOSTEROM, A., AND HUISKAMP, G. Interpolation on a triangulated 3D surface. *J Comput Phys* 80, 2 (1989), 331–343.
- [77] PLONSEY, R. *Bioelectric phenomena*. McGraw-Hill, New York, 1969.
- [78] PLONSEY, R. Introductory physics and mathematics. In *Comprehensive electrocardiology: Theory and Practice in Health and Disease*, P. W. Marfarlane and T. D. Veitch Lawrie, Eds., vol. 1. Pergamon Press, Oxford, 1989, pp. 41–76.

-
- [79] PLONSEY, R., AND BARR, R. C. *Bioelectricity, a quantitative approach*, 2 ed. Kluwer Academic / Plenum Publishers, New York, 2000.
- [80] POGGIO, T., AND GRIOSI, F. Network approximation and learning. In *IEEE* (1990), vol. 78-79, pp. 1481–1491.
- [81] ROTHSTEIN, W. G. *American physicians in the nineteenth century : from sects to science*. Johns Hopkins University Press, Baltimore, 1972.
- [82] RUDY, Y., AND BURNS, J. E. Noninvasive electrocardiographic imaging. *Ann. Noninv. Electrocardiol.* 4 (1999), 340–359.
- [83] RUFFY, R. Atrial fibrillation. In *Cardiac Electrophysiology: from Cell to Bedside*, D. P. Zipes and J. Jalife, Eds., 2 ed. Saunders, W. B., Philadelphia, 1995, pp. 682–690.
- [84] SCHOPENHAUER, A. *Die Welt als Wille und Vorstellung vier Bücher*. F. A. Brockhaus, Leipzig, 1819.
- [85] SCHOPENHAUER, A. *The world as will and idea*. Engl. and for. phil. libr. vols. 22-24. London, 1883.
- [86] SIPPENSGROENEWEGEN, A., PEETERS, H. A., JESSURUN, E. R., LINNENBANK, A. C., ROBLES DE MEDINA, E. O., LESH, M. D., AND VAN HEMEL, N. M. Body surface mapping during pacing at multiple sites in the human atrium: P-wave morphology of ectopic right atrial activation. *Circulation* 97, 4 (1998), 369–380.
- [87] SIPPENSGROENEWEGEN, A., SPEKHORST, H., HAUER, R. N. W., VAN HEMEL, N. M., BROEKHUISEN, P., AND DUNNING, A. J. A radiotransparent carbon electrode array for body surface mapping during catheterization. *Proc 9th Ann Conf IEEE-EMBS* (1987), 178–181.
- [88] SLOCUM, J., BYROM, E., MCCARTHY, L., SAHAKIAN, A., AND SWIRYN, S. Computer detection of atrioventricular dissociation from surface electrocardiograms during wide QRS complex tachycardias. *Circulation* 72, 5 (1985), 1028–1036.
- [89] SPACH, M. S., BARR, R. C., WARREN, R. B., BENSON, D. W., WALSTON, A., AND EDWARDS, S. B. Isopotential body surface mapping in subjects of all ages: emphasis on low-level potentials with analysis of the method. *Circulation* 59, 4 (1979), 805–821.
- [90] STEIN, W. D. *Channels, Carriers and Pumps: An Introduction to Membrane Transport*. Academic Press, San Diego, 1990.
- [91] STRIDH, M., AND SORNMO, L. Spatiotemporal QRST cancellation techniques for analysis of atrial fibrillation. *Biomedical Engineering, IEEE Transactions on* 48, 1 (2001), 105–111.
- [92] SUN, T., AND GRIFFITH, S. B. *The art of war*. Oxford University Press, London, 1971.

-
- [93] UIJEN, G. J., HERINGA, A., VAN OOSTEROM, A., AND VAN DAM, R. T. Body surface maps and the conventional 12-lead ECG compared by studying their performances in classification of old myocardial infarction. *J Electrocardiol* 20, 3 (1987), 193–202.
- [94] UIJEN, G. J., AND VAN OOSTEROM, A. On the detection of the number of signals in multi-lead ECGs. *Methods Inf Med* 31, 4 (1992), 247–55.
- [95] UIJEN, G. J., AND VAN OOSTEROM, A. The performance of information-theoretic criteria in detecting the number of independent signals in multi-lead ecgs. *Methods Inf Med* 31, 4 (1992), 256–62.
- [96] UIJEN, G. J. H. *The information content of the electrocardiogram*. PhD thesis, University of Nijmegen, 1991.
- [97] UPTON, G. J., AND FINGLETON, B. *Spatial data analysis by example, volume 2: categorical and directional data*. John Wiley and Sons, Chichester, 1989.
- [98] VAN OOSTEROM, A. Genesis of the T wave as based on an equivalent surface source model. *J Electrocardiol* 34 (2001), 217–227.
- [99] VAN OOSTEROM, A. The dominant T wave and its significance. *J Cardiovasc Electrophysiol* 14, 10 Suppl (2003), S180–187.
- [100] VAN OOSTEROM, A. Singular value decomposition of the T wave: Its link with a biophysical model of repolarization. *International Journal of Bioelectromagnetism* 4 (2003), 59.
- [101] VAN OOSTEROM, A. The dominant T wave. *J Electrocardiol* 37 Suppl (2004), 193–7.
- [102] VAN OOSTEROM, A. Reflections on T waves. In *Advances in Electrocardiology* (2005), H. M, Ed., pp. 807–815.
- [103] VAN OOSTEROM, A., HOEKEMA, R., AND UIJEN, G. J. Geometrical factors affecting the interindividual variability of the ECG and the VCG. *J Electrocardiol* 33 Suppl (2000), 219–227.
- [104] VAN OOSTEROM, A., AND JACQUEMET, V. Genesis of the P wave: atrial signals as generated by the equivalent double layer source model. *Europace* 7, Suppl 2 (2005), S21–S29.
- [105] VIRAG, N., JACQUEMET, V., HENRIQUEZ, C. S., ZOZOR, S., BLANC, O., VESIN, J. M., PRUVOT, E., AND KAPPENBERGER, L. Study of atrial arrhythmias in a computer model based on magnetic resonance images of human atria. *Chaos* 12, 3 (2002), 754–763.
- [106] VULPIAN, A. Note sur les effets de la faradisation directe des ventricules du coeur du chien. *Arch de Physiol* (1874), 975.

- [107] WALLER, A. D. On the electromotive changes connected with the beat of the mammalian heart, and of the human heart in particular. *Phil Trans R Soc B* 180 (1889), 169–194.
- [108] WILSON, R. J. *Introduction to graph theory*. Longman, London, 1975.

Curriculum Vitae

ZENICHI IHARA

Nationality: Japanese

Date of birth: August 11th, 1978

Place of birth: Chiba, Japan.

Gender: Male

Civil state: Single

Chemin de Veilloud 17

CH-1024 Ecublens, SWITZERLAND

Phone: +41 21 626 3433

Mobile: +41 79 501 2349

email: zenichi.ihara@a3.epfl.ch

Objective

To find a role in the mixture of fields, using the technical and academic knowledge of biomedical signal processing as well as the language skills and the management of cultural differences.

Education

- DEC 2001 - JUL 2006 Swiss Federal Institute of Technology Lausanne (EPFL),
School of Engineering, Signal Processing Institute.
– Doctor of Science in Biomedical Engineering.
- FEB 2001 - OCT 2001 Swiss Federal Institute of Technology Lausanne (EPFL),
Department of Physics.
Cycle Postgrade en Ingénierie Biomédicale.
– Master of Science in Biomedical Engineering.
- APR 1997 - MAR 2001 Sophia University, Japan,
Faculty of Science and Technology,
Department of Electrical and Electronics Engineering.
– Bachelor of Science in Electrical Engineering.
- APR 1994 - MAR 1997 Chiba prefectural High School, Japan.
-

Academic works

- DEC 2001 - JUL 2006 Research work as assistant/PhD student.
in biomedical signal processing and biophysics.
*Design and performance of lead systems for the analysis of atrial
signal components in the ECG.*
- FEB 2001 - OCT 2001 MS in biomedical engineering,
biomedical signal processing.
*Detection of particular signal pattern in human walking for integral
pedestrian navigation system.*
- APR 1997 - MAR 2001 BS in electrical engineering,
biomedical signal processing.
*Time-variant auto-regressive identification of the circulatory con-
trol system: power spectra estimation of the cardiovascular signals.*
-

Languages

- JAPANESE Native.
FRENCH Fluent. Spent his childhood in Geneva, CH.
ENGLISH Fluent.
ITALIAN Basic knowledge.
-

Publications

Journal papers

1. Ihara Z, Lemay M, van Oosterom A, Forclaz A, Kappenberger L. *Performance of lead systems dedicated to atrial fibrillation: application to clinical data.* J Electrocardiol, 2006. [to be submitted]
2. van Oosterom A, Ihara Z, Jacquemet V, Hoekema R. *Vectorcardiographic lead systems for the characterization of atrial fibrillation.* J Electrocardiol, 2006. [revised]
3. Ihara Z, van Oosterom A, Jacquemet V, Hoekema R. *Adaptation of the standard 12-lead ECG system dedicated to the analysis of atrial fibrillation.* J Electrocardiol, 2006. [in press]
4. Ihara Z, van Oosterom A, Hoekema R. *Atrial repolarization as observable during the PQ interval.* J Electrocardiol, 2006;39(3):290-297.

5. Dang L, Virag N, Ihara Z, Jacquemet J, Vesin JM, Schlaepfer J, Ruchat P, Kappenberger L. *Evaluation of ablation patterns using a biophysical model of atrial fibrillation*. Ann Biomed Eng, 2005;33(4):465-474.
6. Jacquemet V, Virag N, Ihara Z, Dang L, Blanc O, Zozor S, Vesin JM, Kappenberger L, Henriquez CS. *Study of unipolar electrogram morphology in a computer model of atrial fibrillation*. J Cardiovasc Electrophysiol, 2003;14(10):S172-S179.

Conference papers and abstracts

1. Ihara Z, Jacquemet V, van Oosterom A. *Adaptation of the standard 12-lead ECG system focusing on atrial electric activity*. Computers in Cardiology, Lyon, 2005;32:203-205.
2. Ihara Z, van Oosterom A, Hoekema R. *Atrial repolarization as observable in the PR interval*. SSBE, Lausanne, 2005;10.
3. Ihara Z, van Oosterom A. *On improving vectorcardiographic lead systems for the characterization of atrial electric activity*. Europace, Prague, 2005;7(S1):84.
4. Lemay M, Vesin JM, Ihara Z, Kappenberger L. *Suppression of ventricular activity in the surface electrocardiogram of atrial fibrillation*. ICA, Granada, 2004;1995-1102.
5. Lemay M, Ihara Z, Vesin JM, Kappenberger L. *PhysioNet challenge 2004: AF classification based on clinical features*. Computers in Cardiology, Chicago, 2004;31:669-672.
6. Dang L, Virag N, Ihara Z, Jacquemet V, Blanc O, Vesin JM, Kappenberger L. *Evaluation of ablation patterns by means of a computer model of human atria*. EMBS, Cancun, 2003;1:126-129.
7. Virag N, Blanc O, Dang L, Jacquemet V, Ihara Z, Vesin JM, Henriquez CS, Kappenberger L. *Characterizing anti-tachy pacing efficiency in a numerical model of human atrial arrhythmias*. Eur Heart J, ESC, Vienna, 2003;24:601.
8. Jacquemet V, Virag N, Ihara Z, Dang L, Blanc O, Vesin JM, Henriquez CS, Kappenberger L. *A computer model of sustained atrial fibrillation to study atrial electrograms*. Int J Bioelectromag, ICE, Helsinki, 2003;5(1):181-182.
9. Jacquemet V, Ihara Z, Dang L, Blanc O, Virag N, Vesin JM, Kappenberger L, Henriquez CS. *Analysis of electrogram morphology to detect gross structural remodeling during chronic AF: a model study*. PACE, NASPE, Washington DC, 2003;24(4 part II):1025.
10. Dang L, Ihara Z, Jacquemet V, Virag N, Blanc O, Vesin JM, Kappenberger L. *Optimization of antitachycardia pacing using a computer model of atrial arrhythmias*. PACE, NASPE, 2003;24(4 part II):1025.

Epilogue

Is a thesis a once-in-a-lifetime experience? Some of us write it once and hope never to do it again, while others guide their way into achieving it twice, or more. As for me, I am glad I did it, and I would love to do it again in a field that interests me. This work is not just four months of intense redaction but a compilation of what I have been doing during the past years. It was a fun experience which I enjoyed fully, though I must admit I am relieved it is finished now. After the final correction of this thesis, Professor van Oosterom would probably make me sing: “*Ye see how for a little while I labor and toil, yet have I found much rest.*”^{*} as it resonated inside the Cathedral of Lausanne.

Thank you for reading till the end, my dissertation is nearly finished. What did you find? I am very curious to know. You may have found room for improvement, have you not? There is always. But let’s not worry! It’s too late, now, it will always be too late. Fortunately![†]

^{*}Sehet mich an: Ich habe eine kleine Zeit Mühe und Arbeit gehabt und habe großen Trost funden.⁶

[†]Mais rassurons nous! Il est trop tard, maintenant, il sera toujours trop tard. Heureusement!¹¹

The genius will come through despite everything, for there is something absolute and indomitable in his nature. The so-called “misunderstood genius” is rather a doubtful phenomenon. Generally he turns out to be a good-for-nothing who is forever seeking a soothing explanation of himself.

– CARL GUSTAV JUNG. *The Development of Personality* (1943)⁵⁴ –

With my cordial compliments,

The End



